8-8-2017

Geochemical Signatures of Stream Capture in the Retreating Blue Ridge Escarpment, Southern Appalachian Mountains

David DuBose

GEOCHEMICAL SIGNATURES OF STREAM CAPTURE IN THE

RETREATING BLUE RIDGE ESCARPMENT,

SOUTHERN APPALACHIAN MOUNTAINS

by

DAVID DuBOSE

Under the Direction of Katie Price, PhD

ABSTRACT

Stream capture is a major driver of the retreat of the Blue Ridge Escarpment, but timescales of capture are not well understood. This study examines stream sediment geochemistry to establish a set of sediment source fingerprints which can be used to identify and date the capture of the Tallulah River. Statistical analyses show significant differences in U, Th, and certain REE enrichment. These differences result from variations in bedrock along the lengths of each river and a shift in relative stream powers after capture to favor mobilization or deposition of heavy elements. The observed differences should be sufficient to identify where Tallulah sediment appears in floodplains of the capturing Tugaloo River, facilitating future dating of the capture event. Understanding the timing of river capture will provide insight into the ongoing reshaping and redistribution of river systems and interactions of geomorphic processes in the continuing evolution of the southern Appalachian Mountains.

INDEX WORDS: Stream capture, Blue Ridge Escarpment, Geochemistry, Tallulah River, Southern Appalachians, Sediment, Geomorphology

GEOCHEMICAL SIGNATURES OF STREAM CAPTURE IN THE RETREATING BLUE RIDGE ESCARPMENT, SOUTHERN APPALACHIAN MOUNTAINS

by

DAVID DuBOSE

A Thesis Submitted in Partial Fulfillment of the Requirements for the Degree of

Master of Science

in the College of Arts and Sciences

Georgia State University

2017

GEOCHEMICAL SIGNATURES OF STREAM CAPTURE IN THE

RETREATING BLUE RIDGE ESCARPMENT,

SOUTHERN APPALACHIAN MOUNTAINS

by

DAVID DuBOSE

Committee Chair: Katie Price

Committee: Katie Price

Daniel Deocampo

David S. Leigh

Electronic Version Approved:

Office of Graduate Studies

College of Arts and Sciences

Georgia State University

August 2017

DEDICATION

This thesis is dedicated to my awesome wife Natalie, who stood by me from the start of my career with love and patience through all the long days in the field, all the time on the road, then picking up and moving to go back to school with our little one in tow, and even longer days of research and writing. Through everything and more.

For Pop Pop Charlie, always a hard-working, hard-playing family man, and for Grandma Betty, an educator, a nature lover, always quiet, always strong. Though they didn't get to see me finish, they never had any doubt.

Most of all for little Elliot. At the beginning, she could barely roll over, then she walked, then she ran, then she kept running and started jumping and climbing. Through all of our adventures in the back yard, in the car, playing with rocks, playing with sand and trucks and dinosaurs, watching the birds, reading books and doing puzzles, every day is full of amazement and wonder, and she faces it with fascinated determination and an unquenchable thirst for knowledge like nothing I've ever seen. Look out world, she's coming.

ACKNOWLEDGEMENTS

I want to offer a special thanks to Dr. Katie Price for taking me on as a student when I was new to the department and my tentative area of research interest was basically "Rivers and what they do to mountains." She was very forthcoming with ideas from small to large scales and helped me narrow down a topic by inciting an interest in stream capture, which I did not previously know I had. After digging into the literature, I discovered how surprisingly complex and poorly understood the Appalachian Mountains actually are, and I jumped at the opportunity to fill a knowledge gap related to Tallulah Gorge, a favorite hiking spot of mine. Our meetings and discussions always helped me to refocus when the workload and dataset seemed cumbersome. I always came away with more questions to find answers to and a new determination to find them. Through many plans and iterations and proposals and setbacks and alternate ideas, we finally came away with a good question to answer and a good set of data with which to answer it.

Drs. Dan Deocampo and David Leigh were also instrumental in the formation of this thesis, from our initial meeting to kick around ideas for study areas and methods to later committee discussions about which directions to take the research. I had a top-notch team of researchers to work with and mine for wisdom, and I always came away feeling a little smarter (though even more aware of just how much I *don't* know).

I also must thank all my GSU professors because this thesis truly encompasses the breadth of my graduate school experience. In every class, there has been some topic, assignment, or discussion that flicked on the lightbulb over my head and eventually made its way into influencing the finished thesis. They made me work, and I came out better on the other end for it.

Finally, I would like to thank the numerous U.S. Geological Survey and Department of Energy personnel, whoever and wherever they are, who have collected thousands of samples in the field and analyzed thousands of samples in the lab and compiled all the data to be made available for me to dig through from the relative comfort of my office chair.

TABLE OF CONTENTS

LIST OF TABLES

LIST OF FIGURES

LIST OF ABBREVIATIONS

-AA – Atomic absorption spectrometry

-AOI – Area of Interest

-BA – Base-cation to Aluminum ratio

-BRE – Blue Ridge Escarpment

-DOE – United States Department of Energy

-ECD – Eastern Continental Divide

-EF – Enrichment factor

-Element symbols:

Ag – Silver

Al – Aluminum

Au – Gold

Be – Beryllium

Ca – Calcium

Ce – Cerium

Co – Cobalt

Cr – Chromium

Cu – Copper

Dy – Dysprosium

Eu – Europium

F – Fluorine

Fe – Iron

Hf – Hafnium

K – Potassium

La – Lanthanum

Li – Lithium

Lu – Lutetium

Mg – Magnesium

Mn – Manganese

Mo – Molybdenum

Na – Sodium

Nb – Niobium

Ni – Nickel

P – Phosphorous

Pb – Lead

Sc – Scandium

Sm – Samarium

Sn – Tin

Sr – Strontium

Th – Thorium

Ti – Titanium

U – Uranium

V – Vanadium

W – Tungsten

Y – Yttrium

Yb – Ytterbium

Zn – Zinc

-HSSR – Hydrogeochemical and Stream Sediment Reconnaissance

-HUC – Hydrologic Unit Code

-MRDS – Mineral Resource Data System

-ND – Non-detect

-NGC – National Geochemistry Database

-NHD – National Hydrography Dataset

-NURE – National Uranium Resource Evaluation

-RASS – Rock Analysis Storage System

-SRL-E – Savannah River Laboratory (Eastern Protocol)

-REE – Rare earth element

-USDA – United States Department of Agriculture

-USGS – United States Geological Survey

-WBD – Watershed Boundary Dataset

-WIS – Water Information System

-XRF – X-ray fluorescence spectrometry

1 INTRODUCTION AND BACKGROUND

Many modern and ancient riparian ecosystems are and were closely dependent on fluvial systems for their water and transport of sediments and nutrients. Rivers, however, are not fixed features of the landscape as their courses, discharge, and flow regimes change through time (Davis 1899, Charlton 2008). An ecosystem's water supply and sediment load are functions of the hydrology and geology of the watershed, including climate and tectonic setting (Bishop 1995). Through the processes of erosion and deposition, rivers shift their courses through time, eroding older sediment or bedrock in some places and depositing sediment in others (Bishop 1995). River systems also erode and cut headward into the highlands of the watershed, with their smaller headwater tributaries cutting toward the drainage divides that bound the watershed (Willett et al. 2014). The processes of erosion and deposition make river systems central aspects of the study of landscape and ecosystem evolution.

This study examines the processes that shape fluvial systems and the controls that fluvial systems exert on surrounding landscapes. The principle of stream power is a major driver of erosional and depositional processes along a river's length, and stream capture is a major geomorphological shift that alters these processes. Stream capture is prevalent in tectonically active settings, but is also a major geomorphological factor in the tectonically dormant southern Appalachian Mountains. The heavily faulted and structurally complex rock units of the southern Appalachians result in varied geochemical compositions of stream sediment in river basins throughout the region. The focus of this study is the Tallulah River capture event, in which the Savannah River captured flow from the Tallulah River and cut off flow from the Chattahoochee

River. Geochemical variations between adjacent river basins were used to establish sediment source fingerprints for identifying sediment from one basin in the river channel of another after the capture event. With these signatures it will be possible to identify and distinguish sediment sourced from different basins and date a capture event from the record of floodplain deposits.

1.1 Fluvial Processes and Stream Capture

1.1.1 Stream Power and Erosion

River systems make up an interlocking network of drainage basins that channel surface water, groundwater, and sediment from high points in the watershed to some local, regional, and ultimate base level (Charlton 2008). Sediment transport is a function of the erosive power of a stream's flowing water and the stream's capacity to carry sediment grains of a given size, quantified by the equation for stream power:

$$\Omega = \rho g Q S$$

where Ω is stream power of the stream channel (in power per unit length), ρ is the density of the fluid, g is the acceleration due to gravity, Q is the stream discharge (in volume per unit time), and S is the water surface slope (unitless gradient) (Charlton 2008). As demonstrated in the stream power equation, a river's erosive power over a given channel length is directly proportional to the volumetric velocity of water flowing through it and the channel's gradient, represented by the elevation drop from its high point to its low point (Charlton 2008). It is often useful to express stream power in terms of power per area of channel bed to allow for comparisons of relative erosive power between streams of varying channel widths. Specific stream power is defined as a streams power per unit area of channel bed, calculated by the equation

$$\boldsymbol{\omega = \Omega/W}$$

where ω is specific stream power (in power per unit area), Ω is stream power (in power per unit length), and W is channel width (Charlton 2008). Because of this relationship a small highland river flowing through steep terrain can have a higher erosive power per channel bed area than a larger, flatter lowland river into which it flows, and this principal is a fundamental control on the development of river profiles from their headwaters to the river mouth (Knighton 1998).

Numerous erosion processes act on streambeds as flowing water interacts with sediment and exposed bedrock. One such process is abrasion, by which moving sediment grains (sand, gravel, cobbles, etc.), through repeated impacts, loosen and break apart pieces of bedrock exposed in the river channel (Cook et al. 2013). In rocks with jointing or cleavage planes, the process of plucking, by which larger blocks of bedrock are loosened and removed along planes of weakness, tends to dominate (Hartshorn et al. 2002). Sediment being transported through the channel is derived from upstream erosional processes such as tree throw, stream bank erosion, gully erosion, soil creep, frost-wedged rockfalls, and other mass hillslope movement (Jungers et al. 2009; Linari et al. 2016). Varying sediment flux and stream flow can have complicated interactions related to overall erosion rates of the stream bed. The “tools effect” results from high sediment flux, which leads to more individual impacts on the bedrock and higher channel erosion rates (Cook et al. 2013). The “cover effect,” by contrast, is caused by sediment deposited on the stream bed, unmoved by the current, which shields the underlying sediment and bedrock from impacts, decreasing channel erosion rates (Cook et al. 2013). Because river erosion is driven by flowing water, climate factors such as precipitation magnitude and frequency also exert controls on rivers' erosive power. All these erosive actions contribute to the quantity and nature of a stream's sediment supply.

At the basin scale, channel erosion processes work to reshape the topography of the basin itself, expanding watersheds through headward erosion and cutting through underlying rock via knickpoint migration and gorge incision. The process of headward erosion occurs at the headwater tributaries of a river, as small-scale erosion processes extend the reach of the channels upstream (Bishop 1995). Knickpoints are sharp convexities where a river flows steeply or abruptly from a high elevation to a lower elevation and represent a disequilibrium between river basin area and channel gradient – either resulting from differential resistance of underlying rock units, recent tectonic uplift, or other geomorphological changes (Gallen et al. 2013; Willett et al. 2014). Gorge incision is the combined product of headward erosion, knickpoint migration, and hillslope erosion as a river channel erodes downward to a local base level, gorge walls retreat through rockfalls, and the upland region is dissected as knickpoints erode and migrate upstream and tributary streams also incise and migrate upstream (Nott et al. 1996).

1.1.2 Stream Capture

As a stream erodes its headwaters, it can eventually cut into an adjacent stream basin, whereby one river gains new streamflow, groundwater, and sediment, one river loses streamflow, groundwater, and sediment, and entire watersheds shift their boundaries and flow directions – a process called stream capture or river capture (Bonnet 2009; Bloxom & Burby 2015). Stream capture typically occurs in upland areas where there is sufficient potential energy (as stream power increases with gradient) to drive erosion at a stream's headwaters as well as significant elevation differences between adjacent watersheds separated by a low-relief divide (Bishop

1995). The capture takes place when one river actively cuts into the low-relief divide and expands into an adjacent river basin through headward erosion (Bishop 1995), as shown in ***Figure 1-1***. The process of stream capture is one mechanism by which landscapes adjust towards equilibrium between tectonic uplift and river erosion (Willett et al. 2014).

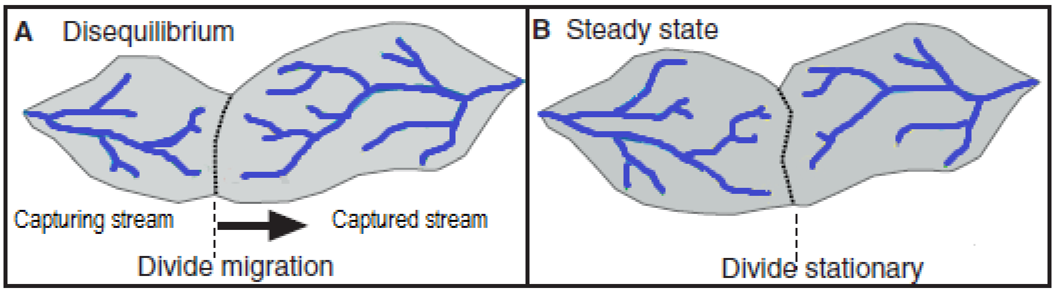

Figure 1-1 *Watershed divide migration and stream capture.*
The watershed divide migrates from a disequilibrium state at time ***A*** *to a steady state condition at time* ***B****. The divide migrates as headwater tributaries of the left basin erode through the divide and capture flow from headwater tributaries of the right basin. After a steady state is reached, both basins continue to erode at equal rates, and the divide erodes downward without migrating laterally (Modified from Willett et al. 2014).*

Stream capture is most often observed in tectonically active settings where active or recent uplift generates high topographic relief (i.e. steep slopes) and drainage divides migrate as erosion propagates upstream, all resulting in the continual reorganization of river networks (Gallen et al. 2013; Willett et al. 2014). This uplift-induced change in base level is often manifested in the formation of knickpoints which migrate upstream as they erode (Gallen et al. 2013). However, there are several complicating factors that can account for high relief conditions without active tectonic uplift. Disequilibrium conditions also exist in tectonically dormant regions, such as the southeastern United States, where divide migration and escarpment retreat result in significant river capture events and landscape reorganization (Prince et al. 2010, 2011). In piedmont regions, where eroded mountain sediment tends to be deposited, stream capture also occurs where low elevation streams capture and divert sediment from larger rivers at higher elevations

(Pastor et al. 2012). Stream capture therefore represents a fundamental process in the ongoing reshaping and redistribution of river systems in both tectonically active and inactive regions.

There are several clues and lines of evidence for identifying regions of stream capture and establishing a chronology of capture events. Stream captures have been studied in actively eroding landscapes throughout the world, including the eastern U.S. (Voss et al. 1995; Jones et al. 2006; Kozak et al. 2006; Prince et al. 2010, 2011; Bloxom & Burby 2015), western U.S. (Mikesell et al. 2010; Aslan et al. 2014; Hood et al. 2014), western Canada (Andrews et al. 2012), Mexico (Schonhuth et al. 2011), Iran (Walker & Allen 2012), Kyrgyzstan (Oskin & Burbank 2007), Lithuania (Linkeviciene 2009), Morocco (Pastor et al. 2012), and Spain (Mather 2000). Several studies of phylogeography and gene lineage of aquatic river vertebrate species have identified separate populations of the same species in adjacent, presently disconnected river basins in the southern Appalachian Mountains (Voss et al. 1995; Jones et al. 2006), northern Appalachian Mountains (Kozak et al. 2006;), and the Sierra Madre Occidental Mountains in Mexico (Schonhuth et al. 2011). Through analysis of genetic variations, these studies have constrained timescales of river capture events to account for species migration throughout presently disconnected basins (Jones et al. 2006, Schonhuth et al. 2011, Voss et al. 1995, Kozak et al. 2006). For example, in the southern U.S., the presence of isolated populations of aquatic river salamander species and studies of genetic variation among the populations suggest that the drainages of the Tennessee, Chattahoochee, and Savannah Rivers were once connected to allow species dispersal until river capture events that established the modern drainage divides and separated the populations (Voss et al. 1995; Jones et al. 2006). More modern instances of stream capture have been documented through cartographic studies in Lithuania, where the Ula River captured headwater streams of the Katra River basin in the late nineteenth century (Linkeviciene 2009). The drainage area of the Ula River basin has increased by 62% with a 63% increase in mean discharge, and the Katra River's drainage basin area has decreased by 23% with a 27% reduction in mean discharge (Linkeviciene 2009). Because this capture occurred in modern times, it has significant and observable impacts on water resources and ecosystems within the region. These indicators can be used to hypothesize regions of past stream capture that can then be studied for geologic evidence to corroborate and date the events in the geologic record.

Several basin geometry and sedimentological clues can be used to infer where a stream capture has occurred. These include the locations and elevations of knickpoints, which can be correlated to reconstruct a paleo-terrace surface and trace the propagation of erosion after an ancient stream capture, as in the central Appalachians (Prince et al. 2010). Elsewhere in the Appalachians, groundwater basin capture associated with river capture was observed based on hydraulic gradient and groundwater tracer studies (Bloxom & Burby 2015). In Canada's Fraser River system, several geomorphological clues indicate a drainage reversal of the entire river due to ancient glacial controls on surface water hydrology: regional slopes not parallel to the channel; barbed drainage patterns; bedrock canyons; elevated terraces and hanging paleovalleys (Andrews et al. 2012). These clues were combined with age data from volcanic dams from the ancient Fraser River basin to confirm the reversal of the Fraser River (Andrews et al. 2012). In the Kuh Banan fault zone of Iran, tectonic controls on stream capture are observed based on strike-slip faulting and offset rivers (Walker & Allen 2012). In the piedmont of the High Atlas Mountains of Morocco lowland river capture occurs when small streams capture flow and sediment from larger rivers at higher elevations, resulting in the formation of step-shaped pediments (Pastor et al. 2012). In the Colorado Plateau in the western U.S., Unaweep Canyon is a fluvial canyon abandoned as the result of river capture and diversion (Aslan et al. 2014). The ancestral Colorado River captured the ancestral Gunnison River, which led to the canyon's abandonment and subsequent river readjustment, knickpoint migrations, and canyon erosion as rivers adjusted to a new base level, as suggested by stranded river gravels and provenance studies (Aslan et al. 2014). A stratigraphic study of lake and river sediments revealed that the river capture and canyon abandonment were initiated by one or more landslide events which created a lake that eventually drained by spillover into its new channel (Hood et al. 2014). In the Sorbas Basin of Spain, basin sediment and water budgets have undergone measurable changes through geologic time as a result of river capture Spain (Mather 2000). Modeling of the erosive power of streams and landscape evolution indicates that stream capture increases the power of the receiving stream to erode, which amplifies channel incision and provides positive feedback to initiate additional captures, as observed in the Tien Shan Mountains of Kyrgyzstan (Oskin & Burbank 2007). Field evidence of this capture signature appears as relaxed channel gradients downstream of the capture and a knickzone that expands upstream from the capture (Oskin & Burbank 2007). Identifying a stream capture event therefore requires a combined approach, integrating several lines of evidence, to serve as the background for a focused geological study of the sedimentary record of capture.

In addition to water from a captured basin, stream capture also results in a shift in sediment sources for adjacent watersheds. Tracing sediment deposited in one basin back to a presently disconnected basin is one way to determine the timing and extent of a stream capture event in the sedimentary record. There are several methods to determine the provenance of stream sediment by chemical and physical parameters. Tectonic provenance of stream sediments can be determined by analyzing detrital zircon grains for U-Pb age dating (Craddock & Kylander-Clark 2013). This technique is useful in river systems in geologically complex settings, such as fold-and-thrust belts, where streams erode through bedrock of several various types and ages within their basins (Hietpas et al. 2011). Surface soils can be used to generate a unique fingerprint signature of chemical parameters that can be used to trace the sediment source area of stream deposits (Walling 2005). Those same geochemical fingerprints can be used to identify the proportions of source input (e.g. topsoil and subsoil/channel bank) in floodplain sediment cores at sample intervals, and those proportions can be correlated with depositional dates (***Figure 1-2***) to identify events of significant changes in sediment flux (e.g. changes in land use and land management practices) (Walling 2005). If deposits of river sediment can be identified within a basin in the absence of present-day flowing water, their provenance can be traced based on lithology as well as roundness and sorting (as proxies for transport distance), and this provenance data in the stratigraphic record can be used to date stream capture events from adjacent basins (Mikesell et al. 2010; Prince et al. 2010). Multivariate mixing models can incorporate silt grain-size fraction along with trace and heavy metal concentrations, base cations, organic constituents, and color to differentiate between surface and subsurface or channel and non-channel sediment sources (Grimshaw & Lewin 1980; Collins et al.1998). X-ray crystallography, x-ray diffraction, and magnetic properties can be used to assess the presence and abundance of minerals in fluvial sediment to identify sources (Klages & Hsieh 1975; Wall & Wilding 1976; Bunte 2010). Rare earth elements (REE) have been used as tracers in sediment source studies in multiple environments (Kimoto et al. 2006; Polyakov et al. 2010). Mixing models used in conjunction with principal component analysis can be used to incorporate multiple mineralogical and geochemical constituents to identify sediment source fingerprints and evaluate relative concentrations of sediment from each source in downstream locations (Collins et al. 1997; Helsel & Hirsch 2002). Other applications of geochemical sediment source fingerprinting studies include those by Horowitz (1991), Oldfield et al. (1979), Walden et al. (1997), and Walling et al. (1979). Determining which sedimentary clues to use when investigating a stream capture event will depend on the study area and a preliminary evaluation of available techniques that might provide the clearest data.

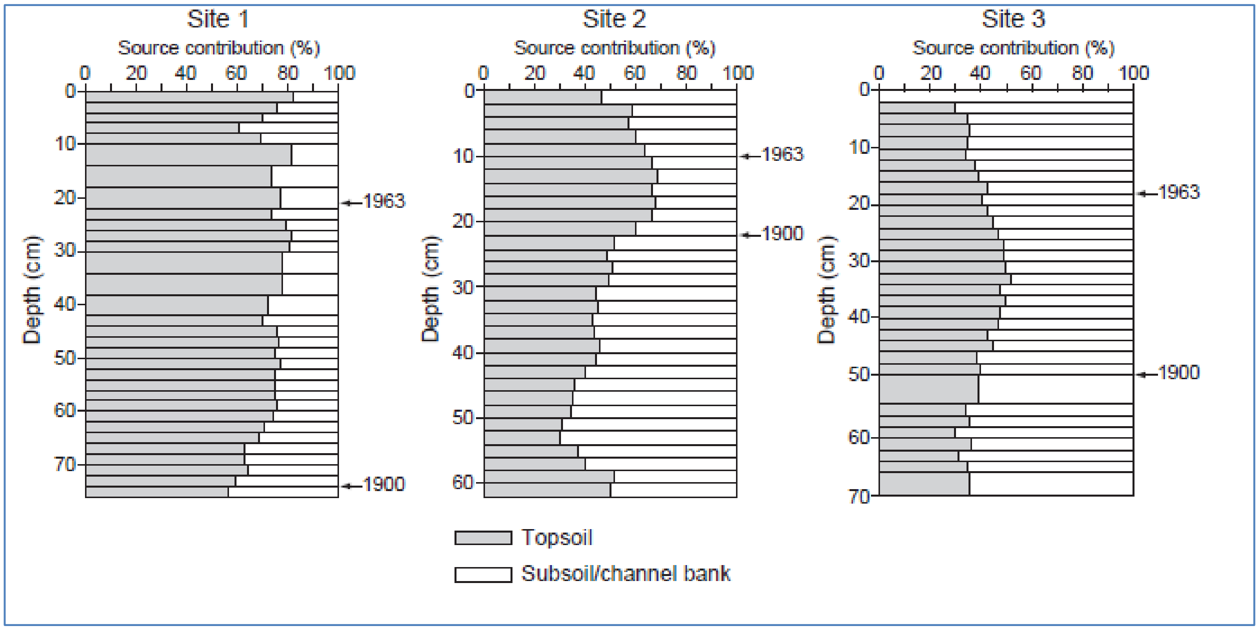

***Figure 1-2** Sediment source study using chemical fingerprinting*
Sediment source fingerprints used in floodplain sediment cores to differentiate proportion of source input by topsoil and subsoil/channel bank, and correlated with dates of deposition from radionuclide analysis (from Walling 2005)

1.2 Study Area and Geologic Setting

1.2.1 Southern Appalachian Geomorphology

The southern Appalachian Mountains comprise an ancient and continually evolving landscape with many unresolved questions, dating back over a century of scientific inquiry. These mountains formed as the result of a series of continental collisions during the Paleozoic Era (Chew 1988), as illustrated in ***Figure 1-3***. The Alleghenian Orogeny in the Permian period (299-251 Ma) – the latest Appalachian mountain-building episode – established the present tectonic structure of the region and represents the final stage of tectonic uplift before erosional processes dominated regional geomorphological change (Chew 1988). From an initial state of high relief and ruggedness (Pazzaglia & Gardner 1994; Slingerland & Furlong, 1989), the Appalachians have continually eroded, and a complex pattern of steep valleys and irregular peaks formed as the result of variable weathering resistance of the bedrock units (Adams & Spotila 2005). Following continental rifting in the Triassic (~200 Ma) that opened the Atlantic Ocean, the region experienced rift margin uplift through the Mesozoic (Linari et al. 2016). As the mountains continued to erode through summit lowering and basin denudation after active uplift ceased, the rift margin formed an escarpment which separates high-relief uplands from gently sloping lowlands, and this escarpment has eroded by downwearing and parallel retreat from its original position (Matmon et al. 2003; Prince et al. 2010). Topographic relief in the Appalachian Mountains has increased by more than 150% since the Miocene as fluvial incision and dissection have outpaced summit lowering rates long after tectonic uplift, rifting, and subsequent erosion (Gallen et al. 2013; Miller et al. 2013). Study of knickpoint migration suggests that the present-day Appalachian river systems are adjusting to a new base level imposed during the Miocene (before Pliocene glaciation-induced sea level cycles), possibly induced by mantle processes causing crustal bulging and uplift of the Appalachian region (Gallen et al. 2013). The southern Appalachians were not glaciated during the Pleistocene (Richmond and Fullerton 1986; Barron 1989), so glacial isostatic rebound effects, such as those observed in northern Appalachians (Sella 2007), are not likely, and as such the nature and mechanisms of recent uplift in the southern Appalachian region remain uncertain (Graf 1987; Gallen et al. 2013; Miller et al. 2013). The structural and lithological complexity of the southern Appalachians represents varied igneous, metamorphic, hydrothermal, and erosive processes that have transported and concentrated distinctive mineral assemblages from deep within the earth and exposed them at the surface. This variation in mineralogy, in turn, accounts for spatial variations in stream sediment mineralogy throughout the region.

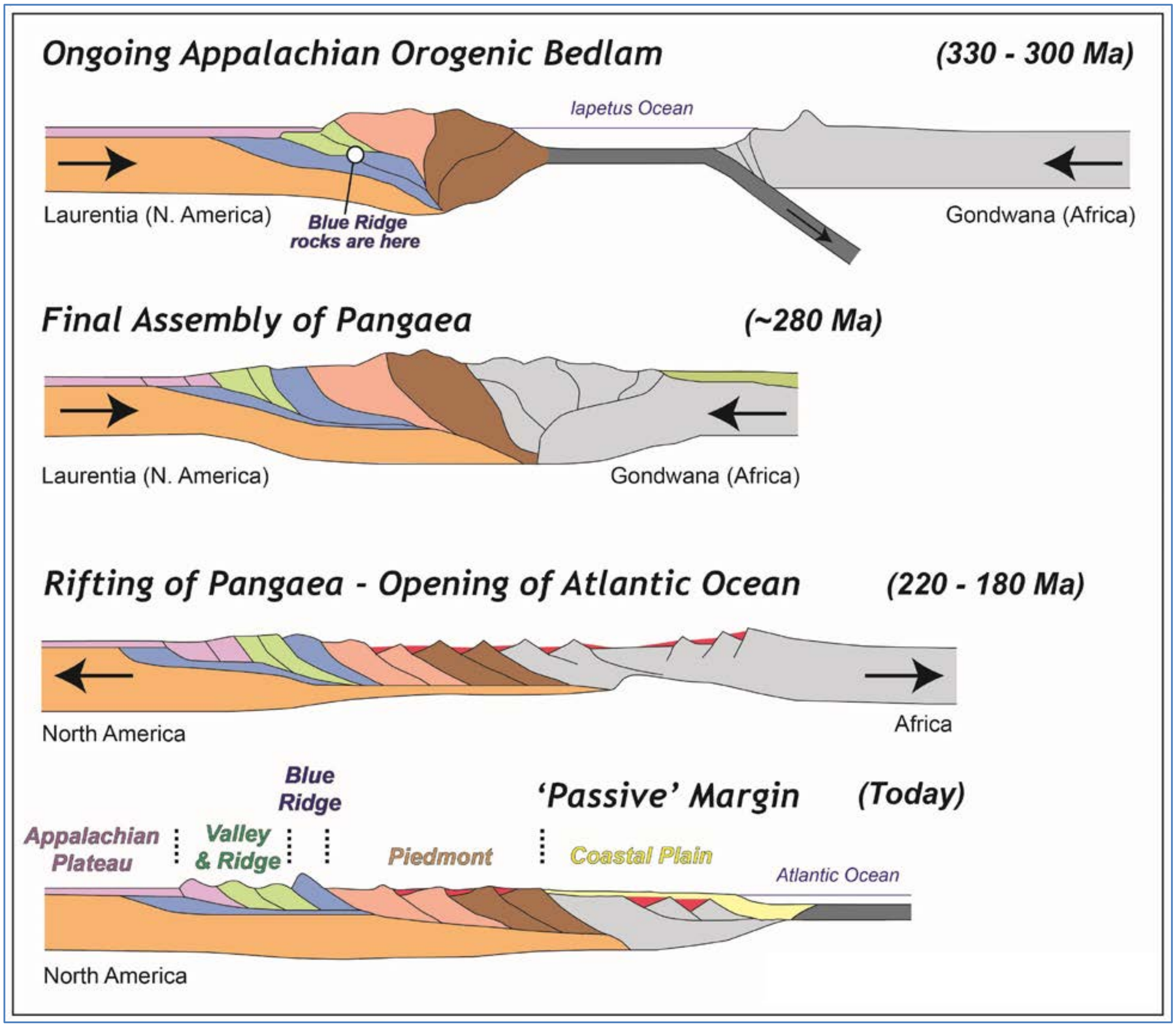

Figure 1-3 *Stages of Appalachian evolution.*

The present exposure of Blue Ridge rocks in the southern Appalachians reflect deep metamorphic processes during mountain building, as seen at 330-300 Ma (from Bailey 2006).

In the southern Appalachians, the Blue Ridge Escarpment (BRE) represents a sharp topographic contact between the high-relief Blue Ridge uplands and the low-lying Piedmont region. The steep slopes along the eastern face of the escarpment do not correspond to lithologic boundaries and likely represent a regional scale erosional feature associated with ongoing escarpment retreat long after continent-scale rifting in the Triassic (Spotila et al. 2004; Prince et al. 2010). In the Blue Ridge Mountains, stream capture is a major driver of long-term landscape evolution as the mountains are eroded and drainage divides migrate and rearrange (Prince et al. 2011). Significant, continental-scale capture events occur when rivers draining the Atlantic side of the BRE capture basins of headwater streams from the Blue Ridge province that flowed west ultimately to the Gulf of Mexico (Prince et al. 2010, 2011), as illustrated in ***Figure 1-4***. The Blue Ridge and Piedmont regions are eroding at a rate of 1.5-106 m/Ma, through both summit lowering and basin-wide denudation (Judson & Ritter 1964; Matmon, et al. 2003; Pelletier 2004; Spotila et al. 2004; Reiners & Brandon 2006; Hancock & Kirwan 2007; Portenga & Bierman 2011; Duxbury et al. 2015; Linari et al. 2016;), and the BRE is retreating locally by episodic capture events at a rate of 1-10 km/Ma, though escarpment-wide erosion rates are similar to those of the highlands and lowlands (Prince et al. 2010; Linari et al. 2016). Stream capture is therefore a major factor in the continuing retreat of the BRE (Prince et al. 2010) and represents a fundamental process in the ongoing reshaping and redistribution of river systems. Significant research is still needed to determine the timescales of river capture and gorge incision in the southern Appalachians, and a geochemical analysis of stream sediment provenance is an important step in building on that research.

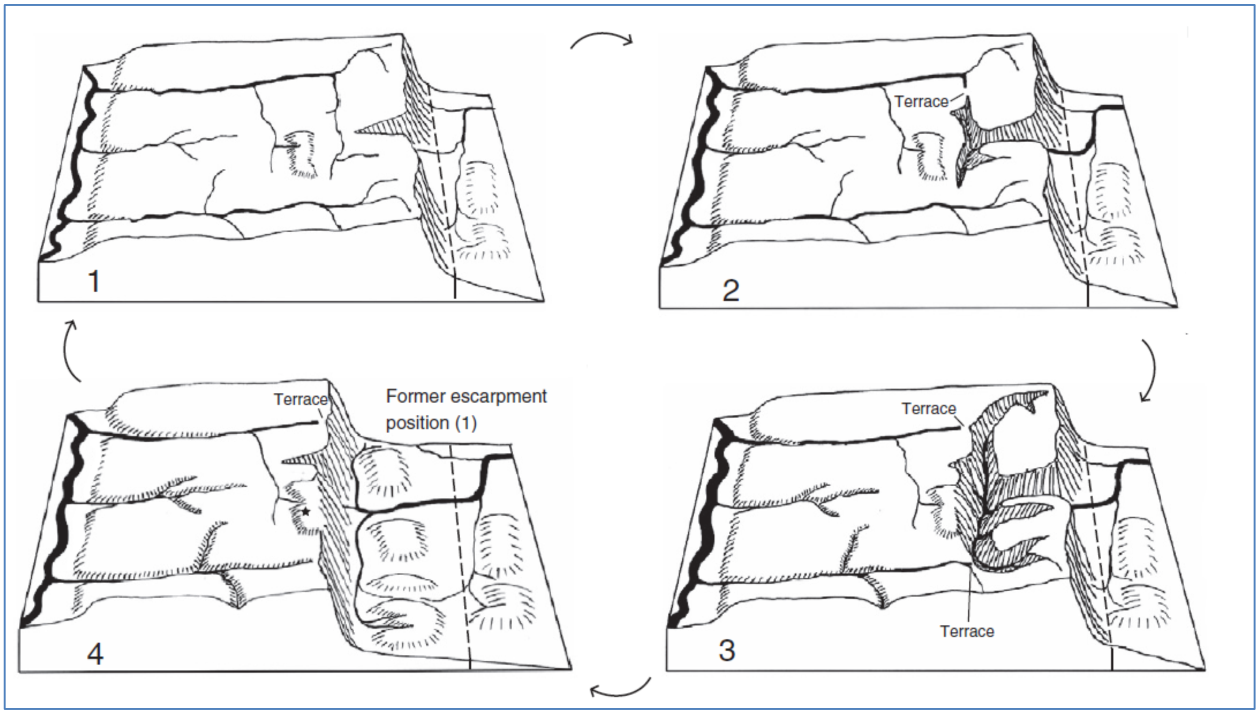

__Figure 1-4__ Escarpment retreat driven by stream capture.
A cycle of escarpment retreat by (1) gorge incision, (2) stream capture, (3) plateau dissection, and (4) parallel migration of the escarpment face (From Prince et. al 2010).

1.2.2 Northeast Georgia, Northwest South Carolina River Systems

The study area lies in northeast Georgia and northwest South Carolina, as denoted by the blue star in ***Figure 1-5***. The Eastern Continental Divide (ECD) separates rivers flowing to the Gulf of Mexico from Rivers flowing to the Atlantic Ocean. The Savannah River drains the eastern face of the ECD, and the Apalachicola-Chattahoochee-Flint Watershed drains the western face of the ECD.

Figure 1-5 *Study area on the Eastern Continental Divide, Savannah River and Apalachicola-Chattahoochee-Flint Watersheds*

This study focuses on the Soque River, a tributary to the Chattahoochee, and the Tugaloo and Tallulah Rivers, both part of the Savannah River system (***Figure 1-6***). The region is underlain by a complex geologic structure as described in the following sections. These various lithologic assemblages account for variations in stream sediment element concentrations between the river basins and downstream from the parent rock sediment sources.

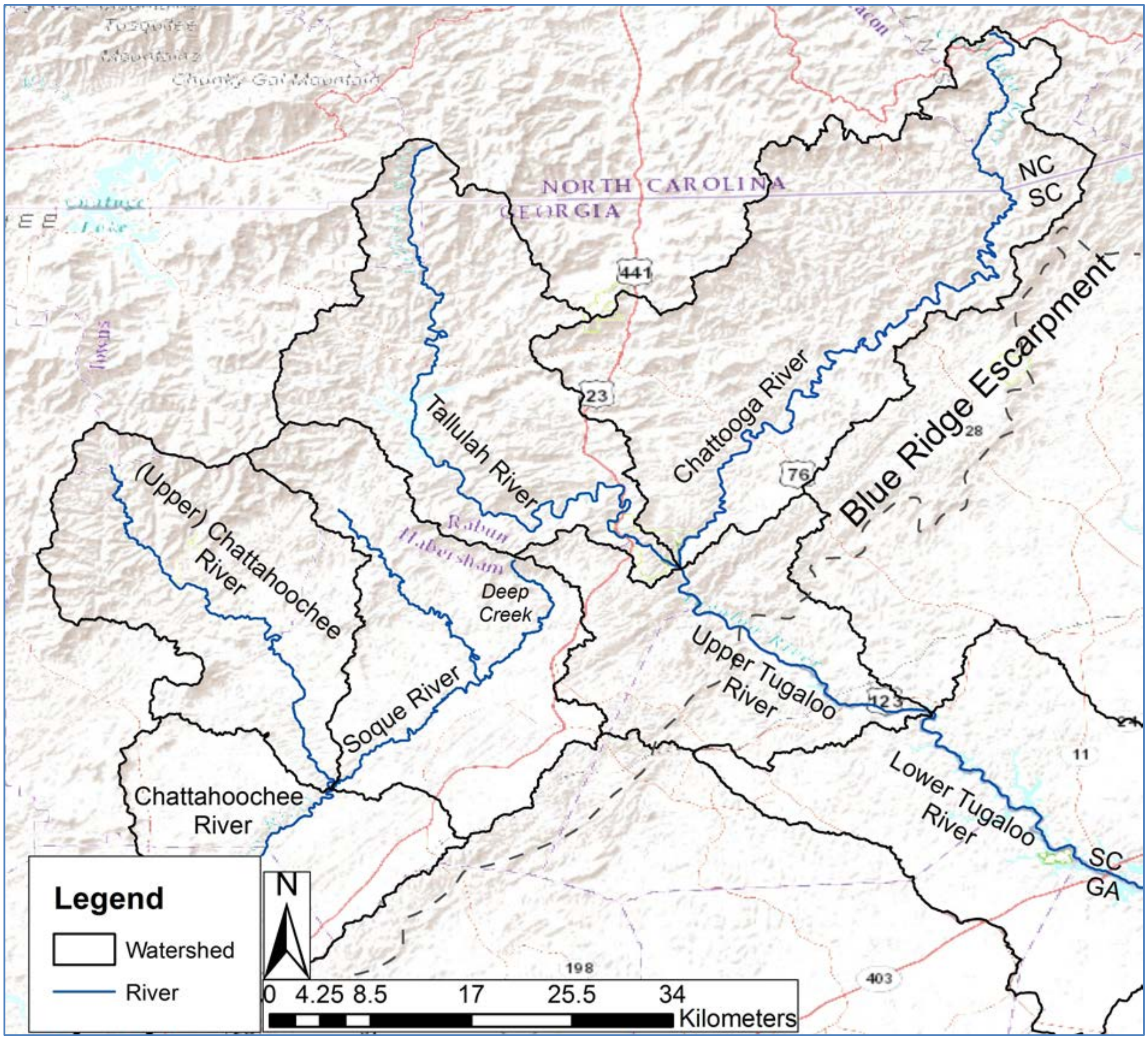

Figure 1-6 Study area map, northeast Georgia and northwest South Carolina. The Tallulah River and Chattooga River converge to form the Tugaloo River, which flows southeast to the Savannah River and Atlantic Ocean. The Soque River flows ino the Chattahoochee River, which flows southwest and joins the Flint River to form the Apalachicola River and flows to the Gulf of Mexico (Source: ESRI, DeLorme, USGS, NPS).

Tallulah River Basin

The Tallulah River basin lies in the Blue Ridge Mountains of northeast Georgia. It flows 80.45 km (USGS National Hydrography Dataset (NHD) 2017) from its headwaters draining the ECD to where it joins the Chattooga River to form the Tugaloo River in the larger Savannah River drainage, which flows into the Atlantic Ocean. The basin covers an area of 490.41 km^2 with steep terrain ranging from 270 m to 1,676 m in elevation, draining loamy soils, residuum saprolite, and bedrock gorges (Mast and Turk 1999; USGS Watershed Boundary Dataset (WBD) 2017). The boundary of the Tallulah River basin includes within it three distinct structural and lithologic features: the Richard Russell, Helen, and Tallulah Falls thrust sheets (Nelson et al. 1998), as shown in ***Figure 1-7***. These thrust sheets are members of the Blue Ridge thrust stack, part of the larger thrust complex underlying the Blue Ridge and Piedmont Provinces (Lesure et al. 1992), as illustrated in the cross-section in ***Figure 1-8***. These thrust sheets represent the westward translation and uplift of Late Proterozoic to Paleozoic-age rocks ending with the Alleghenian Orogeny, and each consists of characteristic assemblage of metamorphosed crystalline rock (Chew 1988; Nelson 1989).

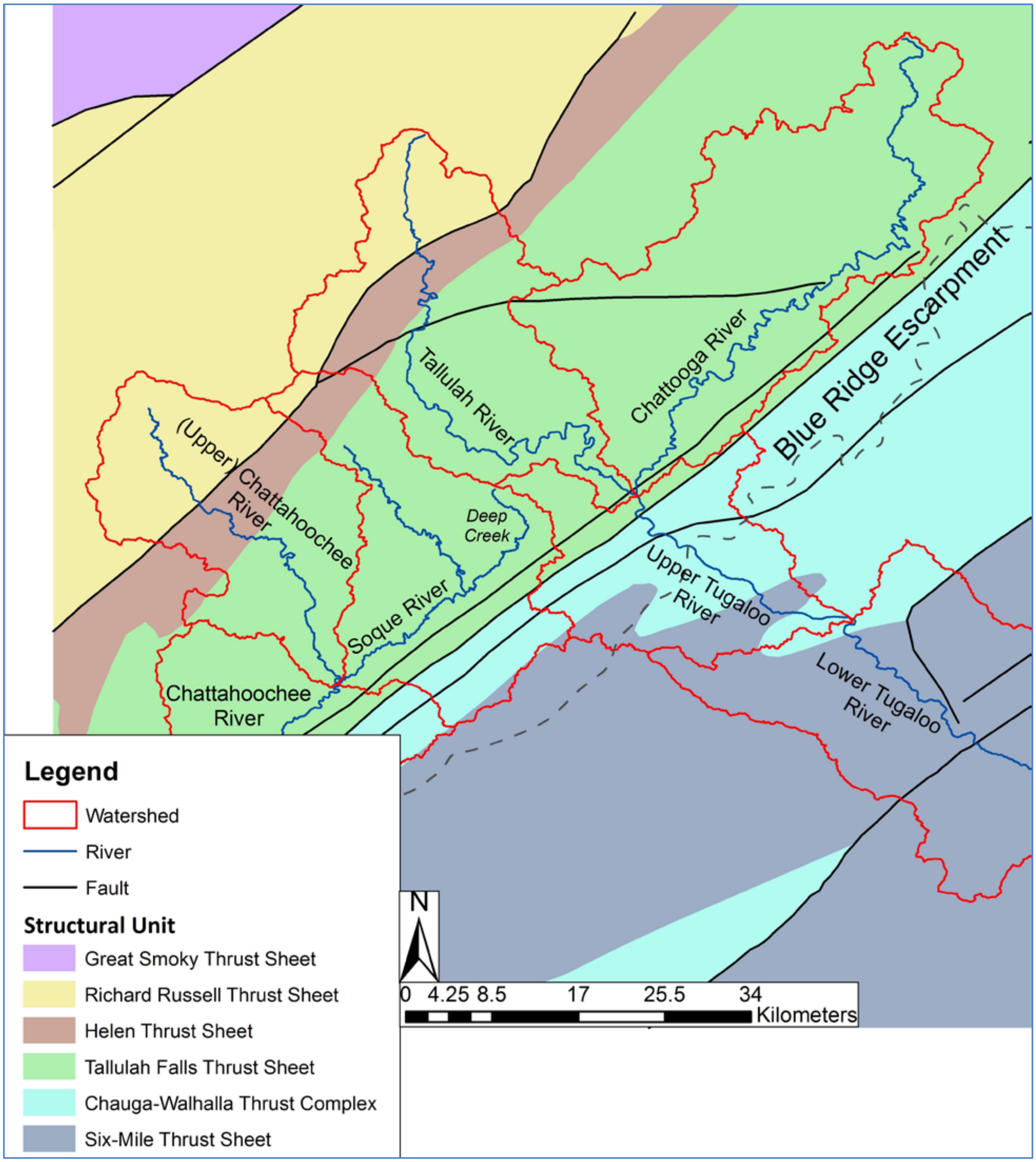

***Figure 1-7** Study area map with structural geologic units.*

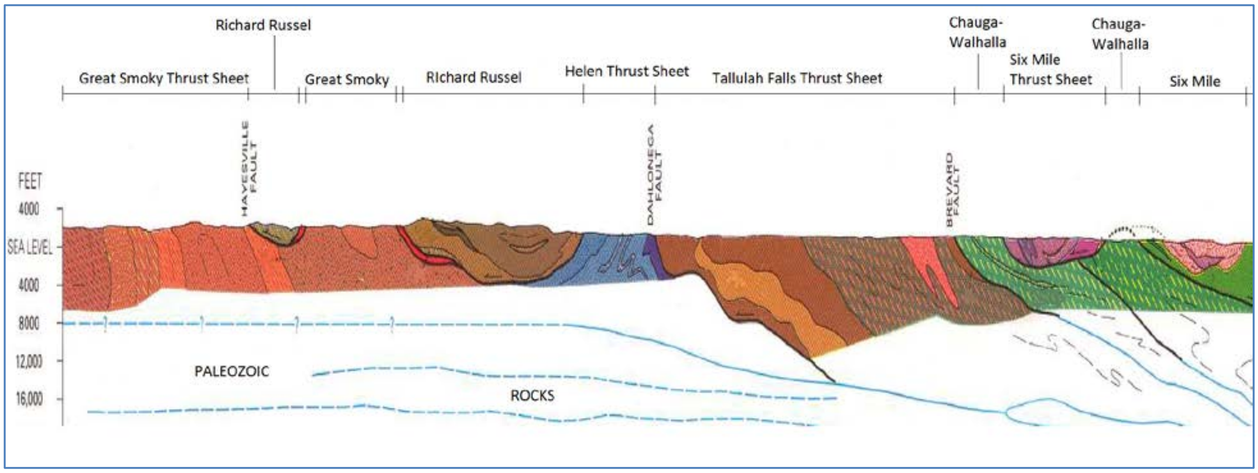

Figure 1-8 *Geologic cross-section of Blue Ridge and Piedmont thrust complexes (modified from Nelson et. al 1998)*

The Richard Russell thrust sheet consists mainly of metasedimentary and metaigneous rock of Middle Proterozoic age (Nelson and Gillon 1985; Nelson 1988), including metasandstone, quartzofeldspathic gneiss, metagraywacke, biotite gneiss, and mica schist, with smaller amounts of amphibolite, granitic gneiss, granodiorite gneiss, and granitic pegmatite (Nelson and Gillon, 1985). This thrust sheet also contains isolated copper- and zinc-bearing massive sulfide deposits (Peper et al. 1991). The Helen thrust sheet consists of interlayered metasedimentary and metavolcanic rocks of Late Proterozoic to early Paleozoic age (Nelson 1989), including micaceous and quartzofeldspathic gneiss and schist, quartzite, iron- and magnesium-rich quartz schist, amphibolite, metagabbro, granitic to dioritic gneiss, and metatrondhjemite (Cook and Burnell 1986). This thrust sheet also includes the Dahlonega Gold Belt, which hosts several gold-bearing hydrothermal ore deposits and the source of historically productive gold mining operations (Peper et al. 1991). Though present prospects for gold occurrence are low, gold is detectable in very low concentrations in a few sediment samples throughout the region (Peper et al. 1991; Smith 2006). The Tallulah Falls thrust sheet consists of interlayered and folded metasedimentary and metaigneous rocks mostly of Late Proterozoic to early Paleozoic age

(Nelson 1989; Lesure et al. 1992), including metagraywacke, mica schist, amphibolite, aluminous schist, quartzite, biotite gneiss, biotite schist, quartzofeldspathic gneiss, amphibolite, and several types of granitoid rock (Nelson 1989).

Soque River Basin

The Soque River drains and area of 414.04 km^2 (USGS WBD 2017) and flows 47.3 km (USGS NHD 2017) to its confluence with the Chattahoochee River, which flows southwest ultimately to the Gulf of Mexico. The Soque River basin lies mostly within the Tallulah Falls thrust sheet, with headwater tributaries extending northward into rocks of the Helen and Richard Russel thrust sheets (***Figure 1-7***).

Upper Tugaloo River Basin

The Tugaloo River drains an area of 336.2 km^2 (USGS WBD 2017) and flows 102.0 km (USGS NHD 2017). The Upper Tugaloo River basin lies almost entirely within the Chauga-Walhalla thrust complex, a member of the Inner Piedmont thrust stack (Nelson et al.1987), as shown in ***Figure 1-7*** above. Within the Chauga-Walhalla complex are smaller thrust sheets separated by poorly defined thrust faults or slides (Lesure et al. 1992). The rocks of this thrust sheet consist of metasedimentary and metaigneous rock of Late Proterozoic to early Paleozoic age (Lesure et al. 1992). These include abundant amphibolite interlayered with quartzofeldspathic and micaceous gneiss and schist, metasandstone, metasiltstone, carbonate rocks, quartzite, phyllonitic schist, and pegmatite (Lesure et al. 1992).

1.2.3 Tallulah Gorge and Tallulah River Capture

Tallulah Gorge is located at the southeastern extent of the Tallulah River, where the Tallulah River joins the Chattooga River to form the Upper Tugaloo River. The gorge is steeply incised into the quartzite-schist member of the Tallulah Falls formation (Nelson 1989). Drainage networks and topographic patterns suggest that the Tallulah River once flowed into the Chattahoochee River and into the Gulf of Mexico and later was captured by the Upper Tugaloo River, channeling water eastward to the lower elevation Piedmont, into the Savannah River and the Atlantic Ocean (Johnson 1907). ***Figure 1-9*** shows a map of the study area with elevation and drainage patterns, present-day watersheds and the former course of the Tallulah River in relation to the BRE. The presence of isolated populations of fish and aquatic salamander species suggest that the Tallulah River and Chattahoochee River were once connected to allow species dispersal until the Tallulah River capture event established the modern drainage divides, separated the populations, and allowed the Tallulah populations to spread into the Savannah River (Voss et al. 1995; Jones et al. 2006). Through the study of genetic diversity and gene lineages in these populations across the presently disconnected basins, this capture event was constrained to as recently as the Pleistocene (Voss et al. 1995, Jones et al. 2006). During the capture period, the Upper Tugaloo River eroded headward and incised into the east-facing slope of the BRE until it eroded into the ancestral Tallulah drainage and channeled water down the steeper gradient (shorter river distance to base level) eastward to the lower elevation Piedmont, cutting off the Chattahoochee's former headwaters (Johnson 1907). This process is evident in the knickpoint at Tallulah Falls within Tallulah Gorge, where the river incises downward and erodes from the BRE headward up the Tallulah River as the Savannah River system moves toward equilibrium between its drainage area and elevation profile (Willett et al. 2014). The gorge incision represents the Tallulah River's readjustment to a new base level – from a local base level at the elevation of its former confluence with Deep Creek to its new local base level at the elevation of the Upper Tugaloo River (Johnson 1907; Willett et al. 2014). Because bedrock gorge incision rates and plateau dissection rates outpace plateau and lowland denudation rates at actively eroding escarpments (Nott e al. 1996; Prince et al. 2011), stream capture and gorge incision dates are necessary for a full understanding of escarpment retreat. However, erosion rates and exposure dating data have not conclusively identified the time of the Tallulah River capture or incision rate of Tallulah Gorge (Leigh et al. 2014).

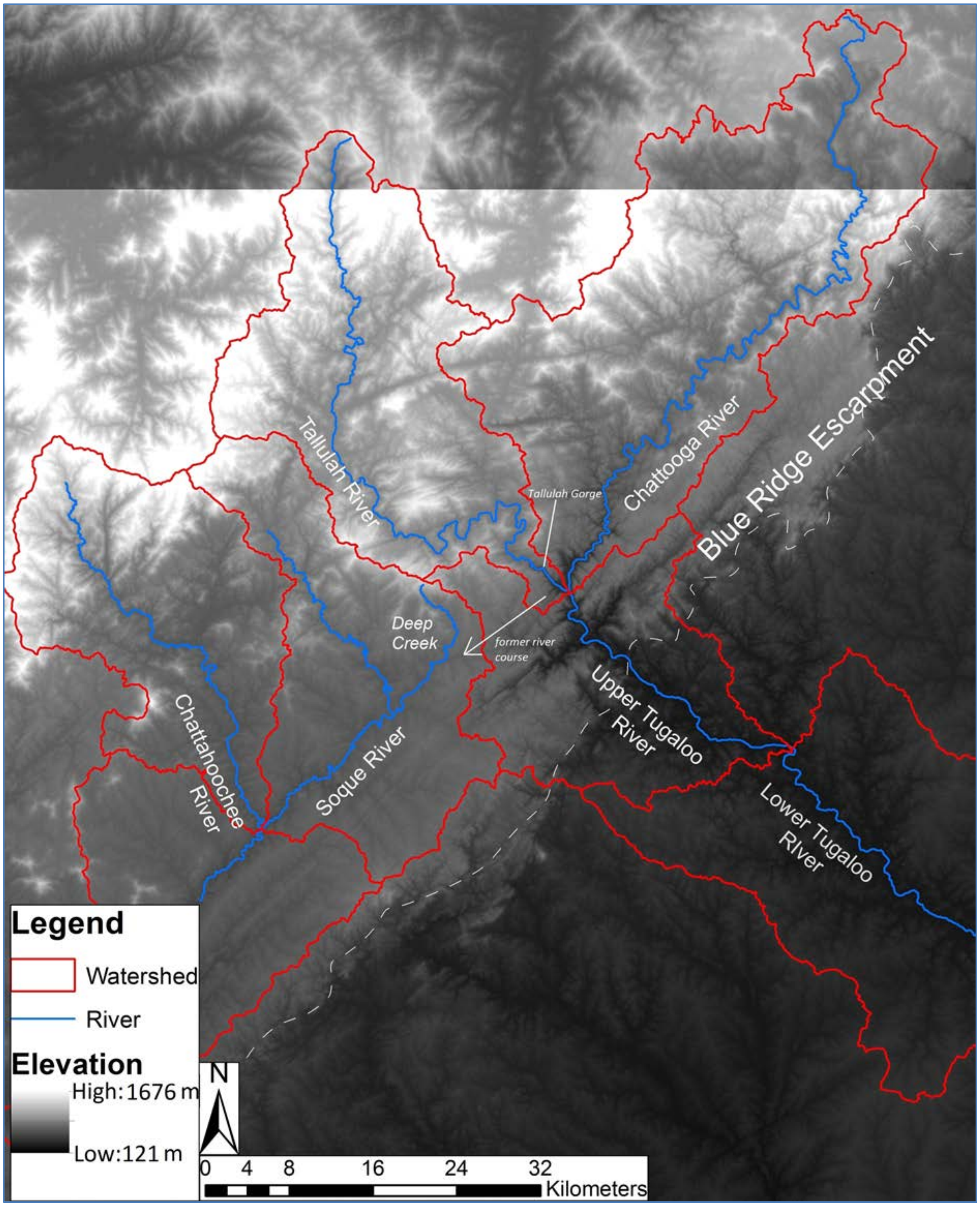

Figure 1-9 *Study area map with watershed boundaries and surface topography. The former course of the Tallulah and Chattooga Rivers entered the Chattahoochee watershed at Deep Creek.*

1.3 Research Objectives

Previous studies of river drainage and topographic patterns, along with biological and genetic evidence suggest that the Tallulah River was captured by the Tugaloo River possibly as recently as the Pleistocene. The purpose of this study is to employ geochemical and geospatial methodologies to both corroborate and refine the timescale of this capture event. The first step in dating the capture event is to establish sediment source fingerprints for the river basins involved in the capture. With those fingerprints established, future work can continue to identify stream sediment provenance in Tugaloo and Soque River floodplain deposits and date the stratigraphic layer where Tallulah sediment first appears in the Tugaloo basin and the layer where Tallulah sediment input ceases in the Soque basin.

This research will seek to answer the following questions: (1) What unique geochemical signatures exist between stream sediment derived from the Tallulah, Soque, and Upper Tugaloo River basins? (2) What differences in weathering extent exist between stream sediment in the Tallulah, Soque, and Upper Tugaloo Rivers? (3) What differences in erosive power and sediment mobility exist between the Tallulah, Soque, and Upper Tugaloo Rivers? (4) How can these differences be evaluated together to identify unique sediment source fingerprints?

To answer the above research questions, this research employed the following objectives: (1) Evaluate statistics of element concentrations in stream sediment samples previously collected by the United States Geological Survey (USGS) in order to identify unique geochemical signatures in stream sediment from the Tallulah, Soque, and Upper Tugaloo River basins. (2) Evaluate element concentrations in bedrock from the Tallulah River basin and determine characteristics of element enrichment/depletion in stream sediment samples relative to Tallulah basin parent rock in order to assess differences in the extent of weathering of stream sediment between the Tallulah, Soque, and Upper Tugaloo River basins. (3) Evaluate stream power from modern drainage network measurements in order to assess differences in sediment transport capacity between the Tallulah, Soque, and Upper Tugaloo River basins and how their relative capacities changed from pre-capture to post-capture conditions. (4) Combine and evaluate the distinct characteristics of the Tallulah, Soque, and Upper Tugaloo River basins to establish a unique sediment source fingerprint for each basin that can be used to identify where in the sedimentary record Tallulah sediment input begins in the Tugaloo River and where Tallulah sediment input ceases in the Soque River.

2 METHODS

2.1 Data Collection and Analyses

To identify distinguishing characteristics of sediment derived from the Tallulah River basin, a literature review was conducted to evaluate various resources from the USGS, including geologic maps, watershed boundary data, mineral resource evaluation papers, and geochemical databases.

2.1.1 Stream Sediment Samples

Stream sediment samples were collected by the USGS as part of the hydrogeochemical and stream sediment reconnaissance (HSSR) phase of the National Uranium Resource Evaluation (NURE) program and compiled into the NURE-HSSR database version 1.40 (Smith 2006), and the Rock Analysis Storage System (RASS) sediment database (USGS 2001). These databases include, among other data, mass concentration of 38 elements from stream sediment samples collected throughout the U.S.: Ag, Al, Au, Be, Ca, Ce, Co, Cr, Cu, Dy, Eu, F, Fe, Hf, K, La, Li, Lu, Mg, Mn, Mo, Na, Nb, Ni, P, Pb, Sc, Sm, Sr, Th, Ti, U, V, W, Y, Yb, and Zn. The majority of samples used in this study are from the NURE-HSSR database; the RASS database was used only for Ca concentrations because the NURE-HSSR program did not include Ca analyses. The NURE-HSSR samples were collected by USGS personnel between July 3 and August 9, 1976 and were analyzed by the U.S. Department of Energy (DOE) Savannah River Laboratory (Eastern Protocol) (SRL-E) between August 22 and September 6, 1977 [note: analysis dates missing from some samples]. The samples were collected from flowing stream channels, sieved to sample the <150 μm size fraction (clay to fine sand grain sizes) and dried at less than or equal to 110°C (Smith 2006). The geochemical data, available to the public (https://mrdata.usgs.gov/mrds) and accessible through mapping and database software, were separated based on present-day watershed boundaries of the USGS Hydrologic Unit Code (HUC) system. The HUC system divides U.S watersheds based on the hierarchical succession of tributaries and assigns each watershed a number based on which larger watersheds the river feeds into (USGS WBD 2017). For example, the two-digit HUC "03" represents the South Atlantic/Gulf Region; within the "03" HUC, the four-digit HUC "03 06" represents the Ogeechee-Savannah watershed; within the "0306" HUC, the six-digit HUC "0306 01" represents the Savannah River watershed; and within the "030601" HUC, the eight-digit HUC "030601 02" represents the Tugaloo River. This study focused on three 10-digit HUC watersheds: the Tallulah River (HUC 0306010201), Soque River (HUC 0313000102), and Upper Tugaloo River (HUC 0306010204). From the U.S. Department of Agriculture (USDA) Natural Resources Conservation Service Geospatial Gateway online national map interface (USDA 2017), an Area of Interest (AOI) was selected to include the study area. The 10-digit HUC Watershed Boundary Dataset (WBD) and the National Hydrography Dataset (NHD) map and database files were selected, and the data were downloaded, limited to data available within the geographic AOI boundaries. From the USGS Mineral Resource Data System (USGS MRDS 2017) online national map interface, an AOI was selected to include the study area and access the NURE-HSSR and RASS map and database files limited to the AOI. The NURE-HSSR database includes the eight-digit HUC for each sample location but does not specify further to the 10-digit HUC. The 10-digit HUC WBD map, the NURE-HSSE sample map, and the RASS sample map were compiled into a working study area map using ESRI ArcView GIS v. 10.1, and the samples were visually separated and identified based on 10-digit HUC watershed boundaries and individual sample identification numbers. The sample data were then compiled into separate databases for each river basin for statistical analysis.

2.1.2 Bedrock Samples

An analysis was conducted to evaluate the enrichment and depletion of certain elements from the weathering of parent rock to the deposition of stream sediment. Parent rock samples were collected by the USGS and analyzed for major element geochemistry as part of the National Geochemistry (NGC) Rock Database (USGS NGC 2008). The database includes, among other data, mass concentration of 11 major element oxides from in situ bedrock samples collected throughout the U.S.: SiO_2, Al_2O_3, Fe_2O_3, FeO, MgO, CaO, Na_2O, K_2O, TiO_2, P_2O_5, and MnO. The NGC rock samples were collected by USGS personnel from exposed bedrock at outcrops or road cuts and were analyzed by x-ray fluorescence (XRF) spectrometry or atomic absorption (AA) spectrometry between July 3, 1967 and August 6, 1988 (USGS NGC 2008). The data, available to the public (https://mrdata.usgs.gov/mrds) and accessible through mapping and database software, were separated to include only rock samples from the Tallulah River basin; there were insufficient rock samples from the Soque and Tugaloo basins to make statistical comparisons. From the USGS MRDS online interface (USGS MRDS 2017), an AOI was selected to include the study area and access the NGC map and database files limited to the AOI. The NGC sample map was added to the working study area map using ESRI ArcView GIS v. 10.1, and the samples were visually separated and identified based on 10-digit HUC Tallulah River watershed boundaries and individual sample identification numbers to construct a separate database for Tallulah River rock samples. These parent rock data were used for comparisons to stream sediment data from the HSSR-NURE and RASS databases.

2.2 Statistical Analyses

As part of the data formatting for this study, non-detection (ND) results for a particular element in a sample were adjusted to [0.5 x lowest element reading in dataset] or [0.5 x detection limit] (after Cannon & Horton 2009) using Microsoft Excel 2016 so that the sample would not be omitted from the sample means and statistical trend analyses. Elements with greater than 55% ND results were removed from consideration for use in sediment source fingerprinting. A frequency distribution analysis was conducted using IBM's SPSS Statistics 22 software for each analyzed element to determine its suitability for trend analysis. Ideal elements exhibit a normal distribution of concentrations across the basin to demonstrate that the number of samples is sufficiently large to represent the basin as a whole. An ideal normal distribution is evaluated as having a skewness value near zero and a kurtosis value less than three. Using the NURE-HSSE sampling data for 37 elements, a correlation matrix was developed for each river basin to determine which elements show strong positive or strong negative correlations, using

VassarStats (Lowery 2017). Only NURE-HSSE samples were used, because the concentrations represent the same set of individual samples; RASS samples were collected from different locations than the NURE-HSSE samples and were used in this study for Ca concentrations only, so Ca was not included in the correlation matrices. Difference of means tests were performed to determine the statistical significance of differences between mean element concentrations from each basin. The sample means and element correlations were used to determine a set of potential fingerprint ratios that could be used to distinguish between sediment source basins. Selected ratios were plotted for each basin to identify which could be used to best distinguish between the basins. Fingerprint ratios were selected for evaluation based on significant differences between the ratio values for each river basin, based on basin means and relative scatterplot trends.

2.3 Weathering Assessment

Calculation of enrichment factors (EF) and molar base metal-aluminum ratios (molar BA ratios) are two methods of assessing the extent of weathering along a weathering profile from in situ parent rock to soil (Ryan 2014; Birkeland 1999). EF values are used to quantify the relative enrichment or depletion of individual elements in weathered soil by comparing the concentration in soil to an initial concentration in the unweathered parent rock. Molar BA ratios compare relative enrichment or depletion of the four soluble/mobile base metal cations (Mg, Ca, Na, and K) normalized to the concentrations of insoluble/immobile Al. These methods were modified for this study by taking a basin-wide approach to assess general weathering trends from parent rock to stream sediment – where mean stream sediment and parent rock element concentrations were averaged over each studied river basin. With this method, extent of chemical weathering in stream sediment is used as a proxy for distance from sediment source to assess pre-capture and post-capture sediment transport distances, similar to the reasoning of Prince et al. (2010), who used the physical weathering signatures of clast roundness and sorting as proxies for fluvial transport distances.

EF was calculated for major elements Al, Fe, Mg, Ca, Na, K, Ti, P, and Mn using the following formula:

$$\mathbf{EF = [x]_{sed} / [x]_{rock}}$$

where $[x]_{sed}$ is the concentration (weight percent) of the mean element concentration in stream sediment, and $[x]_{rock}$ is the mean element concentration in parent rock. EF was calculated relative to Tallulah River basin bedrock samples. Molar BA ratios were calculated for sediment samples and rock samples as follows:

$$\mathbf{Molar\ BA\ Ratio = ([Mg] + [Ca] + [Na] + [K]) / [Al]}.$$

For each river basin, sediment to parent rock BA ratios were also calculated, as follows:

$$\mathbf{Sed\ to\ rock\ BA\ Ratio = BA_{sed} / BA_{rock}}.$$

2.4 Stream Power Assessment

Stream power and specific stream power reflect the potential energy released by the action of flowing water, and specific stream power has been shown to be proportional to sediment discharge rates (Bagnold 1966; Yang 1974). Specific stream power was assessed for this study to make generalized comparisons of the capacity for sediment transport between river basins both before and after the Tallulah River capture event. The stream power of each river was assessed based on publicly available data and measurements from the USGS and mapping software. Discharge measurements were taken from USGS stream gauges located as close as possible to the downstream extent of each river. Discharge measurements were compiled from the USGS Water Information System (WIS) for all years of available data to calculate a mean discharge (m^3/s) for the available measurement period for each river (USGS WIS 2017). The length of each river was gathered from the USGS NHD for each river. The slope of each river was calculated by measuring the elevation of the upstream extent of each river – using USGS hydrography and digital mapping software – and subtracting the provided elevation of the stream gauge. The channel width of each river was also measured at each stream gauge. After compiling these measurements for each river, each river's stream power and specific stream power were calculated. Additionally, stream power was estimated for the pre-capture ancestral Soque River using the combined length of the Tallulah River, the former course to Deep Creek, and the length of Soque River below the Deep Creek confluence together with the combined discharge of the Tallulah, Chattooga, and Soque Rivers. Stream power was estimated for the post-capture Tallulah-Tugaloo River system using the combined length of the Tallulah and Tugaloo Rivers together with discharge of the Tugaloo River (the Tugaloo River discharge already incorporates discharge from the Tallulah and Chattooga Rivers). By the nature of available data, stream power calculations refer to average conditions of late 20th to early 21st century for general comparative purposes between river basins only and may not reflect conditions of the past.

3 RESULTS

3.1 Data Collection and Analyses

3.1.1 Stream Sediment Samples

Stream sediment samples selected from the USGS HSSR-NURE database, version 1.40 (Smith 2006) and the RASS sediment database (USGS 2001) were separated based on present-day watershed boundaries of the 10-digit USGS HUC: the Tallulah River (HUC 0306010201), Soque River (HUC 0313000102), and Upper Tugaloo River (HUC 0306010204). The databases include mass concentration analyses of 38 elements from stream sediment samples across each river basin, with 70 samples within the Tallulah River basin, 65 samples within the Soque River basin, and 50 samples within the Upper Tugaloo River basin. ***Figure 3-1*** shows the locations of stream sediment samples within each river basin. ***Table 3-1*** includes the mean concentrations of 38 analyzed elements (with corrected ND values) from each of the three river basins.

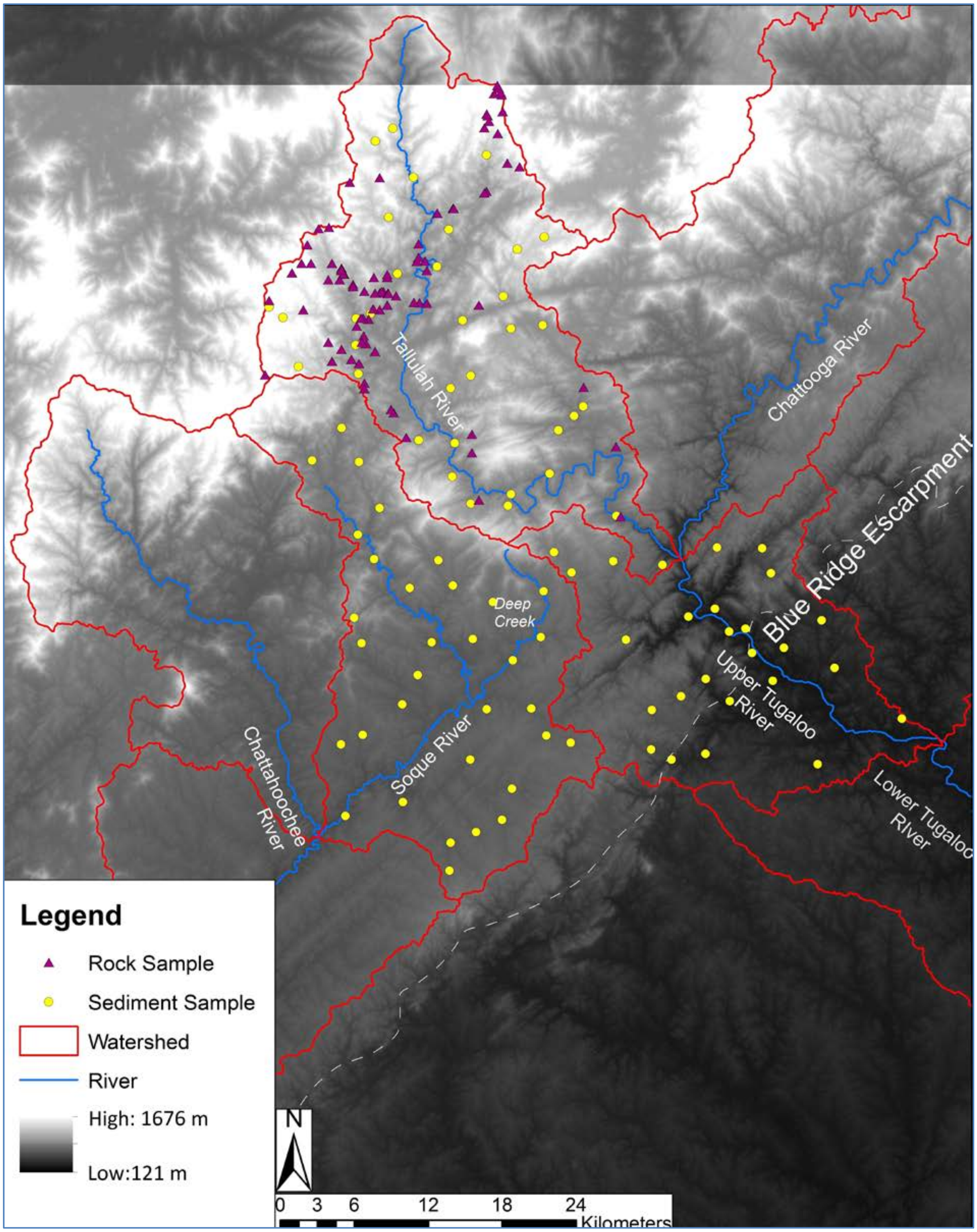

Figure 3-1 *Sample location map with watershed boundaries.*
Sample site elevations range from 480 m to 900 m in the Tallulah basin, 400 m to 520 m in the Soque basin, and 210 m to 480 m in the Upper Tugaloo basin.

***Table 3-1** – Geochemistry of Stream Sediment*

Geochemistry of Stream Sediment from Tallulah River, Soque River, and Upper Tugaloo River Watersheds
Data Source: USGS NURE Sediment Database

		Ag	std. dev.	Au	std. dev.	Be	std. dev.	Ce	std. dev.	Co	std. dev.	Cr	std. dev.
Mean Concentrations (mg/kg)	Tallulah (n = 70)	0.37	0.14	0.01	0.03	0.89	0.52	140	104	5.6	3.4	3.2	1.9
	Soque (n = 65)	0.28	0.098	0.03	0.1	0.78	0.38	468	616	3.7	2.1	7.6	5.0
	Tugaloo (n = 50)	0.25	0.00	0.01	0.01	0.80	0.40	166	336	5.2	4.3	3.3	2.0
		Cu	std. dev.	Dy	std. dev.	Eu	std. dev.	F	std. dev.	Hf	std. dev.	La	std. dev.
	Tallulah (n = 70)	7.5	4.9	14.4	8.0	2.4	3.1	200	300	62.8	56.2	77	60
	Soque (n = 65)	6.9	5.9	36.0	34.5	3.9	5.1	190	310	147	159	260	360
	Tugaloo (n = 50)	6.7	5.1	16.5	19.4	1.7	3.1	150	110	75.3	117	87	150
		Li	std. dev.	Lu	std. dev.	Mo	std. dev.	Nb	std. dev.	Ni	std. dev.	Pb	std. dev.
	Tallulah (n = 70)	4.4	2.1	2.5	2.1	2.5	0.0	14	8.8	7.0	4.4	9.3	3.4
	Soque (n = 65)	6.3	2.5	4.7	4.4	2.7	0.75	17	15	5.2	4.0	6.3	2.8
	Tugaloo (n = 50)	6.4	4.0	2.3	2.3	2.5	0.0	10	10	4.8	3.0	7.0	3.9
		Sc	std. dev.	Sm	std. dev.	Sn	std. dev.	Sr	std. dev.	Th	std. dev.	U	std. dev.
	Tallulah (n = 70)	9.13	5.19	14	10	8.9	6.8	32	27	21	15	7.14	4.01
	Soque (n = 65)	8.02	4.23	78	210	8.1	5.0	26	4.7	75	100	18.8	17.2
	Tugaloo (n = 50)	12.9	7.81	34	87	20	12	26	6.3	24	45	7.99	6.35
		V	std. dev.	W	std. dev.	Y	std. dev.	Yb	std. dev.	Zn	std. dev.		
	Tallulah (n = 70)	150	200	1.1	0.37	18	4.9	10.0	4.87	30	12		
	Soque (n = 65)	93	66	1.1	0.35	64	63	18.9	14.9	23	11		
	Tugaloo (n = 50)	83	53	1.2	0.82	25	26	11.1	10.9	24	13		
		Al	std. dev.	Ca*	std. dev.	Fe	std. dev.	K	std. dev.	Mg	std. dev.	Mn	std. dev.
Major Element Mean Concentrations (wt. %)	Tallulah (n = 70)	7.09	2.16	0.501		3.87	3.32	1.60	0.888	0.241	0.133	0.121	0.0670
	Soque (n = 65)	5.11	1.94	0.297		2.86	1.54	1.25	0.657	0.195	0.112	0.119	0.0846
	Tugaloo (n = 50)	5.32	1.81	0.666		2.34	1.39	1.01	0.426	0.215	0.0818	0.0969	0.0480
		Na	std. dev.	P	std. dev.	Ti	std. dev.						
	Tallulah (n = 70)	0.906	0.498	0.0677	0.0402	2.04	1.65						
	Soque (n = 65)	0.516	0.246	0.130	0.0537	2.16	1.68						
	Tugaloo (n = 50)	1.02	0.647	0.0517	0.0300	0.957	0.966						

Watershed boundaries based on USGS 10-digit HUC
Includes adjusted Non-Detect values in calculations
*Ca values from USGS RASS sediment database samples

3.1.2 Bedrock Samples

Bedrock samples from the Tallulah River basin were selected from the USGS NGC Rock Database (USGS 2008), as shown in ***Figure 3-2***. These 36 parent rock samples were analyzed for major element geochemistry for comparison to stream sediment concentrations in the three river basins. ***Table 3-2*** includes the mean sample concentrations of 11 major element oxides from the bedrock samples.

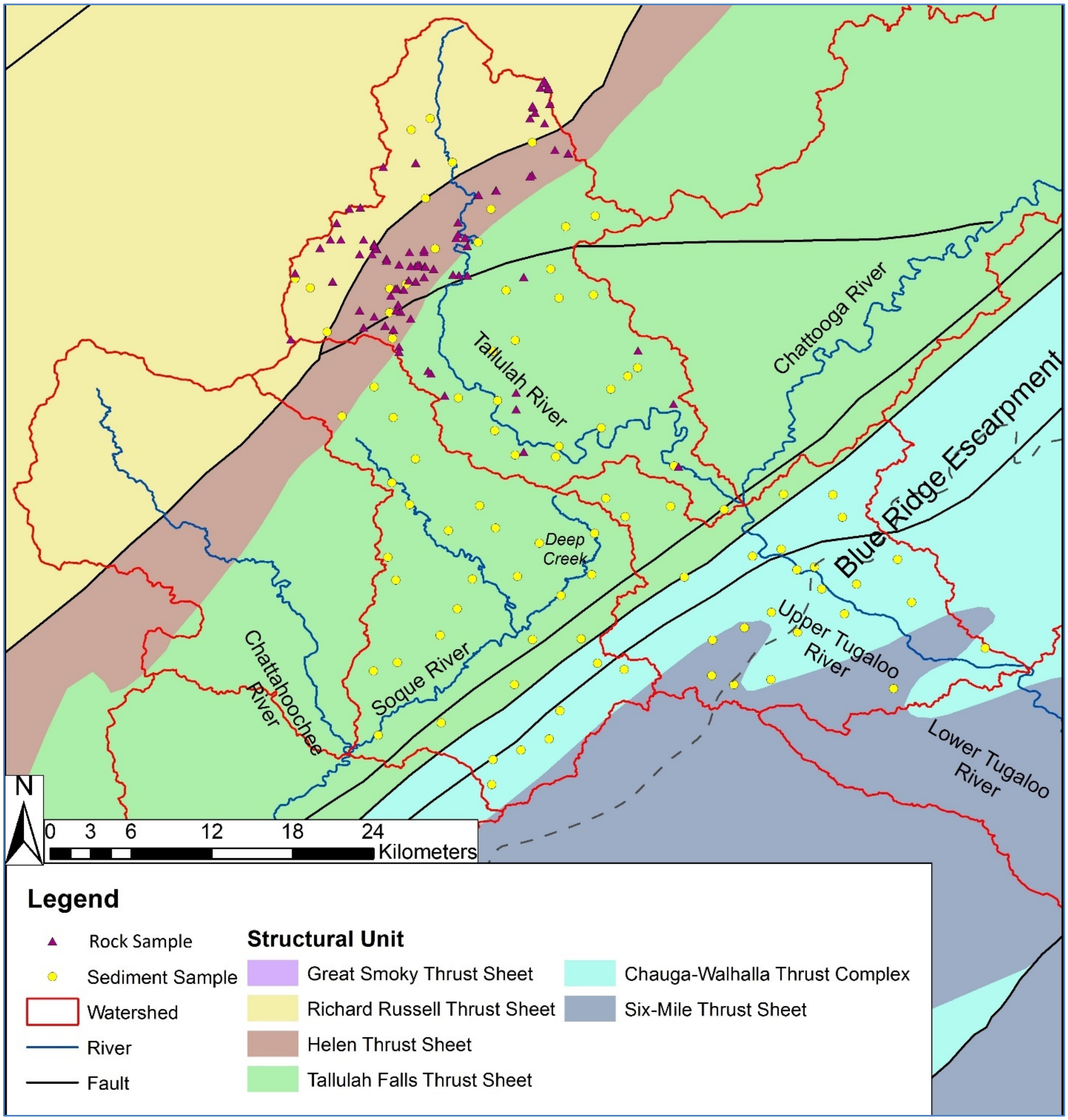

***Figure 3-2** Sample location map with structural geologic units*

***Table 3-2** – Geochemistry of Bedrock*

Geochemistry of Bedrock Samples from Tallulah River Watershed Data Source: USGS NGC Rock database													
Mean Concentrations (wt. %)		SiO2	std. dev.	Al2O3	std. dev.	Fe2O3	std. dev.	FeO	std. dev.	MgO	std. dev.	CaO	std. dev.
	Tallulah (n = 36)	50.3	10.090	13.8	5.16	7.98	4.61	7.66	3.21	10.9	11.8	7.41	4.21
		Na2O	std. dev.	K2O	std. dev.	TiO2	std. dev.	P2O5	std. dev.	MnO	std. dev.	LOI	std. dev.
	Tallulah (n = 36)	1.57	0.912	0.522	0.730	0.918	0.851	0.109	0.0581	0.172	0.0510	1.62	2.18
	Watershed boundary based on USGS 10-digit HUC Includes adjusted Non-Detect values in calculations LOI = loss on ignition												

3.2 Statistical Analyses

The mean element concentrations for sediment samples from each river basin are summarized in ***Table 3-1*** above, including ND adjustments. A frequency distribution analysis was conducted for each analyzed element to determine its suitability for trend analysis. Elements with greater than 55% ND results were removed from consideration for use in sediment source fingerprinting. **Appendix A** includes sample statistics for the entire dataset and for each subset of river basin samples. **Appendix B** includes the correlation matrices for samples from each river basin based on NURE-HSSR samples. ***Table 3-3*** summarizes the strongest correlations (R>0.800; R<-0.600) of element concentrations for each of the three river basins. REE such as Ce have a strong positive correlation with other REE and metals such as Cu, Ni, Zn, and Th. Other REEs such Lu have a strong negative correlation with alkali/alkaline earth elements such as Mg, Na, K, Be as well as the metals Zn and Pb. However, each river basin displayed a unique assemblage of strongest and weakest correlations. A t-test was performed to determine the statistical significance of differences between mean element concentrations from each basin. A summary of t-test results is included in ***Table 3-4*** through ***Table 3-6***, calculated for a one-tailed 95% confidence interval. Significant differences appear in the means of the nine analyzed REE: Ce, Dy, Eu, La, Lu, Sc, Sm, Y, and Yb. Significant differences also appear between mean U concentrations, mean Fe, Co, Cu concentrations, mean P, mean Sn, and mean Th concentrations. **Appendix C** includes histograms of the REE concentrations. The Tallulah River basin sediment exhibited a relative enrichment in Al, Cu, Pb, Sr, and V. The Soque River basin sediment exhibited a relative enrichment in U, Th, Hf, and the REE Ce, Dy, Eu, La, Lu, Sm. The Upper Tugaloo River basin sediment exhibited a relative enrichment of the REE Sc and depletion in Ti. The sample means and element correlations were used to determine a set of potential fingerprint ratios that could be used to distinguish between sediment source basins. These preliminary ratios are summarized in ***Table 3-7*** and include Ti/mean REE, U/mean REE, Lu/Zn, U/Ti, U/Th, and U/Pb. In addition to these element ratios, several individual REE ratios and REE/Ti ratios were plotted, as shown in ***Figure 3-3*** through ***Figure 3-22***, to identify patterns which could be used to best distinguish between the basins. These plots are meant to visualize distinctive patterns, such as relative trendline slope (e.g. Tugaloo slope > Soque slope), basin clusters (where data from one basin plots in a different x,y range than others), and strength of correlation (e.g. Tugaloo R value >> Tallulah or Soque R values). Major elements were omitted from consideration for sediment source fingerprinting due to their susceptibility to post-depositional weathering reactions.

***Table 3-3** – Stream Sediment Element Correlations*

Tallulah

Correlation	R	p (1-tailed)	N
Cu : mean Co, Ni,	0.975	0.000	35
Co : mean Co, Ni,	0.941	0.000	35
Cu : Ni	0.920	0.000	35
Ce : Sm	0.902	0.000	70
Th : mean REE	0.884	0.000	70
Hf : U/Pb	0.881	0.000	35
Fe : V	0.880	0.000	70
La : Th	0.880	0.000	70
Ce : La	0.879	0.000	70
Co : Cu	0.878	0.000	35
Ce : Th	0.868	0.000	70
Co : Ni	0.863	0.000	35
Eu : Eu/Ti	0.861	0.000	63
La : Sm	0.854	0.000	70
Cu : mean Cu, Pb,	0.848	0.000	35
Th : light REE	0.848	0.000	70
Mn : Ti	0.845	0.000	69
Sm : Th	0.835	0.000	70
U : U/Pb	0.824	0.000	35
U : La	0.815	0.000	70
Ti : V	0.806	0.000	69
Co : mean Cu, Pb,	0.803	0.000	35
Cu : Zn	0.760	0.000	35
Ce : Ce/Ti	0.736	0.000	69
Cu : Sc	0.715	0.000	35
K : mean Cu, Pb, Zn	-0.614	0.000	35
Cu : K	-0.704	0.000	35
K : mean Co, Ni, Cu	-0.714	0.000	35
K : Ni	-0.734	0.000	35
K : Sc	-0.742	0.000	35

Soque

Correlation	R	p (1-tailed)	N
Ce : Th	0.990	0.000	64
Ce : La	0.988	0.000	65
Th : mean REE	0.987	0.000	64
La : Th	0.983	0.000	64
Th : light REE	0.967	0.000	64
Th : heavy REE	0.964	0.000	64
Sm : Th	0.950	0.000	64
Mn : Ti	0.945	0.000	65
Mn : mean Al, Fe, Ti	0.945	0.000	65
La : Sm	0.934	0.000	65
Ce : Sm	0.933	0.000	65
U : La	0.917	0.000	65
U : mean REE	0.917	0.000	65
U : light REE	0.913	0.000	65
U : Dy	0.908	0.000	65
Dy : Y	0.904	0.000	32
U : Ce	0.901	0.000	65
U : heavy REE	0.896	0.000	65
U : Th	0.889	0.000	64
Cu : Zn	0.884	0.000	32
Zn : mean Co, Ni, Cu	0.879	0.000	32
La/Lu : Sm/Yb	0.876	0.000	65
Au : heavy REE	0.869	0.000	32
La/Lu : Ce/Yb	0.866	0.000	65
Dy : La	0.864	0.000	65
Th : Sm/Ti	0.859	0.000	64
Ce : Dy	0.852	0.000	65
Au : Sm	0.850	0.000	32
Th : La/Ti	0.849	0.000	64
Sm/Yb : Ce/Ti	0.844	0.000	65
Sm/Yb : La/Ti	0.843	0.000	65
Au : mean REE	0.842	0.000	32
U : Sm	0.840	0.000	65
Dy : Yb	0.838	0.000	65
Al : Zn	0.834	0.000	32
Ce/Lu : Sm/Yb	0.833	0.000	65
Ce : La/Ti	0.832	0.000	65
Dy : Th	0.832	0.000	64
Th : Ce/Ti	0.829	0.000	64
Ag : mean Co, Ni, Cu	0.827	0.000	32
Au : light REEE	0.821	0.000	32
Cu : Ni	0.821	0.000	32
Au : Ce	0.820	0.000	32
Ce : Sm/Ti	0.819	0.000	65
Au : La	0.818	0.000	32
Au : Th	0.816	0.000	31
Co : mean Cu, Pb, Zn	0.814	0.000	32
La : Sm/Ti	0.813	0.000	65
Hf : Ti	0.812	0.000	65
Hf : mean Al, Fe, Ti	0.812	0.000	65
Lu : Yb	0.809	0.000	65
Ce/Lu : La/Yb	0.809	0.000	65
U : Yb	0.806	0.000	65
Y : Yb	0.806	0.000	32
Co : Cu	0.801	0.000	32
U/Pb : Sc/Ti	-0.612	0.000	32
U/Th : Ce/Ti	-0.627	0.000	64

Tugaloo

Correlation	R	p (1-tailed)	N
Ce : Th	0.994	0.000	48
Th : mean REE	0.989	0.000	48
Ce : La	0.983	0.000	43
La : Th	0.982	0.000	43
Th : light REEE	0.974	0.000	48
Th : heavy REE	0.966	0.000	48
Ce : Sm	0.951	0.000	43
Sm : Th	0.948	0.000	43
La : Sm	0.926	0.000	43
Eu : Sm	0.921	0.000	43
Eu : Th	0.917	0.000	47
Sr : Sc/Ti	0.916	0.000	23
Ce : Eu	0.909	0.000	47
U : Th	0.894	0.000	48
Eu : Sm/Yb	0.887	0.000	40
U : Ce	0.886	0.000	48
Zn : mean Co, Ni, Cu	0.885	0.000	24
U : La	0.883	0.000	43
Eu : La	0.882	0.000	43
Co : mean Cu, Pb, Zn	0.881	0.000	24
Ce : Dy	0.880	0.000	47
Co : Zn	0.880	0.000	24
Dy : Th	0.878	0.000	47
Th : Sm/Yb	0.871	0.000	40
Ce : Sm/Yb	0.857	0.000	40
Dy : La	0.849	0.000	42
Co : Ni	0.848	0.000	24
Cu : Ni	0.843	0.000	24
Cu : Zn	0.842	0.000	24
La : Sm/Yb	0.834	0.000	40
U : Yb	0.830	0.000	42
Sr : Y/Ti	0.830	0.000	23
U : Eu	0.817	0.000	47
Co : Cu	0.802	0.000	24
Cu : Pb	0.800	0.000	24
Na : Nb	-0.633	0.000	24

***Table 3-4** – T-test results for Tallulah-Tugaloo comparisons*
Selected elements for which the most significant differences are observed between basins ($p < 0.05$)

Tallulah (1) > Tugaloo (2)				
Element	t	df	Critical value	p-value (1-tailed)
Ag	5.191	34.000	2.03	0.000
Al	4.853	115.014	1.98	0.000
Fe	3.445	99.351	1.98	0.000
K	3.388	52.013	2.01	0.001
Li	-2.209	31.649	2.04	0.017
Mn	2.247	117.996	1.98	0.013
Ni	2.358	56.990	2	0.011
P	1.753	56.530	2	0.043
Pb	2.422	44.226	2.01	0.010
Sc	-2.978	79.149	1.99	0.002
Sn	-4.15	33.834	2.03	0.000
Ti	4.434	112.033	1.98	0.000
V	2.839	82.577	1.99	0.003
Zn	1.954	46.788	2.01	0.028
Ti / 9REE	2.772	100.948	1.98	0.003
U / 9REE	-2.207	62.424	2	0.016
Co / Fe	-1.73	33.575	2.03	0.046
Cu / Fe	-1.808	31.511	2.04	0.040
Mean_Fe_Co_Cu_ppm	3.076	101.891	1.98	0.001
U / Ti	-4.544	53.417	2	0.000
Mean Cu, Pb, Zn	1.864	45.324	2.01	0.034
Mean Al, Fe, Ti	4.48	13.696	2.16	0.000
Sc/Ti	-3.327	47.161	2.01	0.001
Y/Ti	-2.593	22.603	2.07	0.008
La/Ti	-2.63	57.770	2	0.005
Ce/Ti	-2.429	58.335	2	0.009
Sm/Ti	-2.036	42.982	2.02	0.024
Dy/Ti	-4.071	56.384	2	0.000
Yb/Ti	-3.847	42.796	2.02	0.000
Lu/Ti	-3.561	54.724	2	0.000

H0 = No difference in samples from Basin 1 and Basin 2
H1 = Basin 1 sample concentrations > Basin 2 sample concentrations
H1 confirmed with 95% confidence for the element concentrations showr
($p < 0.05$, 1-tailed)

***Table 3-5** – T-test results for Tallulah-Soque comparisons*
Selected elements for which the most significant differences are observed between basins ($p < 0.05$)

Tallulah (1) > Soque (2)				
Element	t	df	Critical value	p-value (1-tailed)
U	-5.347	70.450	1.99	0.000
Ag	3.123	61.668	2	0.001
Al	5.584	132.849	1.98	0.000
Ce	-4.244	67.374	1.99	0.000
Co	2.739	56.889	2	0.004
Cr	-4.659	37.664	2.02	0.000
Dy	-4.943	70.329	1.99	0.000
Eu	-2.011	103.023	1.98	0.023
Fe	2.287	99.081	1.98	0.012
Hf	-4.036	78.699	1.99	0.000
K	1.838	62.117	2	0.035
La	-3.971	67.249	1.99	0.000
Li	-3.371	59.190	2	0.001
Lu	-3.657	88.952	1.99	0.000
Na	4.445	50.641	2.01	0.000
Ni	1.817	64.989	2	0.037
P	-5.306	55.203	2	0.000
Pb	4.08	64.619	2	0.000
Sm	-2.511	64.308	2	0.007
Th	-4.135	65.389	2	0.000
V	2.413	85.575	1.99	0.009
Y	-4.115	32.409	2.04	0.000
Yb	-4.554	76.903	1.99	0.000
Zn	2.667	64.891	2	0.005
Mean 9REE	-4.068	66.754	1.99	0.000
Ti / 9REE	3.779	76.320	1.99	0.000
U / 9REE	1.703	126.995	1.98	0.045
Zn / 9REE	4.36	54.261	2	0.000
Mean_Fe_Co_Cu_ppm	1.999	103.090	1.98	0.024
U / Ti	-5.568	113.442	1.98	0.000
U / Th	2.844	87.140	1.99	0.003
U / Pb	-5.62	38.219	2.02	0.000
Heavy REE	-3.224	65.097	2	0.001
Light REE	-4.212	67.131	2	0.000
Lu/Zn	-2.937	35.277	2.02	0.003
Mean Cu, Pb, Zn	2.523	64.424	2	0.007
Ce/Lu	-1.866	123.459	1.98	0.032
La/Yb	-2.939	16.202	2.12	0.002
La/Lu	-1.841	116.127	1.98	0.034
Sm/Yb	-3.256	81.150	1.99	0.001
Ce/Yb	-2.757	126.808	1.98	0.003
Y/Ti	-3.393	35.041	2.03	0.001
La/Ti	-4.305	100.143	1.98	0.000
Ce/Ti	-4.375	99.308	1.98	0.000
Sm/Ti	-3.215	67.692	2	0.001
Dy/Ti	-3.726	97.766	1.98	0.000
Yb/Ti	-4.397	105.451	1.98	0.000
Lu/Ti	-3.132	114.895	1.98	0.001

H0 = No difference in samples from Basin 1 and Basin 2
H1 = Basin 1 sample concentrations > Basin 2 sample concentrations
H1 confirmed with 95% confidence for the element concentrations shown ($p < 0.05$, 1-tailed)

***Table 3-6** – T-test results for Soque-Tugaloo comparisons*
Selected elements for which the most significant differences are observed between basins ($p < 0.05$)

Soque (1) > Tugaloo (2)				
Element	t	df	critical value	p-value (1-tailed)
U	4.683	85.156	1.99	0.000
Ag	1.709	31.000	2.04	0.049
Ce	3.336	103.251	1.98	0.001
Cr	4.317	41.996	2.02	0.000
Dy	3.832	104.611	1.98	0.000
Eu	2.889	104.484	1.98	0.002
Fe	1.891	106.559	1.98	0.031
Hf	2.78	112.814	1.98	0.003
La	3.381	91.937	1.99	0.001
Lu	3.705	100.443	1.98	0.000
Mn	1.792	104.821	1.98	0.038
Na	-3.7	29.443	2.04	0.000
Nb	2.219	52.798	2.01	0.015
P	6.884	48.752	2.01	0.000
Sc	-3.988	70.858	1.99	0.000
Sn	-4.631	29.519	2.04	0.000
Th	3.512	90.998	1.99	0.000
Ti	4.816	105.474	1.98	0.000
Y	3.138	43.820	2.02	0.002
Yb	3.126	103.293	1.98	0.001
Mean 9REE	3.367	96.115	1.99	0.001
U / 9REE	-3.025	56.954	2	0.002
Zn / 9REE	-3.536	29.759	2.04	0.001
Co / Fe	-2.534	31.454	2.04	0.008
Mean_Fe_Co_Cu_ppm	1.66	107.289	1.98	0.050
U / Ti	-1.964	61.030	2	0.027
U / Th	-4.454	56.680	2	0.000
U / Pb	4.857	40.760	2.02	0.000
Heavy REE	2.396	93.557	1.99	0.009
Light REE	3.538	96.683	1.99	0.000
Lu/Zn	2.743	36.067	2.04	0.005
Mean Al, Fe, Ti	4.97	105.315	1.98	0.000
La/Yb	2.442	9.938	2.23	0.008
Sm/Yb	2.388	102.95	1.98	0.009
Ce/Yb	2.242	96.289	1.98	0.014
Sc/Ti	-3.403	47.148	2.01	0.001
Yb/Ti	-2.222	47.743	2.01	0.016
Lu/Ti	-1.755	65.190	2	0.042

H0 = No difference in samples from Basin 1 and Basin 2
H1 = Basin 1 sample concentrations > Basin 2 sample concentrations
H1 confirmed with 95% confidence for the element concentrations showr
($p < 0.05$, 1-tailed)

***Table 3-7** – Preliminary Sediment Fingerprint Ratios*

Fingerprint Ratios	Tallulah	Soque	Tugaloo
mean 9 REE	31.85	104.3	39.60
Ti / 9 REE	639.0	207.2	241.7
U / 9 REE	0.2241	0.1805	0.2017
Co / Fe	0.0001452	0.0001300	0.0002229
Cu / Fe	0.0001943	0.0002425	0.0002853
Lu / Zn	0.08363	0.1201	0.1292
mean Fe,Co,Cu	12895	9539	7792
U / Ti	0.0003506	0.0008712	0.0008344
U / Th	0.3377	0.2514	0.3291
U / Pb	0.7638	3.014	1.148
Pb / Zn	0.3070	0.2743	0.2914
Mean Co, Ni, Cu	6.719	5.276	5.549
Mean Al, Fe, Ti	43300	33780	28709
Ce/Lu	56.21	99.70	71.77
La/Yb	7.629	13.63	7.855
La/Lu	30.76	54.84	37.47
Sm/Yb	1.426	4.146	3.062
Ce/Yb	13.94	24.78	15.04
Sc/Ti	0.0004486	0.0003711	0.0013476
Y/Ti	0.0008634	0.002941	0.002620
La/Ti	0.003760	0.01191	0.009069
Ce/Ti	0.006870	0.02165	0.01737
Sm/Ti	0.0007027	0.003622	0.003535
Eu/Ti	0.0001195	0.0001824	0.0001746
Dy/Ti	0.0007057	0.001665	0.001720
Yb/Ti	0.0004928	0.0008736	0.0011545
Lu/Ti	0.0001222	0.0002172	0.0002420

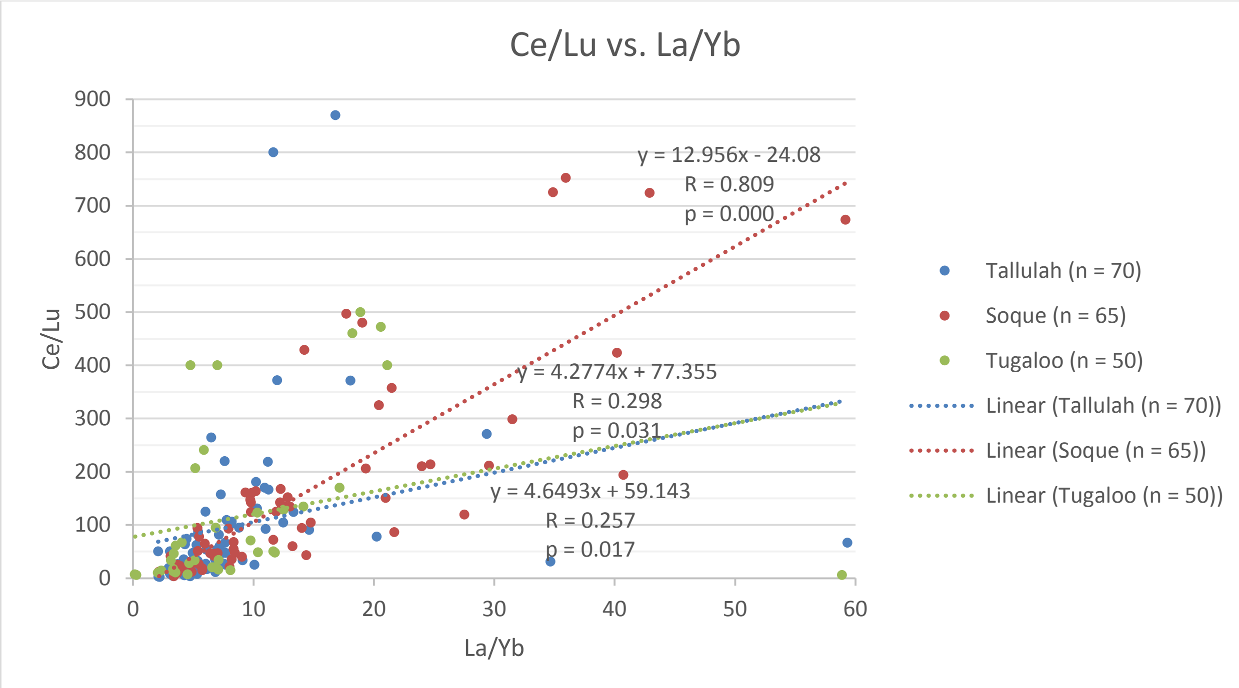

Figure 3-3 *Ce/Lu vs. La/Yb by River Basin*

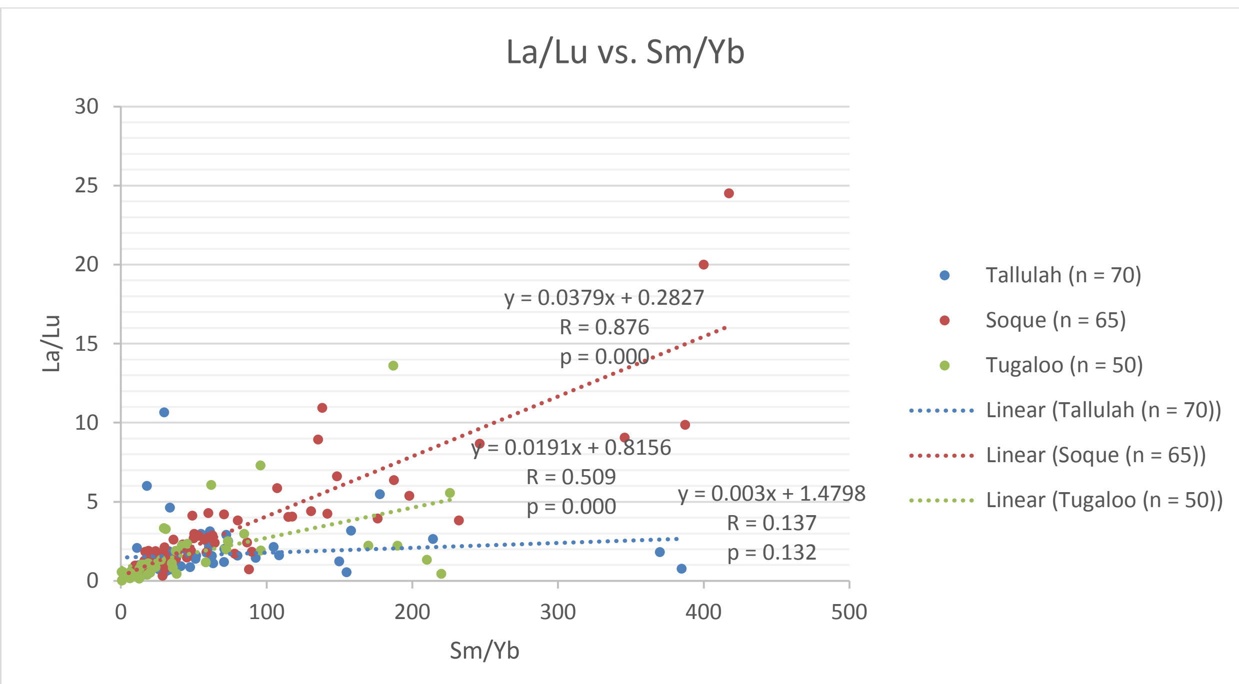

Figure 3-4 *La/Lu vs. Sm/Yb by River Basin*

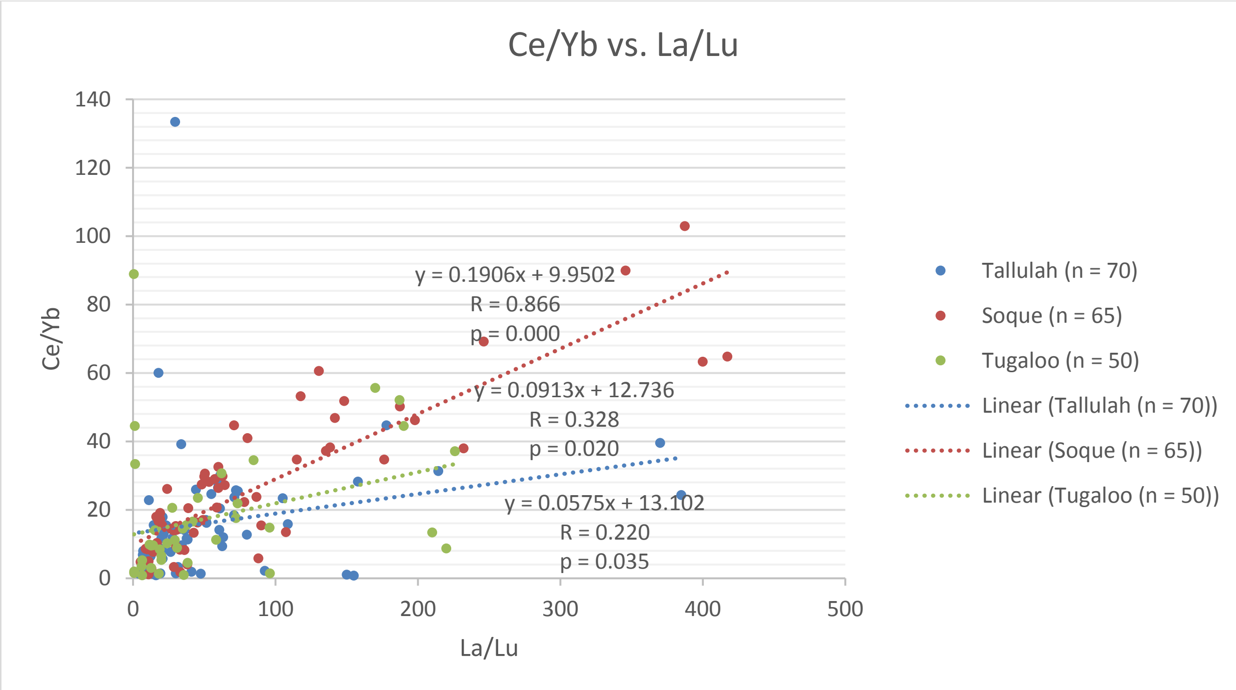

Figure 3-5 *Ce/Yb vs. La/Lu by River Basin*

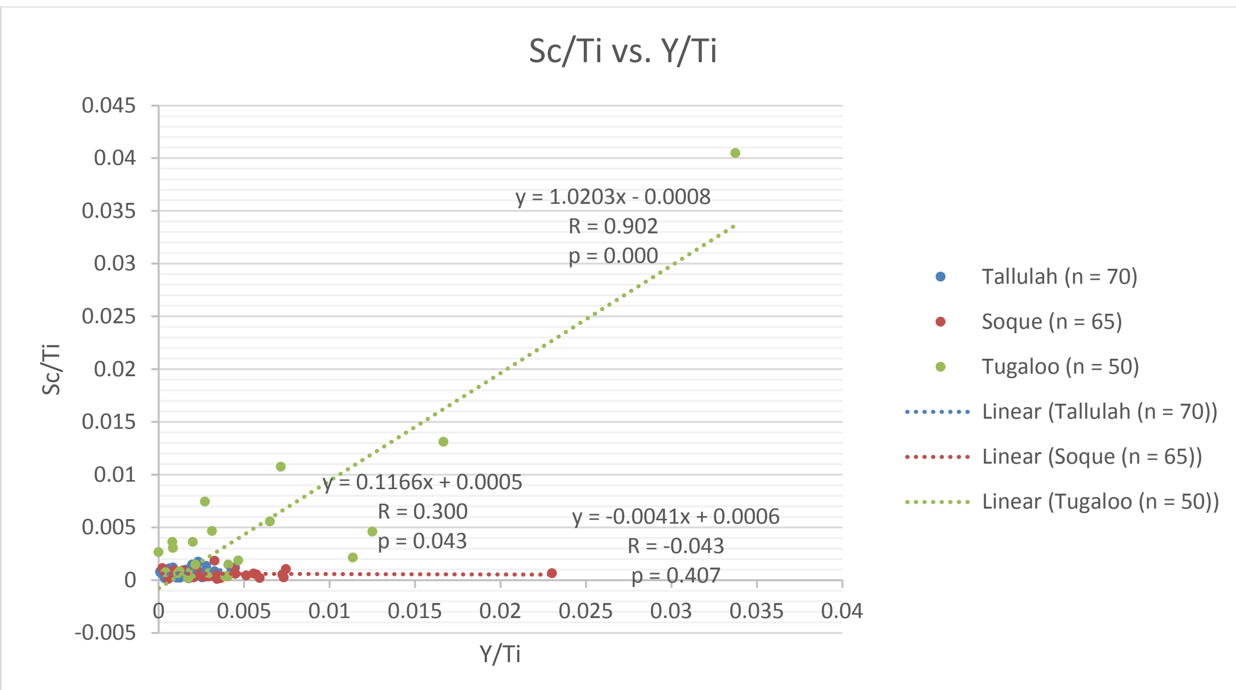

Figure 3-6 *Sc/Ti vs. Y/Ti by River Basin*

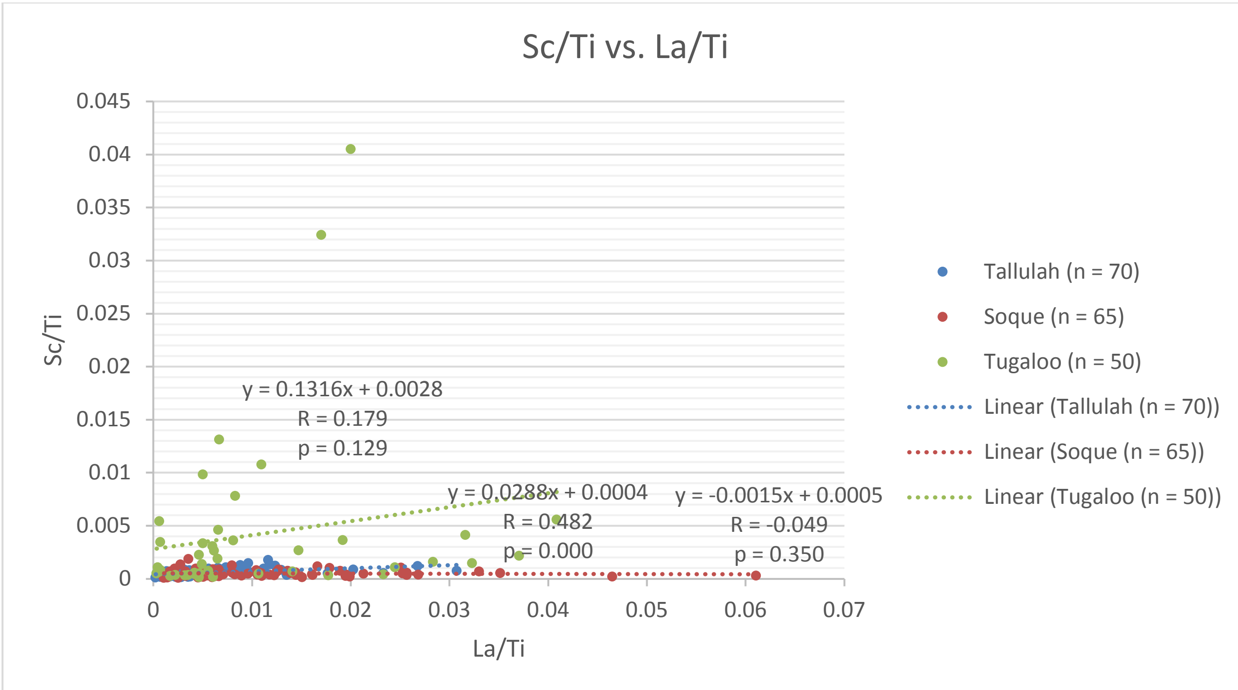

Figure 3-7 *Sc/Ti vs. La/Ti by River Basin*

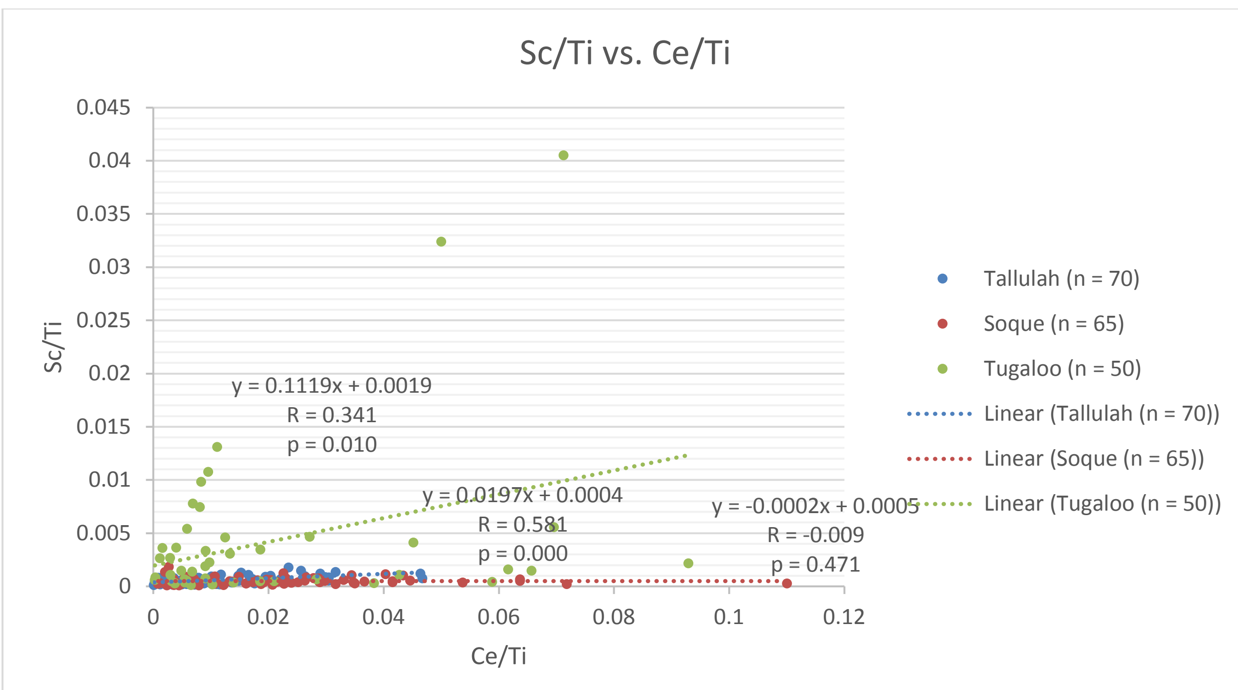

Figure 3-8 *Sc/Ti vs. Ce/Ti by River Basin*

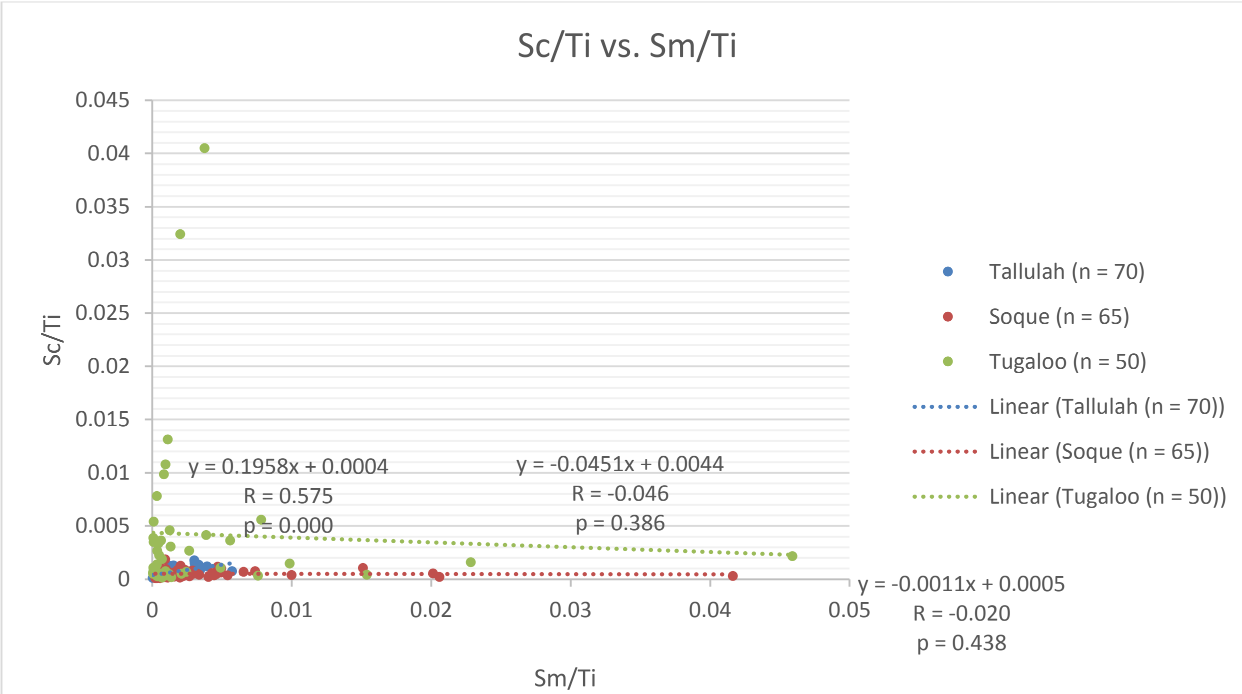

Figure 3-9 *Sc/Ti vs. Sm/Ti by River Basin*

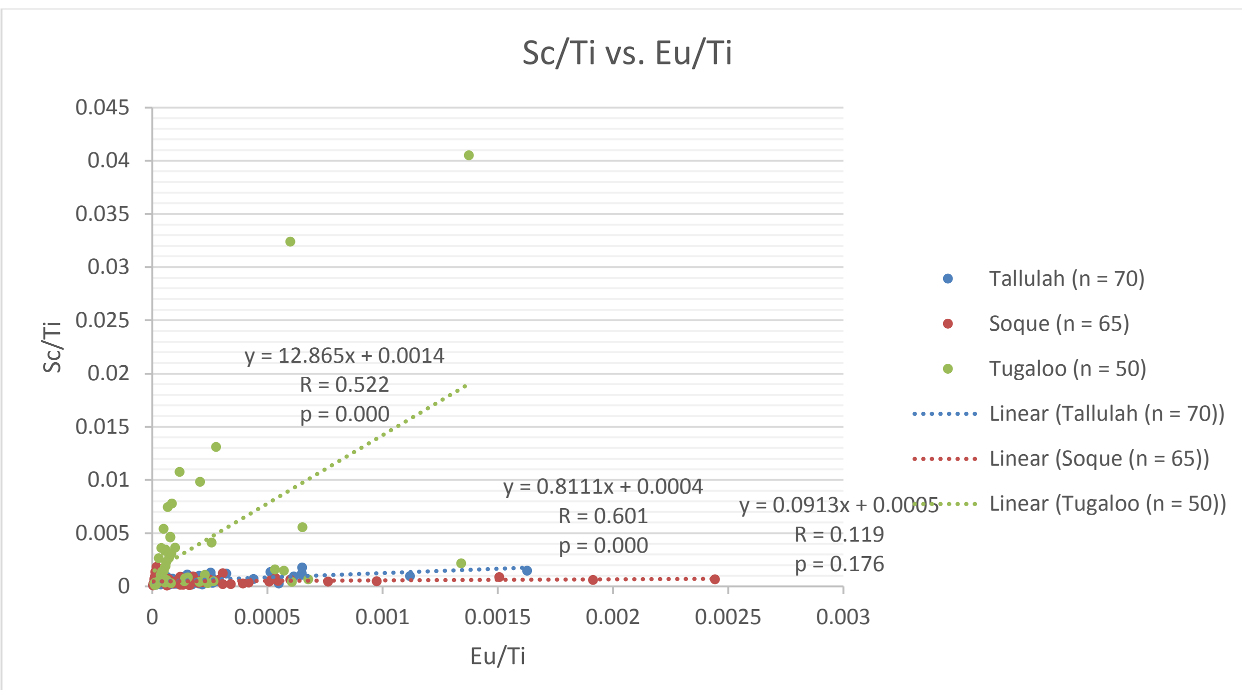

Figure 3-10 *Sc/Ti vs. Eu/Ti by River Basin*

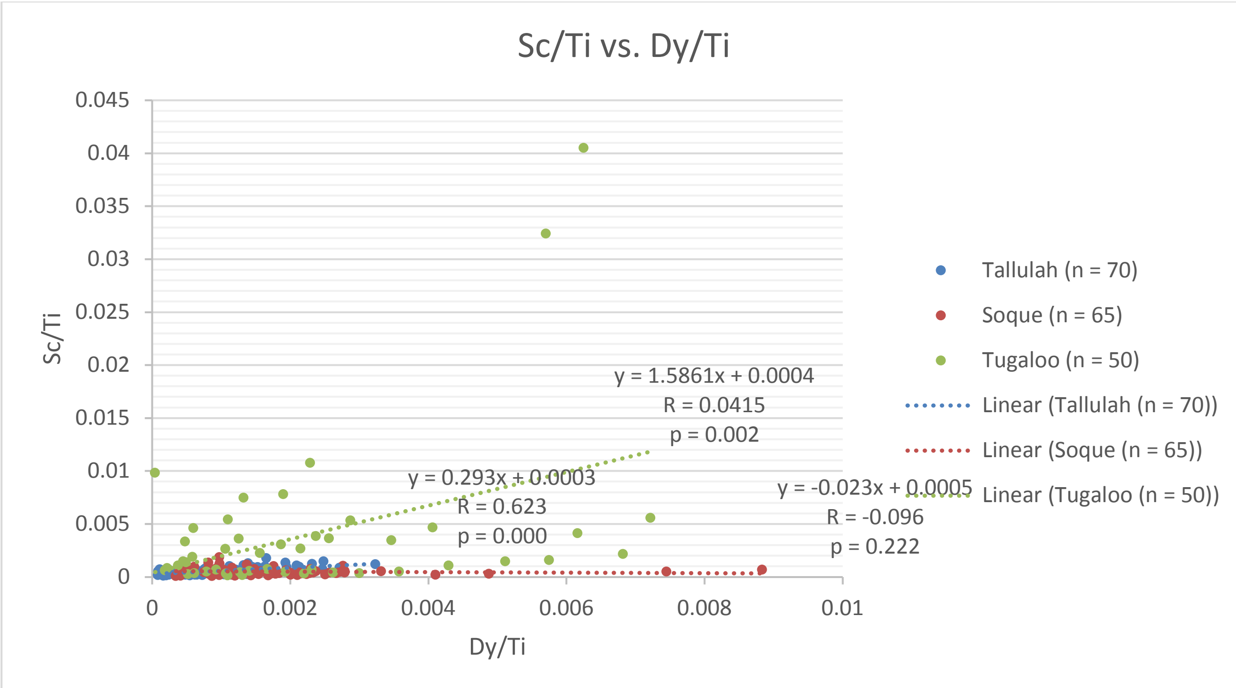

Figure 3-11 *Sc/Ti vs. Dy/Ti by River Basin*

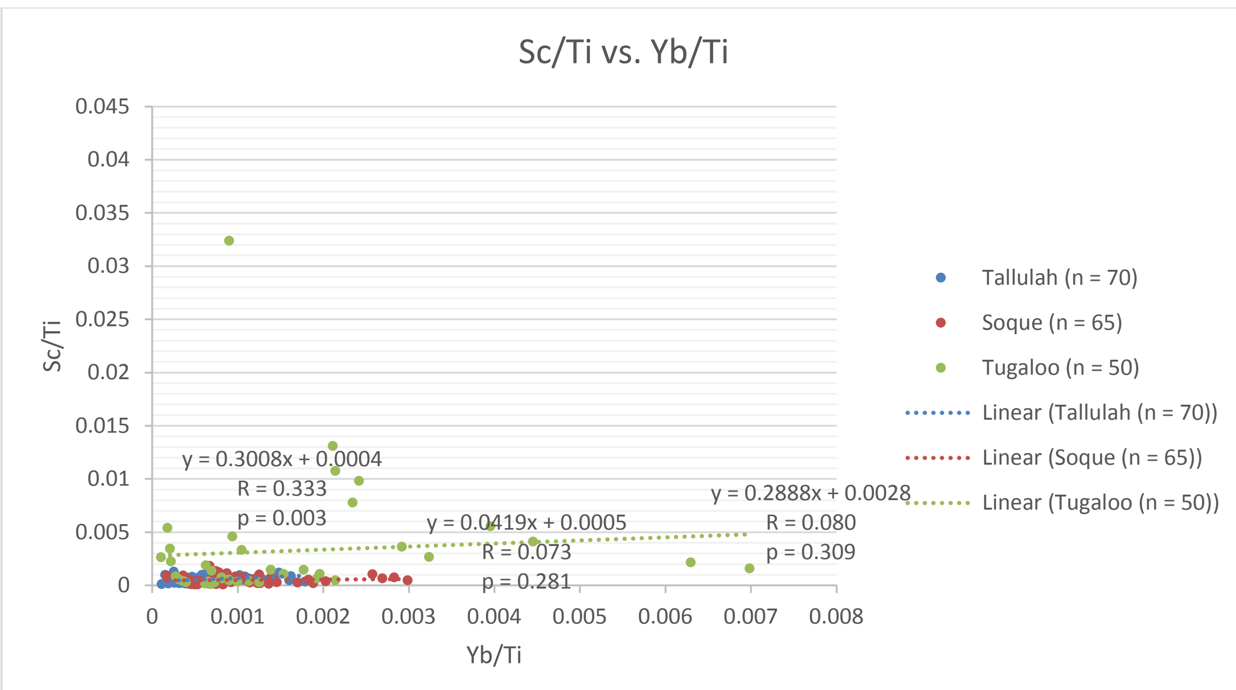

Figure 3-12 *Sc/Ti vs. Yb/Ti by River Basin*

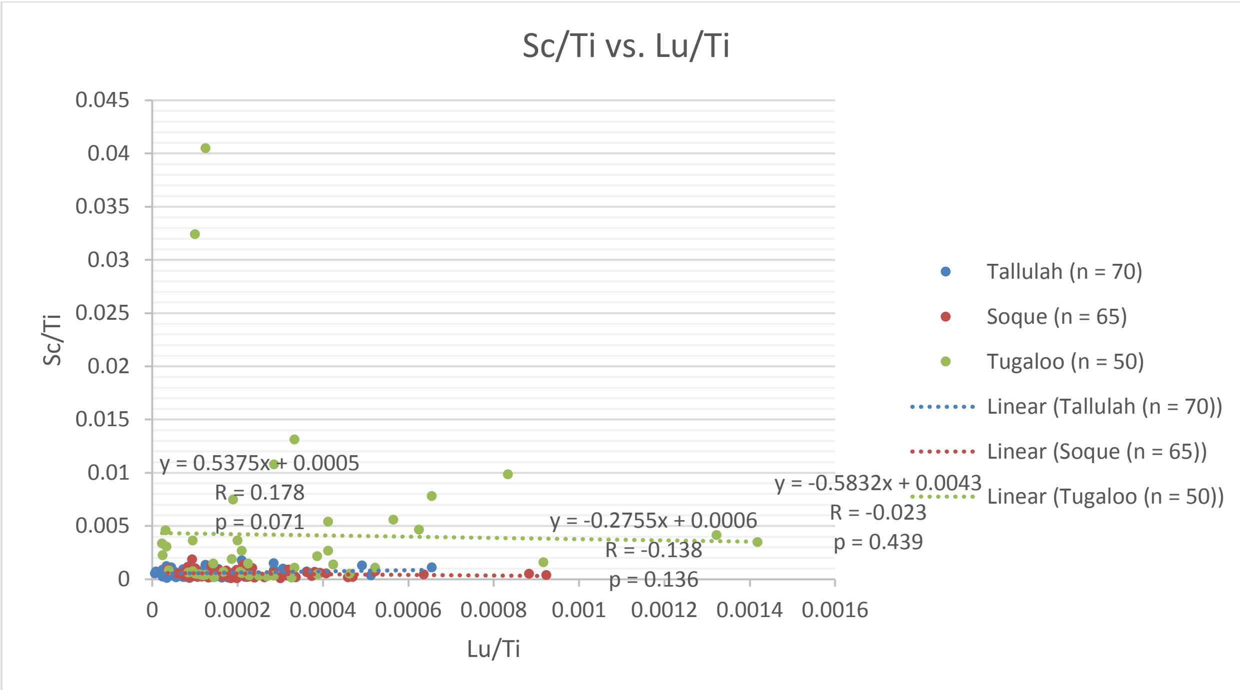

Figure 3-13 *Sc/Ti vs. Lu/Ti by River Basin*

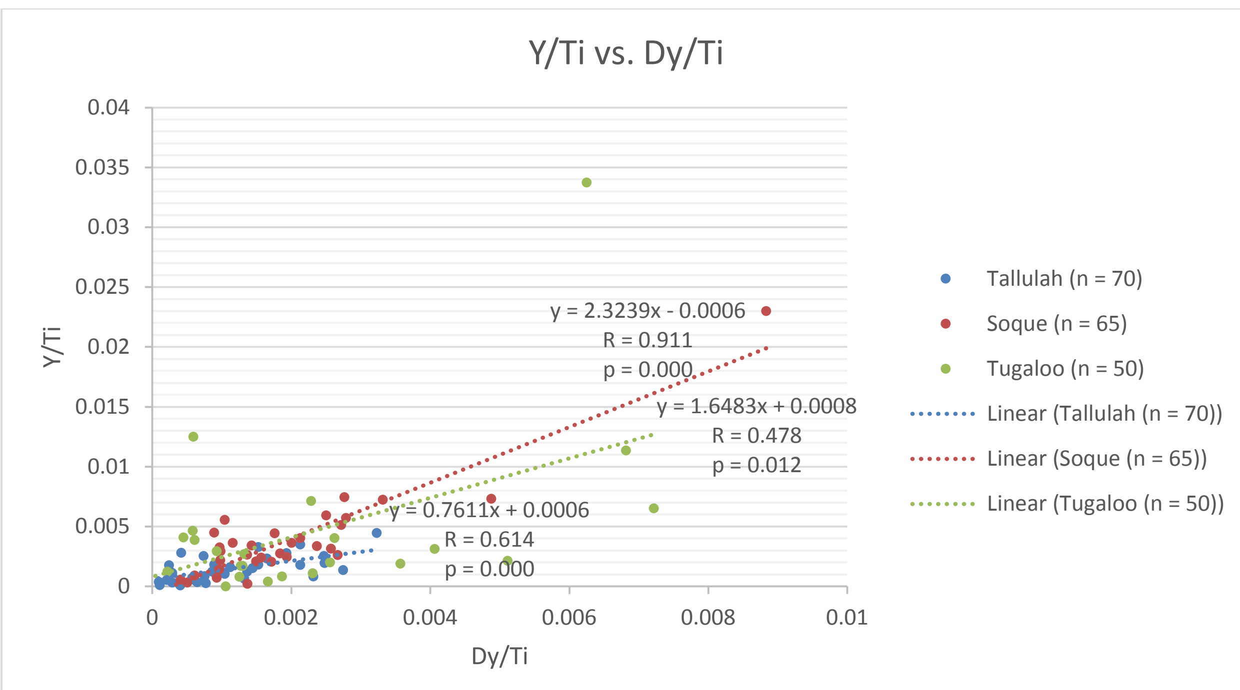

Figure 3-14 *Y/Ti vs. Dy/Ti by River Basin*

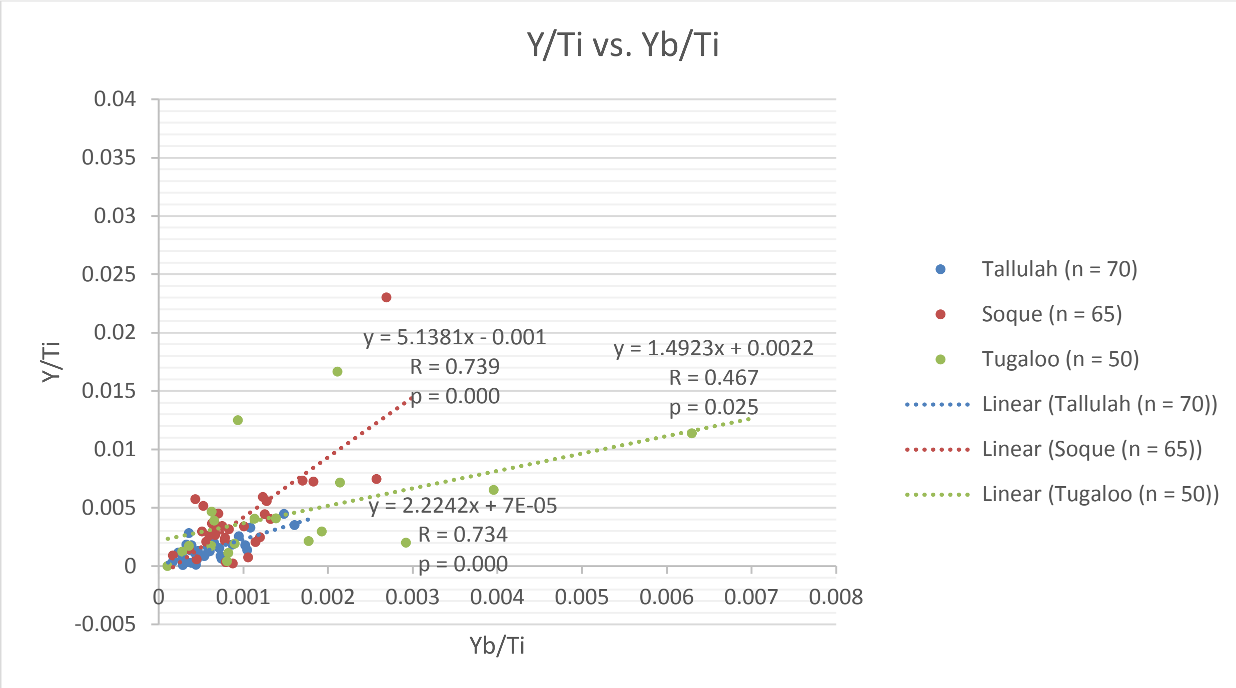

Figure 3-15 *Y/Ti vs. Yb/TI by River Basin*

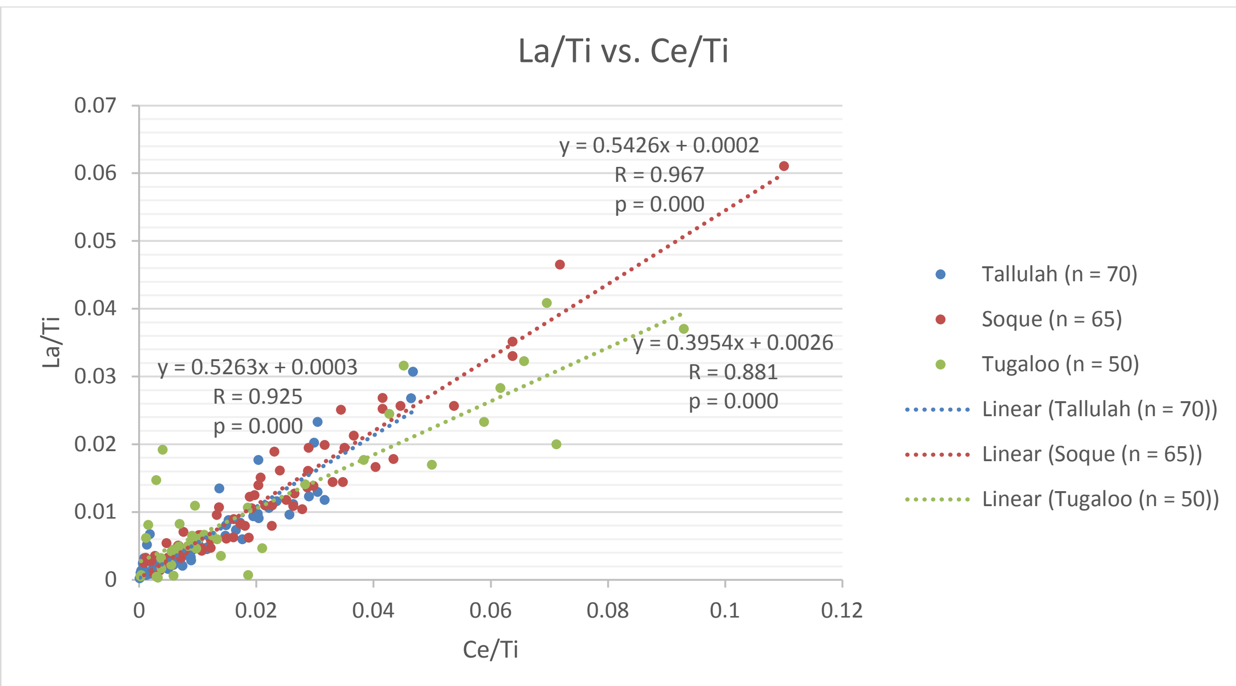

Figure 3-16 *La/Ti vs. Ce/Ti by River Basin*

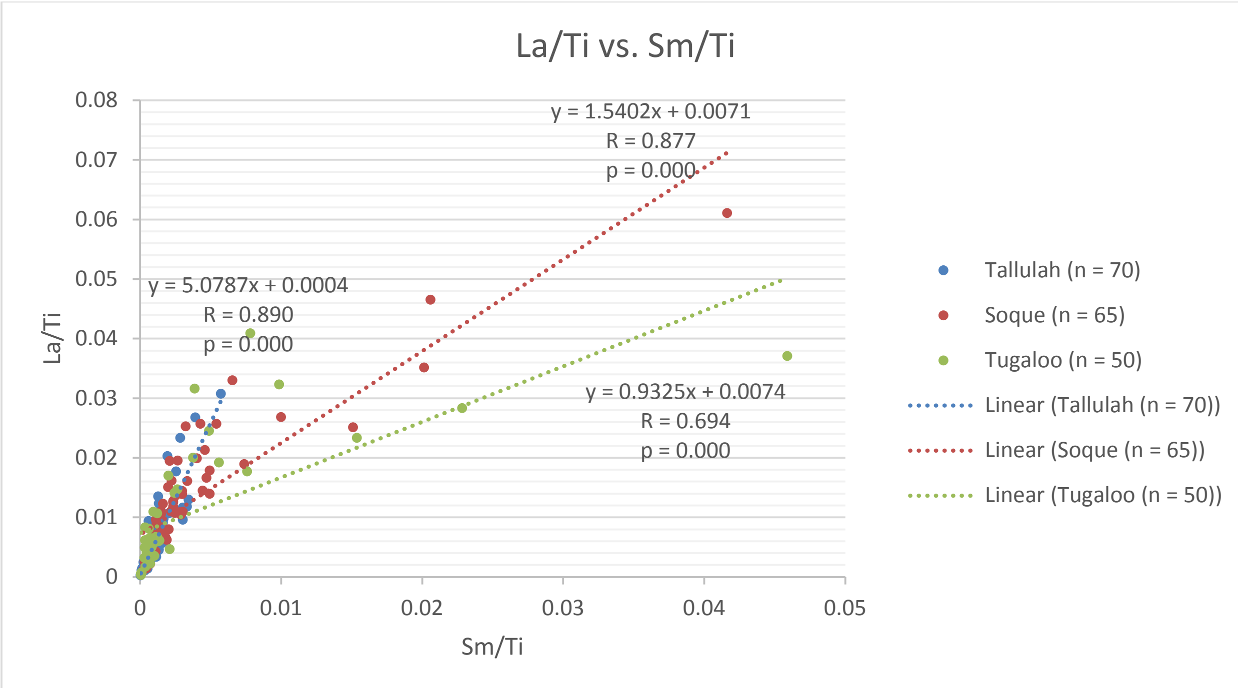

Figure 3-17 *La/Ti vs. Sm/Ti by River Basin*

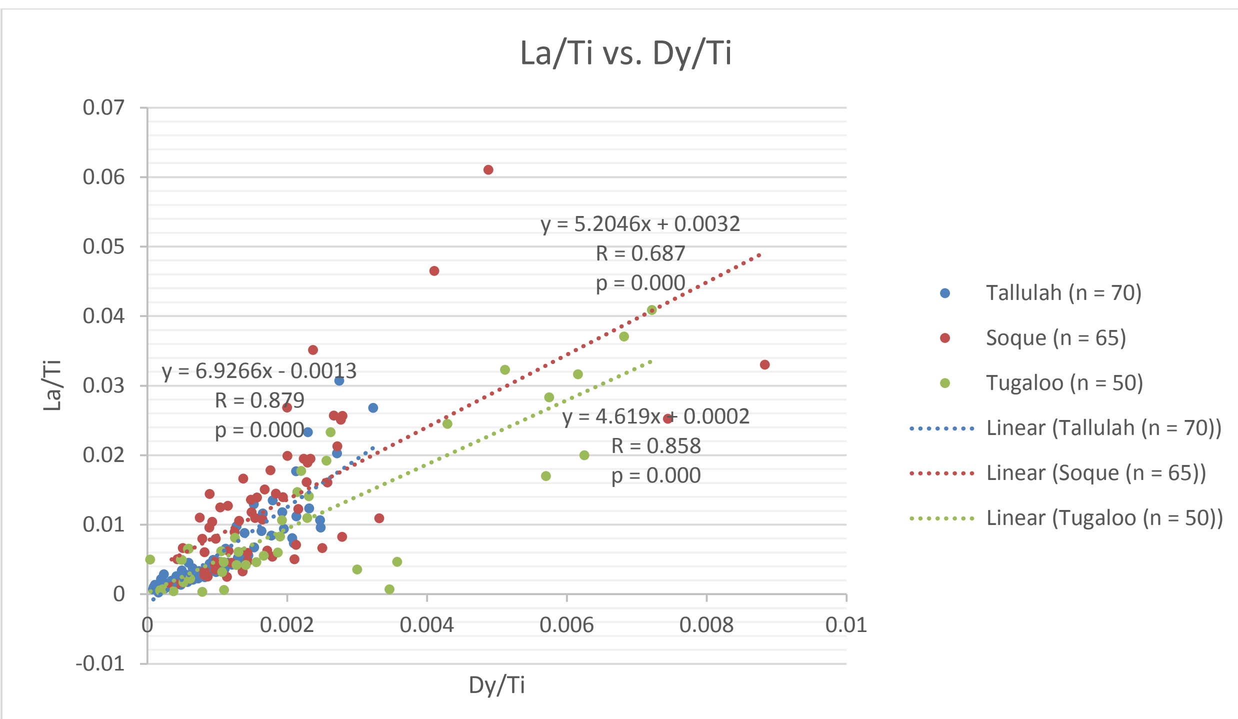

Figure 3-18 *La/Ti vs. Dy/Ti by River Basin*

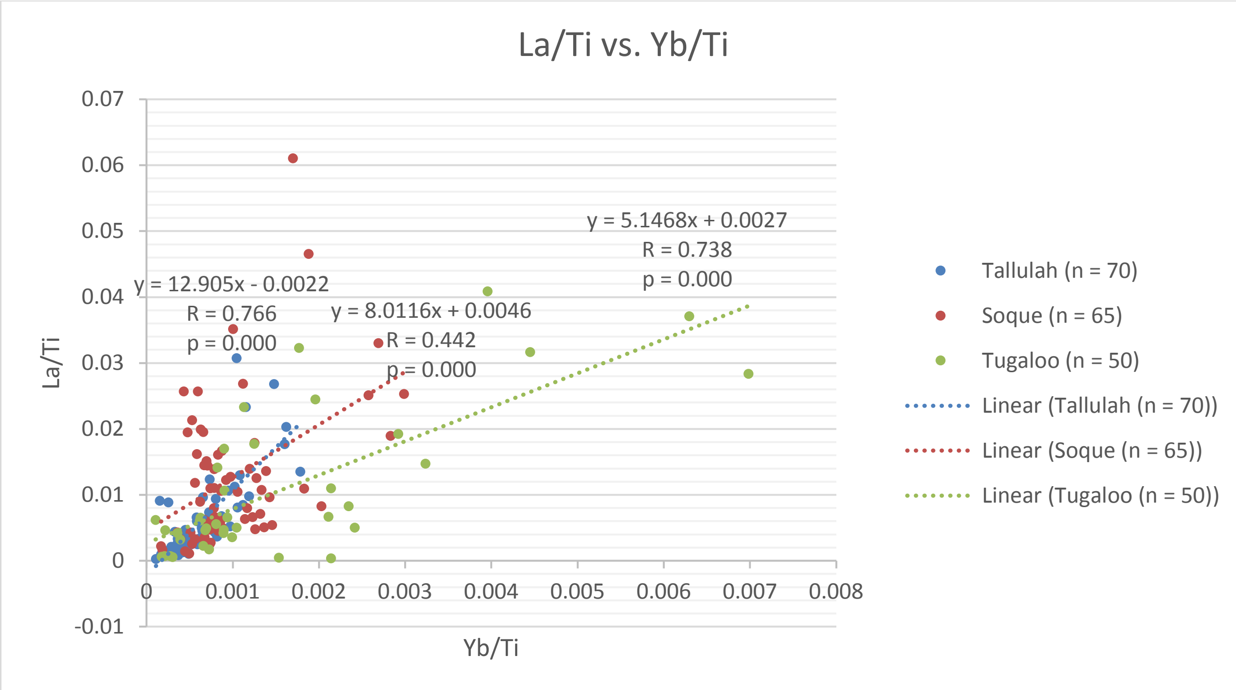

Figure 3-19 *La/Ti vs. Yb/Ti by River Basin*

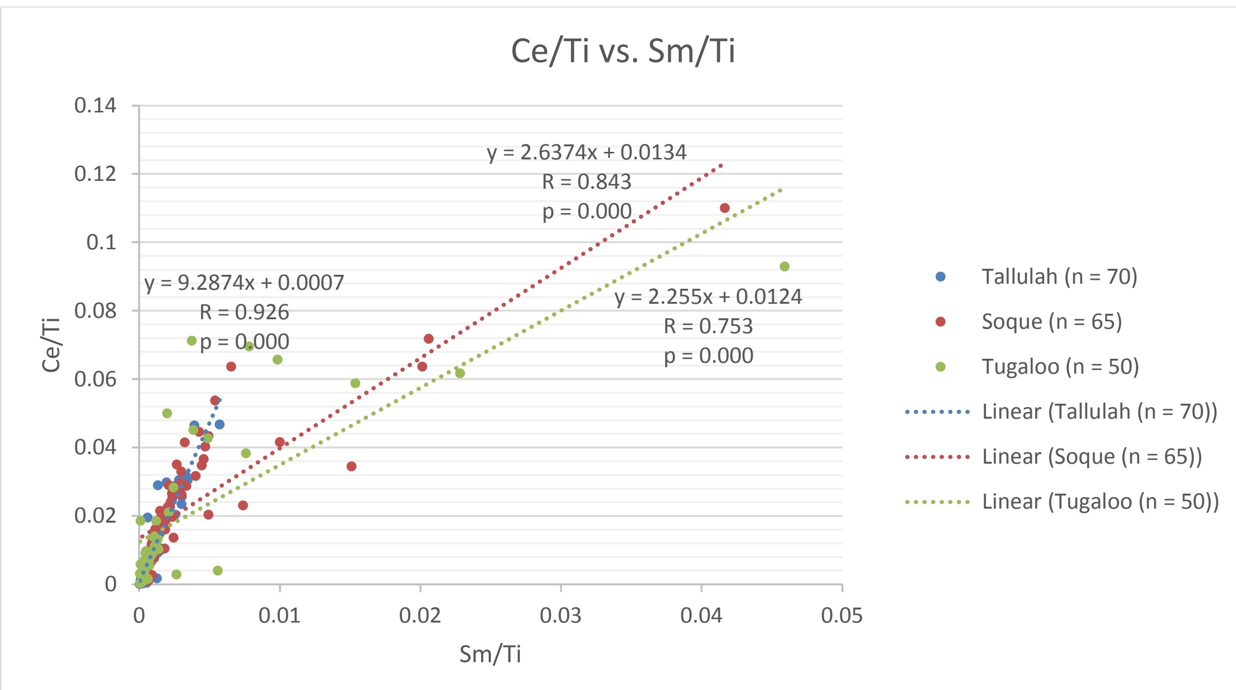

Figure 3-20 *Ce/Ti vs. Sm/Ti by River Basin*

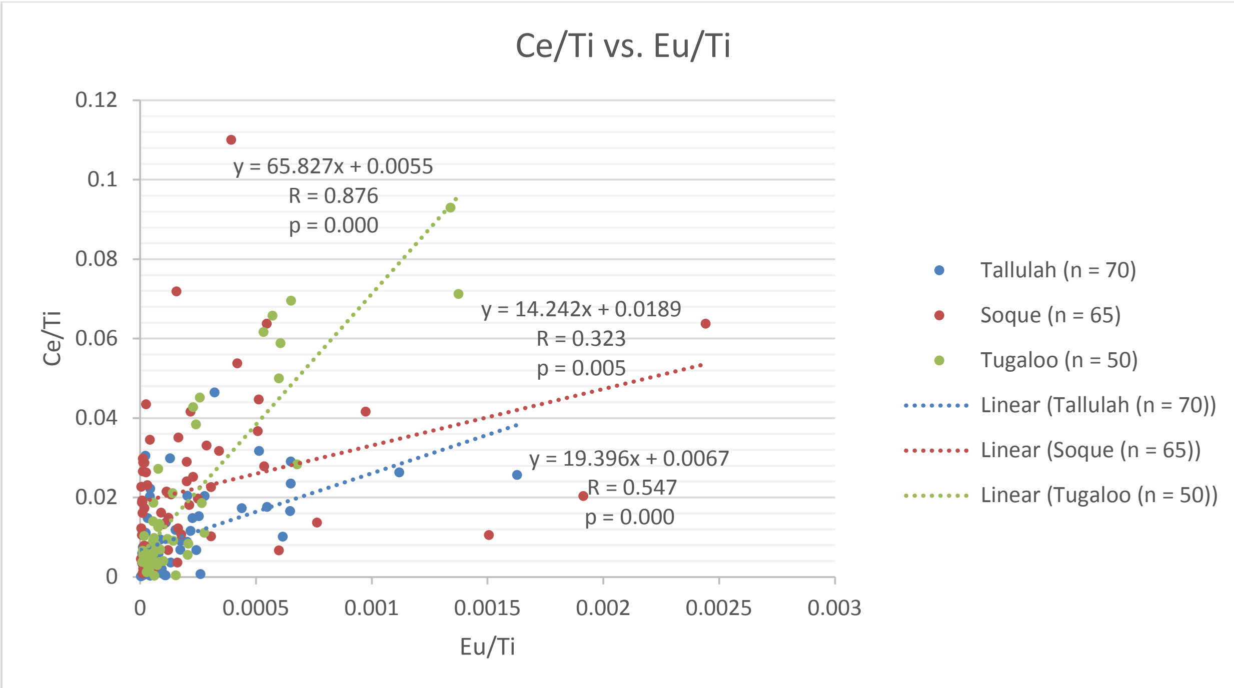

Figure 3-21 *Ce/Ti vs. Eu/Ti by River Basin*

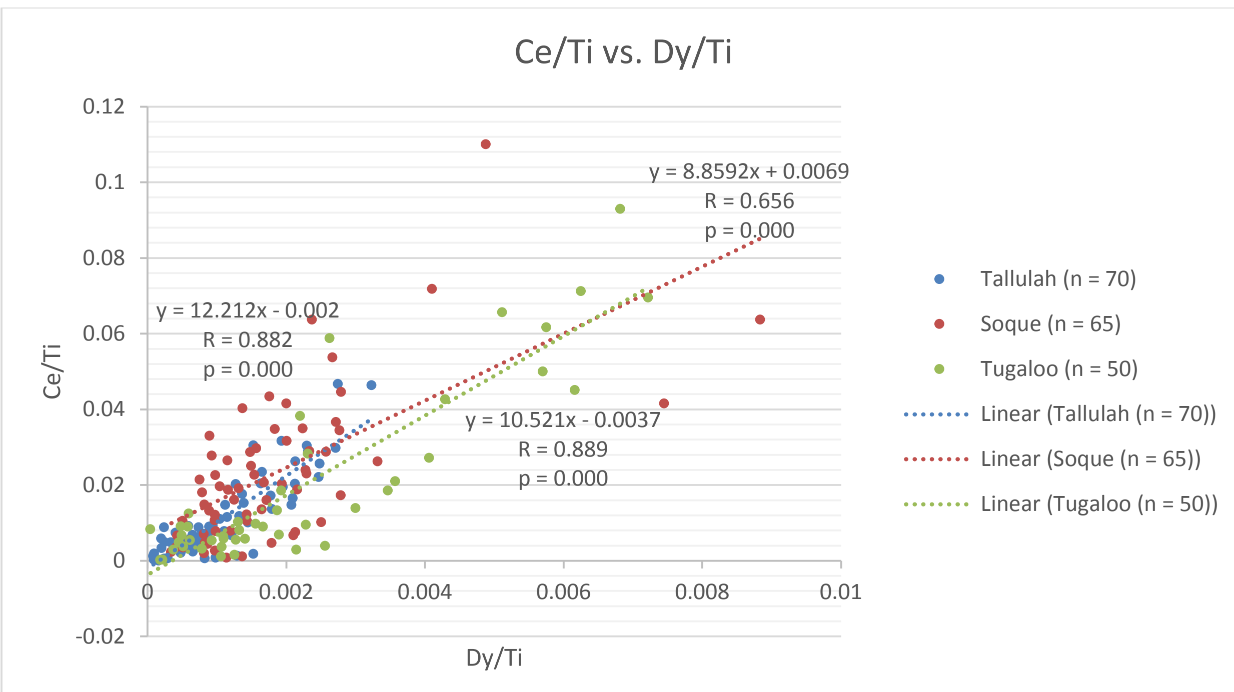

Figure 3-22 *Ce/Ti vs. Dy/Ti by River Basin*

3.3 Weathering Assessment

Table 3-9 includes the mean major element concentrations and Molar BA Ratio of parent rock from the Tallulah River basin. ***Table 3-10*** includes the mean major element concentrations, molar BA ratio and element EF of stream sediment samples from the Tallulah River basin. ***Table 3-11*** includes the mean major element concentrations, molar BA ratio, and element EF of stream sediment samples from the Soque River basin. ***Table 3-12*** includes the mean major element concentrations, molar BA ratio and element EF of stream sediment samples from the Upper Tugaloo River basin.

The results for the Tallulah River sediment show an enrichment (EF >1) of Al, Na, K, Ti, and P relative to Tallulah basin parent rock. The results for the Soque River sediment show an enrichment of Al, K, Ti, and P relative to Tallulah basin parent rock. The results for the Upper Tugaloo sediment show an enrichment of Al, Na, K, Ti, and P relative to Tallulah basin parent rock. It should be noted that NURE stream sediment samples were not analyzed for Si, so Si enrichment could not be evaluated.

The Tallulah River parent rock has a molar BA ratio of 3.210, and each river basin has a lower molar BA ratio by an order of magnitude. The Upper Tugaloo River basin sediment has the highest molar BA ratio (0.485) and the highest sediment-to-rock molar BA ratio (0.151). The Soque River basin sediment has the intermediate molar BA ratio (0.416) and the intermediate sediment-to-rock molar BA ratio (0.129). The Tallulah River basin sediment has the lowest molar BA ratio (0.391) and the lowest sediment-to-rock molar BA ratio (0.122).

***Table 3-8** – Major Element Geochemistry of Bedrock*

Tallulah Basin Parent Rock means, Major Element					
Oxide	Wt. % Oxide	Oxide mw	Metal mw	Wt. % Metal	mol oxide per kg rock
SiO2	50.347	60.084	28.086	23.535	8.379
Al2O3	13.804	101.961	26.982	3.653	1.354
Fe2O3	7.982	159.863	55.933	2.793	0.499
FeO	7.661	71.932	55.933	5.957	1.065
MgO	10.940	40.304	24.305	6.597	2.714
CaO	7.414	56.077	40.078	5.298	1.322
Na2O	1.574	61.979	22.990	0.584	0.254
K2O	0.522	94.195	39.098	0.217	0.055
TiO2	0.918	79.878	47.880	0.550	0.115
P2O5	0.109	141.943	30.974	0.024	0.008
MnO	0.172	70.937	54.938	0.133	0.024
LOI	1.622	--	--	--	--
sum:	103.065				
				Molar BA Ratio:	3.210

***Table 3-9** – Tallulah Basin Enrichment*

Tallulah Basin Stream sediment means (<150µm size fraction)				Enrichment Factors	
Oxide	Wt. % Oxide	Wt. % metal	mol oxide per kg sed		
SiO2*	--	--	--	Si	--
Al2O3	26.783	7.088	2.627	Al	1.940
Fe2O3	11.053	3.867	0.691	Fe***	0.442
FeO**	--	--	--	--	--
MgO	0.400	0.241	0.099	Mg	0.037
CaO****	0.701	0.501	0.125	Ca****	0.095
Na2O	2.442	0.906	0.394	Na	1.552
K2O	3.845	1.596	0.408	K	7.363
TiO2	3.395	2.035	0.425	Ti	3.697
P2O5	0.310	0.068	0.022	P	2.843
MnO	0.156	0.121	0.022	Mn	0.905
		Molar BA Ratio:	0.391		
		BA Ratio (sed) / BA Ratio (rock):	0.122		

***Table 3-10** – Soque Basin Enrichment*

Soque Basin Stream sediment means (<150µm size fraction)				Enrichment Factors	
Oxide		Wt. % metal	mol oxide per kg sed		
SiO2*		--	--	Si	--
Al2O3	19.314	5.111	1.894	Al	1.399
Fe2O3	8.176	2.861	0.511	Fe***	0.327
FeO**	--	--	--	--	--
MgO	0.324	0.195	0.080	Mg	0.030
CaO****	0.415	0.297	0.074	Ca****	0.056
Na2O	1.392	0.516	0.225	Na	0.884
K2O	3.845	1.596	0.408	K	7.363
TiO2	3.607	2.162	0.452	Ti	3.928
P2O5	0.597	0.130	0.042	P	5.471
MnO	0.154	0.119	0.022	Mn	0.896
		Molar BA Ratio:	0.416		
		BA Ratio (sed) / BA Ratio (rock):	0.129		

***Table 3-11** – Tugaloo Basin Enrichment*

Tugaloo Basin Stream sediment means (<150µm size fraction)				Enrichment Factors	
Oxide		Wt. % metal	mol oxide per kg sed		
SiO2*		--	--	Si	--
Al2O3	20.100	5.319	1.971	Al	1.456
Fe2O3	6.678	2.336	0.418	Fe***	0.267
FeO**	--	--	--	--	--
MgO	0.356	0.215	0.088	Mg	0.033
CaO****	0.931	0.666	0.166	Ca****	0.126
Na2O	2.753	1.021	0.444	Na	1.750
K2O	2.429	1.008	0.258	K	4.652
TiO2	1.597	0.957	0.200	Ti	1.739
P2O5	0.237	0.052	0.017	P	2.169
MnO	0.125	0.097	0.018	Mn	0.728
		Molar BA Ratio:	0.485		
		BA Ratio (sed) / BA Ratio (rock):	0.151		

Enrichment factors relative to Tallulah basin parent rock
*Sediment samples not analyzed for Si
** Sediment samples reported as Fe only, calculated here as Fe2O3
***Calculated as Fe2O3(sed) / (Fe2O3 + FeO)(rock)
****Ca from USGS RASS sediment database samples

3.4 Stream Power Assessment

The stream power of each river was assessed based on publicly available data and measurements from the USGS and mapping software. Discharge measurements were taken from USGS stream gauges located as close as possible to the downstream extent of each river. Discharge measurements were compiled from the USGS WIS for all years of available data to calculate a mean discharge (m^3/s) for the available measurement period for each river. ***Table 3-13*** summarizes the mean annual discharge for the Tallulah River from 1999 to 2016. ***Table 3-14*** summarizes the mean annual discharge for the Soque River from 2008 to 2016. ***Table 3-15*** summarizes the mean annual discharge of the Tugaloo River from 1926 to 1960. ***Table 3-16*** summarizes the mean annual discharge of the Chattooga River from 1940 to 2016. The length of each river was gathered from the USGS NHD for each river. The slope of each river was calculated by measuring the elevation of the upstream extent of each river – using USGS hydrography and digital mapping software – and subtracting the elevation of the stream gauge. The channel width of each river was also measured at each stream gauge. After compiling these measurements for each river, each river’s stream power and specific stream power were calculated. ***Table 3-17*** summarizes the measurements and stream power calculations for each river.

***Table 3-12** – Tallulah River Mean Annual Discharge 1999-2016*

Tallulah River

USGS Stream Gauge	Year	Mean Discharge (m^3/s)
2181580	1999	1.66
	2000	1.51
	2001	1.53
	2002	1.52
	2003	1.64
	2004	3.29
	2005	1.65
	2006	1.43
	2007	1.41
	2008	2.00
	2009	2.06
	2010	1.61
	2011	1.09
	2012	1.27
	2013	1.70
	2014	1.37
	2015	1.40
	2016	2.18
	Mean:	**1.68**

***Table 3-13** – Soque River Mean Annual Discharge 2008-2016*

Soque River

USGS Stream Gauge	Year	Mean Discharge (m^3/s)
23312495	2008	3.04
	2009	4.90
	2010	8.15
	2011	4.76
	2012	3.68
	2013	7.58
	2014	6.17
	2015	4.22
	2016	6.80
	Mean:	**5.48**

***Table 3-14** – Tugaloo River Mean Annual Discharge 1926-1960*

Tugaloo River

USGS Stream Gauge	Year	Mean Discharge (m^3/s)
2184000	1926	39.45
	1927	41.74
	1941	41.34
	1942	45.14
	1943	69.32
	1944	57.79
	1945	42.76
	1946	78.38
	1947	46.21
	1948	61.76
	1949	103.13
	1950	65.72
	1951	48.42
	1952	64.17
	1953	50.38
	1954	49.84
	1955	37.66
	1956	36.13
	1957	47.37
	1958	69.15
	1959	47.66
	1960	69.69

Mean:	**55.15**

Table 3-15 *– Chattooga River Mean Annual Discharge 1940-2016*

Chattooga River

USGS Stream Gauge	Year	Mean Discharge (m^3/s)
2177000	1940	13.23
	1950	19.87
	1960	21.52
	1970	14.86
	1980	24.13
	1990	22.84
	1991	21.35
	1992	18.68
	1993	23.89
	1994	19.02
	1995	20.67
	1996	21.85
	1997	20.37
	1998	21.40
	1999	12.83
	2000	12.11
	2001	8.43
	2002	11.03
	2003	22.74
	2004	21.37
	2005	27.40
	2006	12.40
	2007	11.38
	2008	9.28
	2009	16.56
	2010	25.09
	2011	14.52
	2012	12.31
	2013	27.05
	2014	17.07
	2015	13.45
	2016	20.61

	Mean:	**16.95**

***Table 3-16** – Stream Power Calculations*

Stream Power

		Tallulah	Soque	Tugaloo	Tallulah & Soque (pre-capture)*	Tallulah & Tugaloo (post-capture)
Discharge (m^3/s)	*Q*	1.68	5.48	55.15	24.11	55.15
Stream low elev. (m)	*E1*	287	396	174	396	174
Stream high elev. (m)	*E2*	1241	490	269	1241	1241
Stream length (m)	*L*	80450	47288	102010	115450	182460
Stream slope	*S*	0.0119	0.00199	0.000931	0.007319	0.00585
Stream width (m)	*W*	17	25	70	70	70
Water density (kg/m^3)	*ρ*	1000	1000	1000	1000	1000
Accel. due to gravity (m/s^2)	*g*	9.8	9.8	9.8	9.8	9.8
Stream Power (W/m) $\Omega = \rho g Q S$	**Ω**	196	107	503	1729	3160
Specific Stream Power (W/m^2) $\omega = \Omega/W$	**ω**	12	4.3	7.2	24.7	45

* = Stream power based on combined Soque, Tallulah, and Chattooga discharge values and estimated combined length of Tallulah River, Deep Creek, and Soque River below confluence

The Tallulah River has the steepest gradient (S = 0.0119), the lowest discharge (Q = 1.68 m^3/s), the intermediate stream power (Ω = 196 W/m) and the highest specific stream power (ω = 12 W/m^2). The Soque River has the intermediate gradient (S = 0.00199), the intermediate discharge (Q = 5.48 m^3/s), the lowest stream power (Ω = 107 W/m), and the lowest specific stream power (4.3 W/m^2). The Tugaloo River has the shallowest gradient (S = 0.000931), the greatest discharge (Q = 55.15 m^3/s), the highest stream power (Ω = 503 W/m), and the intermediate specific stream power (ω = 7.2 W/m^2). The post-capture Tallulah-Tugaloo system has a higher specific stream power post-capture, compared to the modern Tugaloo system alone. The modern Soque system has a lower specific stream power post-capture, compared to the ancestral Tallulah-Soque system.

4 DISCUSSION

4.1 Sediment Geochemistry Statistics

There are several observed differences between element concentrations between sediment samples from the three river basins. The Tallulah River basin sediment exhibited a relative enrichment in Al, Cu, Pb, Sr, and V. The Soque River basin sediment exhibited a relative enrichment in U, Th, Hf, and the REE Ce, Dy, Eu, La, Lu, Sm. The Upper Tugaloo River basin sediment exhibited a relative enrichment of the REE Sc and depletion in Ti. The selected REE and REE/Ti ratio plots show varied patterns for each river (***Figures 3-3*** through ***3-2***). These patterns include strong correlations for one river but weak correlations for another, differences in relative slope between basins, and Tallulah data points clustered in the low range. Each river basin displayed a unique assemblage of strongest and weakest correlations as well as differences in mean concentrations of individual elements, which reflects the variability of sediment source area geochemistry. This geochemical variability is the fundamental principle in establishing a sediment source fingerprint for each river basin (e.g. Walling 2005).

Land disturbances from historic mining and logging activities in the southern Appalachians (Mast & Turk 1999; Douglass & Hoover 1988) may potentially skew the fingerprint signatures in present-day stream sediment. Increased soil erosion and preferential removal of overburden and heavy minerals will alter the natural processes of sedimentation, and therefore a more reliable sediment source fingerprint can be developed from deeper sub-surface sediment samples of contemporary ages.

4.2 Weathering Assessment

Weathering assessment of sediment in the sampled river basins can be used to compare the relative extent of weathering as a proxy for sediment transport distance (Mikesell et al. 2010; Prince et al. 2010). The present-day Tugaloo River sediment has the highest BA ratio and highest sediment BA to rock BA ratio of three river basins, reflecting increased weathering over a longer stream distance after capture. Increased weathering leads to a decrease in BA ratio in an in situ weathering profile, but in fluvial deposits the deposition of clay minerals (with adsorbed base-metal cations) appears to increases BA ratio because higher elevation streams of higher specific stream power are more leached of base-metal cations. The Tallulah River has the highest specific stream power of the three basins, and the Tugaloo River has the lowest. Therefore, the Tallulah River should experience the least deposition, and the Tugaloo should experience the most deposition, which would result in greater concentrations of fine sediment (more clay with adsorbed base-metal cations) in Tugaloo sediment, which is reflected in the higher molar BA ratio in the Tugaloo basin. Although documentation of the NURE-HSSR samples indicates a size fraction of <150μm, no sample grain size distribution is available to assess the relative abundance of clay to silt and fine sand grains within the <150 μm size fraction.

The identification of a distinct sediment signature for each of the three basins is dependent on the variability of bedrock types and associated sediment across the three basins. Because the Tallulah River crosses such varied metamorphic terranes and ore-bearing mineralization zones, more in-depth mineralogical analysis is required to identify unique minerals and further refine the provenance of clastic sediment deposits. In addition to the NURE sediment database, there are several other USGS databases of available sampling data (including surface sediment, bedrock, and mineral ages) that can be analyzed for future refinement of sediment source fingerprints.

4.3 Stream Power Assessment

Stream power is a major control on the nature and frequency of stream capture events (e.g. Oskin & Burbank 2007), as capture events alter the relative stream powers of the associated rivers. The Tallulah River has the greatest specific stream power of the three rivers. It drains the highest and steepest terrain and experiences the highest annual rainfall (NOAA 2016) of the three rivers. A steeper gradient and greater rainfall (contributing to stream discharge) give the Tallulah River greater stream power and specific stream power than the Soque River. With greater stream power, the Tallulah River can erode and mobilize larger clasts and heavier minerals through higher-energy streamflow. Some heavier elements, such as U and Th, are present in higher concentrations in the Soque River basin, which reflects the effects of stream capture. Prior to stream capture, heavy mineral grains mobilized from the Tallulah River had been transported through and deposited in the Soque River. After stream capture the Soque River, cutoff from its former high elevation headwaters, has lower energy and less capacity to move those heavy minerals (stream power decreases with lower gradient). The Tugaloo River, meanwhile, gains energy from the high elevation Tallulah River and can transport those heavy minerals farther downstream (stream power increases with steeper gradient over the combined Tallulah and Tugaloo length) before they are deposited.

4.4 Sediment Source Fingerprints

A set of unique sediment source fingerprints was established based on the combined factors of heavy element abundance (U, Th), REE element ratio plots, weathering assessment, and stream power to assess the transition of sediment source in Tugaloo and Soque samples from pre-capture to post-capture conditions. The sediment source fingerprints for comparison between the three basins are as follows:

Tallulah River

-Enriched in Al, Cu, Pb, Sr, V

-Low molar BA ratio

-Low Sc/Ti, Y/Ti Ce/Ti, and Sm/Ti, ratios

-High La/Ti vs. Sm/Ti slope; and Ce/Ti vs. Sm/Ti slope

-Low-range clusters in La/Ti vs. Sm/Ti, La/Ti vs. Dy/Ti, La/Ti vs. Yb/Ti, Ce/Ti vs. Sm/Ti, and Ce/Ti vs. D/Ti.

Soque River

-Enriched in U, Th, Hf, Ce, Dy, Eu, La, Lu, Sm

-High Ce/Lu, La/Yb, La/Lu, Ce/Yb ratios

-High Ce/Lu vs. La/Yb slope; La/Lu vs. Sm/Yb slope; Ce/Yb vs. La/Lu slope; Y/Ti vs. Dy/Ti slope; Y/Ti vs. Yb/Ti slope; and La/Ti vs. Ce/Ti slope.

Upper Tugaloo River

-Enriched in Sc

-Depleted in Ti

-High molar BA ratio;

-High Sc/Ti vs. Y/Ti slope; Sc/Ti vs. Ce/Ti slope; Sc/Ti vs. Sm/Ti slope; Sc/Ti vs. Eu/Ti slope; Sc/Ti vs. Yb/Ti slope; and Sc/Ti vs. Lu/Ti slope.

In future work sampling Tugaloo River floodplain cores, a sufficient number of sample locations should be selected to compare means from core samples to means from the stream sediment samples used in this study. Results can then be plotted for each selected core sample interval to compare Tugaloo floodplain core ratio trends against trends from stream sediment from this study. The relative slopes of Tallulah and Tugaloo trend lines should show a transition or abrupt change from pre-capture to post-capture sediment to reflect the addition of Tallulah sediment to the Tugaloo River. Molar BA ratios in selected core sample intervals should also show a transition or abrupt change from pre-capture to post-capture sediment. The same method can be employed for cores from floodplains in the Soque River basin to find where Tallulah River sediment input ceases and the modern Soque signature appears. This approach assumes that post-depositional weathering within the floodplain does not out-pace sediment transport, so that changes in sediment geochemistry reflect changes in sediment source. Additionally, this approach will require bedrock samples from the Tugaloo River basin to represent parent rock of pre-capture Tugaloo River sediment. There were insufficient bedrock samples from the Tugaloo basin available in the USGS NGC database for use in this study.

5 CONCLUSIONS

The results of this study have established a set of sediment source fingerprints for the river basins involved in the Tallulah River capture. These sediment source fingerprints employ geochemical and geospatial methodologies to both corroborate and refine the timescale of the capture event. Future work can continue to identify stream sediment provenance in Tugaloo and Soque River floodplain deposits and date the stratigraphic layer where Tallulah sediment first appears in the Tugaloo basin and the layer where Tallulah sediment input ceases in the Soque basin.

A statistical analysis of element concentrations in stream sediment samples previously collected by the USGS identified unique geochemical signatures in stream sediment from the Tallulah, Soque, and Upper Tugaloo River basins. Element concentrations in bedrock from the Tallulah River basin were evaluated to determine characteristics of element enrichment/depletion in stream sediment samples relative to Tallulah basin parent rock in order to assess differences in the extent of weathering of stream sediment between the Tallulah, Soque, and Upper Tugaloo River basins. Stream power from modern drainage network measurements was estimated in order to assess differences in sediment transport capacity between the Tallulah, Soque, and Upper Tugaloo River basins and how their relative capacities changed from pre-capture to post-capture conditions. These assessments were combined to evaluate the distinct characteristics of the Tallulah, Soque, and Upper Tugaloo River basins in order to establish a unique sediment source fingerprint for each basin that can be used to identify where in the sedimentary record

Tallulah sediment input begins in the Tugaloo River and where Tallulah sediment input ceases in the Soque River.

The analysis of available geochemical data in this study determined that the three river basins possess distinct characteristics sufficient to develop a unique sediment source fingerprint for each basin. REE and heavy element ratios play a significant role in differentiating sediment derived from the Tallulah River basin from sediment derived from the Upper Tugaloo River and Soque River basins. The clearest discriminators for Tallulah River sediment appear to be enrichment in Al, Cu, Pb, Sr, V, and low REE/Ti ratios Sc/Ti, Y/Ti Ce/Ti, and Sm/Ti. The clearest discriminators for Soque River sediment appear to be enrichment in U, Th and REE, and REE ratios Ce/Lu, La/Yb, La/Lu, and Ce/Yb. With these fingerprints established, additional work can continue in sampling a stratigraphic profile in Tugaloo River floodplain sediment to identify the Tallulah River capture event and calculate a more precise date of capture. The Tallulah River and Tallulah Gorge are representative features of the ongoing regional landscape modification in the southern Appalachians. River capture and bedrock gorge incision play vital roles in controlling the overall rate of escarpment retreat, so understanding the timing of such processes will provide insight into the interactions of geomorphic processes and aid in understanding the continuing evolution of the southern Appalachian Mountains.

REFERENCES

Adams, R.K., & Spotila, J.A. (2005). The form and function of headwater streams based on field and modeling investigations in the Southern Appalachian Mountains. *Earth Surface Processes and Landforms, 30*, 1521-1546. doi: 10.1002/esp.1211

Andrews, G.D.M., Russel, J.K., Brown, & S.R., Enkin, R.J. (2012). Pleistocene reversal of the Fraser River, British Columbia. *Geology, 40*, 111-114. doi:10.1130/G32488.1

Aslan, A., Hood.W.C., Karlstrom, K.E., Kirby, E., Granger, D.E., Kelley, S., Crow, R., Donahue, M.S., Polyak, V., & Asmerom, Y. (2014). Abandonment of Unaweep Canyon (1.4-0.8 Ma), western Colorado: effects of stream capture and anomalously rapid Pleistocene river incision. *Geosphere, 10*(3), 428-446. doi:10.1130/GES00986.1

Bailey, C.M., Southworth, S., & Tollo, R.P. (2006). Tectonic history of the Blue Ridge, north-central Virginia. *GSA Field Guides, 8,* p. 113-134.

Bagnold, R.A. (1966). An approach to the sediment transport problem from general physics. *Physiographic and Hydraulic Studies of Rivers: United States Geological Survey Paper 422-I,* United States Department of the Interior, Washington, D.C.

Barron, E.J. (1989). Climate variations and the Appalachians from the Late Paleozoic to the present: results from model simulations: *Geomorphology, 2,* 99-118.

Birkeland, P.W. (1999) *Soils and Geomorphology.* Oxford University Press, New York, 430 p

Bishop, P. (1995). Drainage rearrangement by river capture, beheading and diversion. *Prog Phys Geogr*, *19*(4), 449–473.

Bloxom, L.F. & Burby, T.J. (2015). Determination of the location of the groundwater divide and nature of groundwater flow paths within a region of active stream capture; the New River watershed, Virginia, USA. *Environmental Earth Science, 74*, 2687-2699. doi:10.1007/s12665-015-4290-1

Bonnet, S. (2009). Shrinking and splitting of drainage basins in orogenic landscapes from the migration of the main drainage divide. *Nature Geoscience, 2,* 766-771. doi:10.1038/ngeo666

Bunte, K. (2010). Measurement of gravel transport using the magnetic tracer technique – Temporal variability over a highflow season and field-calibration *in* Gray, J.R., Laronne, J.B., and Marr, J.D.G., Bedload-surrogate monitoring techniques. *U.S. Geological Survey Scientific Investigations Report 2010–5091*, p. 85–106. http://pubs.usgs.gov/sir/2010/5091/

Cannon, W.F. & Horton, J.D. (2009). Soil geochemical signature of urbanization and industrialization – Chicago, Illinois, USA. *Applied Geochemistry, 24 (8)*, 1590-1601. https://doi.org/10.1016/j.apgeochem.2009.04.023

Charlton, R. (2008). *Fundamentals of Fluvial Geomorphology*. Routledge, 233 p

Chew, V.C. (1988). *Underfoot: A Geologic Guide to the Appalachian Trail.* Appalachian Trail Conference, Harpers Ferry

Collins, A.L., Walling, D.E., & Leeks, G.J.L. (1997). Source type ascription for fluvial suspended sediment based on a quantitative composite fingerprinting technique *Catena 29* (1), 1–27. http://dx.doi.org/10.1016/S0341-8162(96)00064-1

Collins, A.L., Walling, D.E., & Leeks, G.J.L. (1998). Fingerprinting the origin of fluvial suspended sediment in larger river basins—Combining assessment of spatial provenance and source type. *Geografiska Annaler—Series A, Physical Geography, 79,* (*4*), 239–254. http://www.jstor.org/stable/521219

Cook, RB., Jr., & Burnell, J .R, Jr. (1986). The trace metal signature of some major lithologic units, Dahlonega district, Lumpkin County, Georgia, *in* Misra, K.C., ed., Volcanogenic sulfide and precious metal mineralization in the southern Appalachians. *Knoxville, University of Tennessee Studies in Geology*, *16*, 206-219

Cook, K.L., Turowski, J.M., & Hovius, N. (2013). A demonstration of the importance of bedload transport for fluvial bedrock erosion and knickpoint migration. *Earth Surface Processes and Landforms, 38,* 683-695. doi: 10.1002/esp.3313

Craddock, W.H., & Kylander-Clark, A.R.C. (2013) U-Pb ages of detrital zircons from the Tertiary Mississippi River Delta in central Louisiana: Insights into sediment provenance. *Geosphere, 9* (6), 1832-1851. doi:10.1130/GES00917.1

Davis, W.M. (1899). The geographical cyle. *The Geographical Journal*, *14*(5), 481-504. http://www.jstor.org/stable/1774538

Douglass, J.E., & Hoover, M.D. (1988). History of Coweeta, in Swank, W.T., and Crossley, D.A., Jr., eds., Forest hydrology and ecology at Coweeta: New York, Springer-Verlag

Duxbury, J., Bierman, P.R., Portenga, E.W., Pavich, M.J., Southworth, S., & Freeman, S. (2015) Erosion rates in and around Shenandoah National Park, Virginia, determined using analysis of cosmogenic ^{10}Be. *American Journal of Science, 315,* 46-76. doi 10.2475/01.2015.02

Gallen, S.F., Wegman, K.W., & Bohnenstiehl, D.R. (2013). Miocene rejuvenation of topographic relief in the southern Appalachians. *GSA Today, 2*(2), 4-10. doi: 10.1130/GSATG163A.1

Graf, W.L. (1987). *Geomorphic Systems of North America*. Geological Society of America

Grimshaw, D.L., & Lewin, J. (1980). Source identification for suspended sediments. *Journal of Hydrology*, *47*,*(1-2)*, 151–162. http://dx.doi.org/10.1016/0022-1694(80)90053-0

Hancock, G. & Kirwan, M. (2007). Summit erosion rates deduced from ^{10}Be: Implications for relief production in the central Appalachians. *Geology*, *35* (*1*), 89-92. DOI: https://doi.org/10.1130/G23147A.1

Hartshorn, K., Hovius, N., Dade, W.B., & Slingerland, R.L. (2002). Climate-driven bedrock incision in an active mountain belt. Science 297: 2036–2038. DOI: 10.1126/science.1075078

Helsel, D.R., & Hirsch, R.M. (2002). Statistical methods in water resources. *U.S. Geological Survey Techniques of Water-Resources Investigations*, book 4, chap. A3, 510 p. http://pubs.usgs.gov/twri/twri4a3/

Hietpas, J., Samson, S., Moecher, D., & Chakraborty, S. (2011). Enhancing tectonic and provenance information from detrital zircon studies: assessing terrane-scale sampling and grain-scale characterization. *Journal of the Geological Society, 168*, 309-318. doi: 10.1144/0016-76492009-163

Hood, W.C., Aslan, A., & Betton, C. (2014). Aftermath of a stream capture: Cactus Park lake spillover and the origin of East Creek, Uncompahgre Plateau, western Colorado. *Geosphere, 10*(3), 447-461. doi:10.1130/GES00970.1

Horowitz, A.J. (1991). A primer on sediment trace element chemistry (2d ed.). *U.S. Geological Survey Open-File Report 91–76*, 136 p., *http://pubs.usgs.gov/of/1991/0076/report.pdf*

Johnson, D.W. (1907). River capture in the Tallulah district, Georgia. *Science*, *2*(637), 428-432

Jones, M.T., Voss, S.R., Ptacek, M.B., Weisrock, D.W., & Tonkyn (2006). River drainages and phylogeography: An evolutionary significant lineage of shovel-nosed salamander (*Desmognathus marmoratus*) in the southern Appalachians. *Molecular Phylogenetics and Evolution, 38*, 280-287. doi:10.1016/j.ympev.2005.05.007

Judson, S. & Ritter, D.F. (1964). Rates of regional denudation in the United States. *Journal of Geophysical Research*, *69*, 3395-3401. DOI: 10.1029/JZ069i016p03395J

Jungers, M.C., Bierman, P.R., Matmon, A., Nichols, K., Larsen, J., & Finkel, R. (2009). Tracing hillslope sediment production and transport with in situ and meteoric ^{10}Be. *Journal of Geophysical Research, 114,* F04020. doi:10.1029/2008JF001086

Kimoto, A., Nearing, M.A., Shipitalo, M.J., & Polyakov, V.O. (2006). Multi-year tracking of sediment sources in a small agricultural watershed using rare earth elements. *Earth Surface Processes and Landforms, 31* (14), 1763–1774. http://dx.doi.org/10.1002/esp.1355

Klages, M.G., & Hsieh Y.P. (1975). Suspended solids carried by the Gallatin River of southwestern Montana—II, Using mineralogy for inferring sources. *Journal of Environmental Quality*, *4,* (*1*), 68–73. http://dx.doi.org/10.2134/jeq1975.00472425000400010016x

Knighton, D. (1998). *Fluvial Forms and Processes: A New Perspective*. Arnold, 400 p

Kozak, K.H., Blaine, R.A., & Larson, A. (2006). Gene lineages and eastern North American paleodrainage basins: phylogeography and speciation in salamanders of the *Eurycea bislineata* species complex. *Molecular Ecology, 15*, 191-207. doi: 10.1111/j.1365-294X.2005.02757.x

Lesure, F.G., D'Agostino, J.P., & Gottfried, D. (1992). Mineral resource assessment of mafic and ultramafic rocks in the Greenville 1° x 2° quadrangle, South Carolina, Georgia, and North Carolina. *U.S. Department of the Interior, U.S. Geological Survey, to accompany Map MF-2198-C.*

Leigh, D.S., Price, K., & McDonald, J. (2014).Geomorphology and physical geography of Tallulah Gorge, northeast Georgia. *Field Trip Guidebook for the Southeastern Division of the Association of American Geographers Conference in Athens, Georgia, November 23, 2014. University of Georgia Geomorphology Laboratory Research Report 6*

Linari, C.L., Bierman, P.R., Portenga, E.W., Pavich, M.J., Finkel, R.C., & Freeman, S. (2016). Rates of erosion and landscape change along the Blue Ridge Escarpment, southern Appalachian Mountains, estimated from *in situ* cosmogenic ^{10}Be. *Earth Surface Processes and Landforms*. doi: 10.1002/esp.4051

Linkeviciene, R. (2009). Impact of river capture on hydrography and water resources: case study of Ula and Katra catchments, south Lithuania. *The Holocene, 19*(8), 1233-1240. Doi: 10.1177/0959683609345081

Lowery, R. (2017). VassarStats: Website for Statistical Computation. Vassarstats.net

Mast, M.A. & Turk, J.T. (1999). Environmental characteristics and water quality of Hydrologic Benchmark Network stations in the Eastern United States, 1963-95. *U.S. Geologic Survey Circular 1173-A*, 158p.

Mather, A.E. (2000). Impact of river capture on alluvial system development: an example from the Plio-Pleistocene of the Sorbas Basin, SE Spain. *Journal of the Geological Society, London, 157*, 957-966

Matmon, A., Bierman, P.R., Larsen, J., Southworth, S., Pavich, M., & Caffee, M. (2003). Temporally and spatially uniform rates of erosion in the southern Appalachian Great Smoky Mountains. *Geology*, *31*(2), 155-158. doi: 10.1130/0091-7613(2003)031<0155:TASURO>2.0.CO;2

Mikesell, L.R., Weissmann, G.S., & Karachewski, J.A. (2010). Stream capture and piracy recorded by provenance in fluvial fan strata. *Geomorphology*, *115*, 267-277. doi:10.1016/j.geomorph.2009.04.025

Miller, S.R., Sak, P.B., Kirby, E., & Bierman, P.R. (2013) Neogene rejuvenation of central Appalachian topography: Evidence for differential rock uplift from stream profiles and erosion rates. *Earth and Planetary Science Letters,369-370*, 1-12. http://dx.doi.org/10.1016/j.epsl.2013.04.007

National Oceanographic and Atmospheric Administration, National Centers for Environmental Information Document Library (accessed 10/25/2016). http://www.ncdc.noaa.gov/img/documentlibrary/clim81supp3/precipnormal_hires.jpg

Nelson, A.E., & Gillon, K.A. (1985). Stratigraphic nomenclature in the Richard Russell and Helen thrust sheets, Georgia and North Carolina, in Stratigraphic Notes, 1984: U.S. Geological Survey Bulletin 1605-A, p. A59-A62.

Nelson, A.E., Horton, J .W., Jr., & Clarke, J.W. (1987). Generalized tectonic map of the Greenville 1° x 2° quadrangle, Georgia, South Carolina, and North Carolina: U.S. Geological Survey Miscellaneous Field Studies Map MF-1898, scale 1:250,000.

Nelson, A. E. (1988). Stacked crystalline thrust sheets and episodes of regional metamorphism in northeastern Georgia and northwestern South Carolina-A reinterpretation: U.S. Geological Survey Bulletin 1822, 16 p.

Nelson, A.E. (1989), Geologic map of the Greenville 1 o x 2° quadrangle, Georgia, South Carolina, and North Carolina: U.S. Geological Survey Open-File Report 89-9, scale 1:250,000, 11 p.

Nelson, A.E., Horton, J.W. Jr., & Clarke, J.W. (1998). Geologic Map of the Greenville 1° x 2° quadrangle, Georgia, South Carolina, and North Carolina: U.S. Geological Survey Map I-2175, scale 1:250,000.

Nott, J., Youn, R., & McDougall, I. (1996). Wearing down, wearing back, and gorge extension in the long-term denudation of highland mass: Quantitative evidence from the Shoalhaven Catchment, Southeast Australia. *Journal of Geology*, *104*, 224-232. Doi: 0022-1376/96/10402-0004S01.00

Oldfield, F., Rummery, T.A., Thompson, R., & Walling, D.E. (1979). Identification of suspended sediment sources by means of magnetic measurements—Some preliminary results. Water Resources Research, 15 (2), 211–218. http://dx.doi.org/10.1029/WR015i002p00211

Oskin, M.E. & Burbank, D. (2007). Transient landscape evolution of basement-cored uplifts: Example of the Kyrgyz Range, Tian Shan. *Journal of Geophysical Research, 112*, F03S03. doi:10.1029/2006JF000563

Pastor, A., Babault, J., Teixell, A., & Arboleya, M.L. (2012). Intrinsic stream-capture control of stepped fan pediments in the High Atlas piedmont of Ouarzazate (Morocco). *Geomorphology, 173-174*, 88-103. doi:10.1016/j.geomorph.2012.05.032

Pazzaglia, F.J., Gardner, T.W. (1994). Late Cenozoic flexural deformation of the middle U. S. Atlantic passive margin: *Journal of Geophysical Research B Solid Earth and Planets, 99*, 12,143-12,157.

Pelletier, J.D. (2004) The influence of piedmont deposition of the time scale of mountain-belt denudation. *Geophysical Research Letters, 31*, L15502. doi:10.1029/2004GL020052

Peper, J.D., Lesure, F.G., Cox, L.J., & D'Agostino, J.P. (1991). Geology, geochemistry, and mineral resource assessment of the Southern Nantahala Wilderness and adjacent roadless areas, Rabun and Towns counties, Georgia, and Clay and Macon counties, North Carolina. *U.S. Geological Survey Belletin 1883*.

Polyakov, V., Kimoto, A., Nearing, M., & Nichols, M. (2010). Tracing sediment movement on a semi-arid watershed using rare earth elements. *Las Vegas, Nevada, 2nd Joint Federal Interagency Conference, June 27–July 1, 2010*. *http://acwi.gov/sos/pubs/2ndJFIC/Contents/4C_Polyakov_06_29_10_paper.pdf*.

Portenga, E. & Bierman, P. R. (2011). Understanding Earth's Eroding Surface with ^{10}Be. *GSA Today, 21 (*8), 4-10.

Prince, P.S., Spotila, J.A., & Henika, W.S. (2010). New physical evidence of the role of stream capture in active retreat of the Blue Ridge escarpment, southern Appalachians. *Geomorphology, 123*, 305-319. doi:10.1016/j.geomorph.2010.07.023

Prince, P.S., Spotila, J.A., & Henika, W.S. (2011). Stream capture as a driver of transient landscape evolution in a tectonically quiescent setting. *Geology, 39*, 823-826. doi:10.1130/G32008.1

Reiners, P.W. & Brandon, M.T. (2006). Using thermochronology to understand orogenic erosion. *Annual Review of Earth and Planetary Science*, *34*, 419-466. doi: 10.1146/ annurev.earth.34.031405.125202

Richmond, G.M. & Fullerton, D.S. (1986). Introduction To Quaternary Glaciations in the United States of America, *in* Sibrava, V, Bowen, DQ, and Richmond, GM, eds., Quaternary Glaciations in the Northern Hemisphere: Oxford, New York, Pergamon Press : 3-10.

Ryan, P.C. (2014). *Environmental and Low Temperature Geochemistry*. Wiley Blackwell. P. 265

Sella, G.F., Stein, S., Dixon, T.H., Craymer, M., James, T.S., Mazzotti, S., & Dokka, R.K. (2007). Observation of glacial isostatic adjustment in "stable" North America with GPS. *Geophysical Research Letters, 34,* L02306. doi:10.1029/2006GL027081

Schonhuth, S., Blum, M.J., Lozano-Vilano, L., Neely, D.A., Valera-Romero, A., Espinosa. H, Perdices, A., & Mayden, L. (2011). Inter-basin exchange and repeated headwater capture across the Sierra Madre Occidental inferred from the phylogeography of Mexican stonerollers. *Journal of Biogeography, 38*, 1406-1421. doi:10.1111/j.1365-2699.2011.02481.x

Slingerland, R. & Furlong, K.P. (1989). Geodynamic and geomorphic evolution of the Permo-Triassic Appalachian Mountains. *Geomorphology*, *2*, 23-37.

Smith, S.M. (2006). National Geochemical Database—Reformatted Data from the National Uranium Resource Evaluation (NURE) Hydrogeochemical and Stream Sediment Reconnaissance (HSSR) Program. *U.S. Department of the Interior, U.S. Geological Survey.*

Spotila, J.A., Bank, G.C., Reiners, P.W., Naeser, C.W., & Henika, W.S. (2004). Origin of the Blue Ridge Escarpment along the passive margin of eastern North America. *Basin Research*, *16*, 41–63. doi:10.1111/j.1365-2117.2003.00219.x

United States Department of Agriculture, Natural Resources Conservation Service (accessed 2017). Geospatial Data Gateway. https://datagateway.nrcs.usda.gov

United States Geological Survey (2001). Geochemistry of unconsolidated sediments in the U.S. from the RASS database: U.S. Geological Survey, Reston, VA.

United States Geological Survey (2008). Geochemistry of rock samples from the National Geochemical Database. U.S. Department of the Interior.

United States Geological Survey (accessed 2017. Mineral Resource Data System. U.S. Department of the Interior. https://mrdata.usgs.gov/mrds

United States Geological Survey (accessed 2017). National Hydrography Dataset. U.S. Department of the Interior

United States Geological Survey (accessed 2017). National Water Information System. U.S. Department of the Interior. https://waterdata.usgs.gov/nwis

United States Geological Survey (accessed 2017). National Watershed Boundary Dataset. U.S.

Department of the Interior

Voss, S.R., Smith, D.G., Beachy, C.K., & Heckel, D.G. (1995). Allozyme variation in Neighboring isolated populations of the plethodontid salamander *Leurognathus Marmoratus. Journal of Herpetology, 29*(3), 493-497.

Walden, J., Slattery, M.C., & Burt, T.P. (1997). Use of mineral magnetic measurements to fingerprint suspended sediment sources—Approaches and techniques for data analysis. *Journal of Hydrology*, *202* (1–4), 353–372. *http://dx.doi.org/10.1016/S0022-1694(97)00078-4*

Walker, F. & Allen, M.B. (2012). Offset rivers, drainage spacing and the record of strike-slip faulting: the Kuh Banan Fault, Iran. *Tectonophysics, 530-531,* 251-263. doi:10.1016/j.tecto.2012.01.001

Wall, G.J., & Wilding, L.P. (1976). Mineralogy and related parameters of fluvial suspended sediments in northwestern Ohio. *Journal of Environmental Quality*, *5* (*2*), 168–173. http://dx.doi.org/10.2134/jeq1976.00472425000500020012x

Walling, D.E., Peart, M.R., Oldfield, F., & Thompson R. (1979). Suspended sediment sources identified by magnetic measurements. *Nature*, *281*, 110–113. *http://dx.doi.org/10.1038/281110a0*

Walling, D.E. (2005). Tracing suspended sediment sources in catchments and river systems. *Science of the Total Environment, 344,* 159-184. doi:10.1016/j.scitotenv.2005.02.011

Willett, S.D., McCoy, S.W., Perron, J.T., Goren, L. & Chen, C. (2014). Dynamic reorganization of river basins. *Science, 343*, 1248765-1-9. doi: 10.1126/science.1248765

Yang, C.T. & Stall, J.B. (1974). Unit stream power for sediment transport in natural rivers. *University of Illinois at Urbana-Champaign Water Resources Center, Research Report No. 88,* Illinois State Water Survey

APPENDICES

Appendix A – Sample Statistics

Appendix A.1 – Statistics: Tallulah Rock

Tallulah Rock Statistics

		SiO2	Al2O3	Fe2O3	FeO	MgO	CaO	Na2O
	Valid	36	36	36	33	36	36	36
N	Missing	0	0	0	3	0	0	0
Mean		50.347222	13.80417	7.982222	7.6606061	10.94	7.4136111	1.5736111
Median		46.4	14.95	6.31	7.8	7.55	9	1.8
Mode		46.4	14.5	2.70000a	10.2	10.90000a	11.20000a	2.5
Std. Deviation		10.085477	5.164755	4.6056	3.20886851	11.75661	4.20742755	0.9122191
Variance		101.717	26.675	21.212	10.297	138.218	17.702	0.832
Skewness		1.199	-1.512	0.645	0.3	1.914	-0.519	-0.409
Std. Error of		0.393	0.393	0.393	0.409	0.393	0.393	0.393
Kurtosis		0.482	1.764	-0.883	1.037	3.056	-1.01	-1.056
Std. Error of		0.768	0.768	0.768	0.798	0.768	0.768	0.768
Range		39.7	21.21	15.6	15.5	45.45	13.79	3.08
Minimum		37.9	0.29	2.4	1.5	0.35	0.01	0.01
Maximum		77.6	21.5	18	17	45.8	13.8	3.09

		K2O	TiO2	P2O5	MnO	LOI
	Valid	36	36	36	36	17
N	Missing	0	0	0	0	19
Mean		0.5222222	0.918333	0.109167	0.1719444	1.622353
Median		0.225	0.905	0.095	0.19	0.85
Mode		.02000a	.34000a	0.05	0.2	.34000a
Std. Deviation		0.7303976	0.851484	0.058082	0.05103609	2.184601
Variance		0.533	0.725	0.003	0.003	4.772
Skewness		2.314	3.364	1.597	-0.446	2.4
Std. Error of		0.393	0.393	0.393	0.393	0.55
Kurtosis		5.068	15.548	3.258	0.092	5.048
Std. Error of		0.768	0.768	0.768	0.768	1.063
Range		3.06	5.02	0.27	0.24	7.69
Minimum		0.02	0.01	0.04	0.05	0.3
Maximum		3.08	5.03	0.31	0.29	7.99

a. Multiple modes exist. The smallest value is shown

Appendix A.2 – Statistics: All Stream Sediment Samples

Statistics - All Samples

		U_ppm	Ag_ppm	Al_pct	Au_ppm	Be_ppm	Ca_pct	Ce_ppm
	Valid	185	91	185	92	90	0	183
N	Missing	0	94	0	93	95	185	2
Mean		11.477	0.3066	5.9152	0.016891	0.8256		263.372
Median		7.4	0.25	5.49	0.005	1		160
Mode		7.4	0.25	6.69	0.005	.50a		10
Std. Deviation		12.226	0.11431	2.19103	0.0594002	0.44249		435.7797
Variance		149.474	0.013	4.801	0.004	0.196		189903.92
Skewness		4.271	1.762	0.701	6.175	0.845		5.1
Std. Error of		0.179	0.253	0.179	0.251	0.254		0.18
Kurtosis		25.829	1.936	0.242	42.351	0.336		33.45
Std. Error of		0.355	0.5	0.355	0.498	0.503		0.357
Range		98.1	0.45	11.57	0.471	1.75		3677
Minimum		2	0.25	1.48	0.005	0.25		10
Maximum		100.1	0.7	13.05	0.476	2		3687

		Co_ppm	Cr_ppm	Cu_ppm	Dy_ppm	Eu_ppm	F_ppm	Fe_pct
	Valid	91	90	91	184	174	93	183
N	Missing	94	95	94	1	11	92	2
Mean		4.841	4.733	7.088	22.5666	2.7739	182.097	3.1082
Median		2.5	2.5	6	14.9	1.05	150	2.34
Mode		2.5	2.5	3	16	.20a	150	1.79a
Std. Deviation		3.4025	3.8797	5.2676	25.26012	4.04552	259.7359	2.43035
Variance		11.577	15.052	27.748	638.074	16.366	67462.741	5.907
Skewness		2.136	3.467	1.69	3.355	2.675	4.032	2.815
Std. Error of		0.253	0.254	0.253	0.179	0.184	0.25	0.18
Kurtosis		6.749	19.228	2.967	15.432	9.691	17.027	11.56
Std. Error of		0.5	0.503	0.5	0.356	0.366	0.495	0.357
Range		19.5	27.5	24	187.85	27.4	1568	18.18
Minimum		2.5	2.5	1	0.05	0.2	15	0.57
Maximum		22	30	25	187.9	27.6	1583	18.75

		Hf_ppm	K_pct	La_ppm	Li_ppm	Lu_ppm	Mg_pct	Mn_ppm
	Valid	185	90	178	90	183	90	185
N	Missing	0	95	7	95	2	95	0
Mean		95.757	1.3184	145.09	5.617	3.227	0.218259	1136.973
Median		56	1	77.5	6	2.1	0.2	930
Mode		29.0a	0.8	3.0a	2.5	1.3	0.23	930
Std. Deviation		122.9059	0.74261	248.3429	2.9386	3.332	0.114719	699.5189
Variance		15105.859	0.551	61674.21	8.635	11.102	0.013	489326.66
Skewness		3.018	1.044	5.761	0.921	2.549	2.007	2.083
Std. Error of		0.179	0.254	0.182	0.254	0.18	0.254	0.179
Kurtosis		10.855	0.357	41.437	1.122	8.687	5.796	7.097
Std. Error of		0.355	0.503	0.362	0.503	0.357	0.503	0.355
Range		762	3.2	2127	13.5	21.5	0.68	4940
Minimum		3	0.4	3	2.5	0.1	0.065	240
Maximum		765	3.6	2130	16	21.6	0.745	5180

a. Multiple modes exist. The smallest value is shown

Statistics - All Samples

		Mo_ppm	Na_pct	Nb_ppm	Ni_ppm	P_ppm	Pb_ppm	Sc_ppm
	Valid	91	92	90	91	90	91	185
N	Missing	94	93	95	94	95	94	0
Mean		2.566	0.8017	14.067	5.78	850	7.626	9.759
Median		2.5	0.61	10	5	850	5	8.1
Mode		2.5	.31a	2.5	2.5	300	5	5
Std. Deviation		0.4485	0.51923	11.9649	3.996	543.656	3.5983	6.0374
Variance		0.201	0.27	143.158	15.968	295561.8	12.948	36.45
Skewness		6.912	1.146	1.328	1.252	1.365	1.115	1.373
Std. Error of		0.253	0.251	0.254	0.253	0.254	0.253	0.179
Kurtosis		48.02	0.734	2.647	0.989	2.91	0.438	1.797
Std. Error of		0.5	0.498	0.503	0.5	0.503	0.5	0.355
Range		3.5	2.27	62.5	15.5	2600	15	29.9
Minimum		2.5	0.12	2.5	2.5	200	5	2.5
Maximum		6	2.39	65	18	2800	20	32.4

		Sm_ppm	Sn_ppm	Sr_ppm	Th_ppm	Ti_ppm	V_ppm	W_ppm
	Valid	179	91	90	182	182	185	91
N	Missing	6	94	95	3	3	0	94
Mean		42.346	11.516	28.4	40.874	17962.09	112.973	1.099
Median		15	10	25	22	14350	70	1
Mode		4.0a	5	25	2.0a	22800	40	1
Std. Deviation		133.4833	9.2103	17.2391	70.2856	15870.98	132.3259	0.5176
Variance		17817.8	84.83	297.187	4940.067	2.52E+08	17510.14	0.268
Skewness		7.928	1.334	7.324	5.665	2.517	4.256	6.044
Std. Error of		0.182	0.253	0.254	0.18	0.18	0.179	0.253
Kurtosis		71.006	1.723	60.249	40.753	8.831	24.421	39.663
Std. Error of		0.361	0.5	0.503	0.358	0.358	0.355	0.5
Range		1394.5	42.5	150	636	103600	1080	4
Minimum		0.5	2.5	25	2	800	20	1
Maximum		1395	45	175	638	104400	1100	5

		Y_ppm	Yb_ppm	Zn_ppm	Mean 9REE	Ti/9REE	U/9REE	Co/Fe (ppm)
	Valid	91	175	91	185	185	185	183
N	Missing	94	10	94	0	0	0	2
Mean		35.736	13.566	26.011	60.625502	631.9207	0.2964	0.000079
Median		20	10.9	22	36.477778	328.8156	0.232848	0
Mode		15	0.9	22	4.1250a	0	.0808a	0
Std. Deviation		44.6408	11.6821	12.4842	99.7332533	976.0217	0.231789	0.0001086
Variance		1992.802	136.472	155.855	9946.722	952618.4	0.054	0
Skewness		3.228	2.773	1.269	5.648	5.801	3.381	1.95
Std. Error of		0.253	0.184	0.253	0.179	0.179	0.179	0.18
Kurtosis		12.155	10.831	2.382	39.949	48.945	16.423	5.636
Std. Error of		0.5	0.365	0.5	0.355	0.355	0.355	0.357
Range		257.5	85.3	72	842.5083	10105.26	1.8459	0.0006
Minimum		2.5	0.9	5	4.125	0	0.0808	0
Maximum		260	86.2	77	846.6333	10105.26	1.9267	0.0006

a. Multiple modes exist. The smallest value is shown

Statistics - All Samples

		Cu/Fe (ppm)	U/Ti	U/Th	U/Pb	Heavy REE	Light REE	Lu/Zn	Mean Cu, Pb, Zn
N	Valid	183	182	182	91	185	185	91	91
	Missing	2	3	3	94	0	0	94	94
Mean		0.000108	0.000883	0.528182	1.710183	16.70303	123.8728	0.08413	13.57509
Median		0	0.00067	0.373547	1.02	8.76	74.1	0.052	12
Mode		0	.0000a	.4000a	0.9	1.8500a	15.5000a	0.04	7.6667a
Std. Deviation		0.000141	0.000791	0.4645555	1.673933	32.42823	201.1167	0.1127406	6.503383
Variance		0	0	0.216	2.802	1051.59	40447.91	0.013	42.294
Skewness		1.389	2.791	2.152	1.898	7.085	5.435	3.69	1.412
Std. Error of		0.18	0.18	0.18	0.253	0.179	0.179	0.253	0.253
Kurtosis		1.842	10.538	4.137	3.605	59.17	38.099	15.899	2.734
Std. Error of		0.357	0.358	0.358	0.5	0.355	0.355	0.5	0.5
Range		0.0007	0.0053	2.1389	8.63	325.8175	1800.767	0.6887	36.6667
Minimum		0	0	0.1111	0.13	0.8625	9	0.0013	4
Maximum		0.0007	0.0053	2.25	8.76	326.68	1809.767	0.69	40.6667

		Mean Co, Ni, Cu	Mean Al, Fe, Ti	Ce/Lu	La/Yb	La/Lu	Sm/Yb	Ce/Yb	Sc/Ti
N	Valid	91	185	183	173	178	173	175	182
	Missing	94	0	2	12	7	12	10	3
Mean		5.90293	58986490	125.71817	10.74409	67.90895	2.384529	20.088296	0.001507
Median		5	47333336	59.677419	7.1875	37.69231	1.369863	14.388489	0.000547
Mode		2.6667	4.2650a	400	3.3333	20	.5556a	1.3699a	.0003a
Std. Deviation		3.914366	52953225	167.7200907	10.30871	81.14143	3.103626	19.986631	0.004139
Variance		15.322	2.8E+15	28130.029	106.27	6583.932	9.632	399.465	0
Skewness		1.566	2.499	2.332	2.622	2.373	3.995	2.316	7.272
Std. Error of		0.253	0.179	0.18	0.185	0.182	0.185	0.184	0.18
Kurtosis		2.405	8.782	5.559	8.147	6.138	21.174	7.743	60.342
Std. Error of		0.5	0.355	0.357	0.367	0.362	0.367	0.365	0.358
Range		18	3.48E+08	867.561	59.1826	416.8551	24.4916	132.6622	0.0404
Minimum		2	4.265	2.439	0.1508	0.4918	0.0251	0.6711	0.0001
Maximum		20	3.48E+08	870	59.3333	417.3469	24.5167	133.3333	0.0405

		Y/Ti	La/Ti	Ce/Ti	Sm/Ti	Eu/Ti	Dy/Ti	Yb/Ti	Lu/Ti
N	Valid	89	176	180	177	172	181	173	180
	Missing	96	9	5	8	13	4	12	5
Mean		0.003429	0.009599	0.017514	0.002624	0.000218	0.001643	0.000989	0.000222
Median		0.00219	0.006066	0.010523	0.001105	0.00008	0.001274	0.000733	0.000167
Mode		.0008a	.0017a	.0001a	.0003a	0.0001	.0000a	0.001	0.0001
Std. Deviation		0.004745	0.009733	0.0185749	0.005573	0.000355	0.001477	0.0009365	0.000211
Variance		0	0	0	0	0	0	0	0
Skewness		4.199	2.024	1.97	5.456	3.353	2.195	3.394	2.738
Std. Error of		0.255	0.183	0.181	0.183	0.185	0.181	0.185	0.181
Kurtosis		21.777	5.396	4.842	35.051	13.796	5.99	15.859	10.269
Std. Error of		0.506	0.364	0.36	0.363	0.368	0.359	0.367	0.36
Range		0.0337	0.0608	0.11	0.0459	0.0024	0.0088	0.0069	0.0014
Minimum		0.0001	0.0002	0.0001	0	0	0	0.0001	0
Maximum		0.0338	0.061	0.1101	0.0459	0.0024	0.0088	0.007	0.0014

a. Multiple modes exist. The smallest value is shown

Appendix A.3 – Statistics: Tallulah Basin Sediment Samples

Tallulah Statistics

		U_ppm	Ag_ppm	Al_pct	Au_ppm	Be_ppm	Ca_pct	Ce_ppm
	Valid	70	35	70	35	35	0	70
N	Missing	0	35	0	35	35	70	0
Mean		7.136	0.37	7.0877	0.009229	0.8857		139.814
Median		5.85	0.25	6.705	0.005	1		148.5
Mode		3.8[a]	0.25	5.25[a]	0.005	1		10
Std. Deviation		4.0116	0.13677	2.16764	0.0250166	0.51927		103.6985
Variance		16.093	0.019	4.699	0.001	0.27		10753.371
Skewness		2.313	0.44	0.657	5.916	0.677		0.91
Std. Error of		0.287	0.398	0.287	0.398	0.398		0.287
Kurtosis		5.346	-1.27	0.085	35	-0.207		1.913
Std. Error of		0.566	0.778	0.566	0.778	0.778		0.566
Range		18.5	0.45	10.2	0.148	1.75		504
Minimum		3.6	0.25	2.85	0.005	0.25		10
Maximum		22.1	0.7	13.05	0.153	2		514

		Co_ppm	Cr_ppm	Cu_ppm	Dy_ppm	Eu_ppm	F_ppm	Fe_pct
	Valid	35	35	35	70	64	35	70
N	Missing	35	35	35	0	6	35	0
Mean		5.614	3.171	7.514	14.3614	2.4313	195.086	3.8671
Median		5	2.5	6	13.9	1.3	150	2.6
Mode		2.5	2.5	4	16	0.35	150	1.59[a]
Std. Deviation		3.4537	1.8902	4.859	7.95313	3.14605	288.8745	3.31651
Variance		11.928	3.573	23.61	63.252	9.898	83448.492	10.999
Skewness		0.949	3.061	1.419	0.629	2.427	3.847	2.174
Std. Error of		0.398	0.398	0.398	0.287	0.299	0.398	0.287
Kurtosis		0.53	8.926	2.591	-0.232	6.871	14.456	5.826
Std. Error of		0.778	0.778	0.778	0.566	0.59	0.778	0.566
Range		13.5	7.5	22	32.3	16.25	1425	18.13
Minimum		2.5	2.5	2	2.4	0.35	20	0.62
Maximum		16	10	24	34.7	16.6	1445	18.75

		Hf_ppm	K_pct	La_ppm	Li_ppm	Lu_ppm	Mg_pct	Mn_ppm
	Valid	70	35	70	35	70	35	70
N	Missing	0	35	0	35	0	35	0
Mean		62.814	1.596	76.514	4.443	2.487	0.241	1205
Median		46.5	1.2	63	5	1.95	0.225	1005
Mode		36.0[a]	0.8	50.0[a]	2.5	0.9	0.23	910
Std. Deviation		56.1972	0.88773	59.9896	2.075	2.0657	0.1334706	670.2579
Variance		3158.124	0.788	3598.746	4.305	4.267	0.018	449245.65
Skewness		2.532	0.702	2.734	0.384	1.467	2.074	1.208
Std. Error of		0.287	0.398	0.287	0.398	0.287	0.398	0.287
Kurtosis		7.637	-0.75	10.061	-1.466	2.05	5.726	1.616
Std. Error of		0.566	0.778	0.566	0.778	0.566	0.778	0.566
Range		312	3.1	336	5.5	9.1	0.68	3430
Minimum		12	0.5	16	2.5	0.2	0.065	240
Maximum		324	3.6	352	8	9.3	0.745	3670

a. Multiple modes exist. The smallest value is shown

Tallulah Statistics

		Mo_ppm	Na_pct	Nb_ppm	Ni_ppm	P_ppm	Pb_ppm	Sc_ppm
	Valid	35	35	34	35	35	35	70
N	Missing	35	35	36	35	35	35	0
Mean		2.5	0.906	13.75	7.029	677.143	9.343	9.129
Median		2.5	0.81	10	6	500	10	7.7
Mode		2.5	.56[a]	10	2.5	300	10	3.9
Std. Deviation		0	0.49771	8.7527	4.3991	402.2625	3.3602	5.1857
Variance		0	0.248	76.61	19.352	161815.1	11.291	26.892
Skewness			1.038	0.626	0.74	0.7	-0.05	0.89
Std. Error of		0.398	0.398	0.403	0.398	0.398	0.398	0.287
Kurtosis			0.898	-0.284	-0.241	-1.005	-0.996	0.095
Std. Error of		0.778	0.778	0.788	0.778	0.778	0.778	0.566
Range		0	2.16	32.5	15.5	1300	10	20.7
Minimum		2.5	0.22	2.5	2.5	200	5	3.1
Maximum		2.5	2.38	35	18	1500	15	23.8

		Sm_ppm	Sn_ppm	Sr_ppm	Th_ppm	Ti_ppm	V_ppm	W_ppm
	Valid	70	35	35	70	69	70	35
N	Missing	0	35	35	0	1	0	35
Mean		14.3	8.929	32.114	21.129	20350.73	152.714	1.086
Median		12	5	25	19	15900	80	1
Mode		5	2.5	25	2	8400.0[a]	30.0[a]	1
Std. Deviation		10.4512	6.7597	26.6135	14.846	16543.89	195.1508	0.3735
Variance		109.228	45.693	708.281	220.404	2.74E+08	38083.83	0.139
Skewness		1.954	0.76	4.907	1.279	2.751	2.969	4.645
Std. Error of		0.287	0.398	0.398	0.287	0.289	0.287	0.398
Kurtosis		6.156	-0.668	26	2.442	10.189	10.331	22.197
Std. Error of		0.566	0.778	0.778	0.566	0.57	0.566	0.778
Range		61	22.5	150	75	100100	1080	2
Minimum		2	2.5	25	2	4300	20	1
Maximum		63	25	175	77	104400	1100	3

		Y_ppm	Yb_ppm	Zn_ppm	Mean 9REE	Ti/9REE	U/9REE	Co/Fe (ppm)
	Valid	35	68	35	70	70	70	70
N	Missing	35	2	35	0	0	0	0
Mean		17.571	10.029	30.429	33.242698	1000.986	0.27804	0.000077
Median		15	9.55	31	31.716319	587.2913	0.219222	0.000021
Mode		15	1.5[a]	31	5.9750[a]	.0000[a]	.1064[a]	0
Std. Deviation		9.8609	4.8715	12.0252	22.0783082	1390.624	0.158738	0.0000972
Variance		97.237	23.731	144.605	487.452	1933835	0.025	0
Skewness		1.021	0.862	0.336	1.605	4.43	1.25	1.209
Std. Error of		0.398	0.291	0.398	0.287	0.287	0.287	0.287
Kurtosis		2.187	1.131	-0.15	4.765	26.44	0.66	0.649
Std. Error of		0.778	0.574	0.778	0.566	0.566	0.566	0.566
Range		47.5	25.1	52	116.75	10105.26	0.6195	0.0004
Minimum		2.5	1.5	5	5.975	0	0.1064	0
Maximum		50	26.6	57	122.725	10105.26	0.7258	0.0004

a. Multiple modes exist. The smallest value is shown

Tallulah Statistics

		Cu/Fe (ppm)	U/Ti	U/Th	U/Pb	Heavy REE	Light REE	Lu/Zn	Mean Cu, Pb, Zn
	Valid	70	69	70	35	70	70	35	35
N	Missing	0	1	0	35	0	0	35	35
Mean		0.000098	0.000511	0.557494	0.881857	8.887571	67.70655	0.051074	15.76191
Median		0.000029	0.000382	0.33875	0.65	7.815	63.27083	0.038095	15.66667
Mode		0	.0000[a]	1.9	.5300[a]	7.7	15.5000[a]	.0290[a]	9.6667
Std. Deviation		0.000115	0.000372	0.5464063	0.738926	4.707937	47.0935	0.0460683	6.101843
Variance		0	0	0.299	0.546	22.165	2217.798	0.002	37.232
Skewness		0.77	1.425	2.096	3.09	1.281	1.596	2.33	0.435
Std. Error of		0.287	0.289	0.287	0.398	0.287	0.287	0.398	0.398
Kurtosis		-0.628	1.709	3.105	11.777	1.997	4.982	7.441	-0.004
Std. Error of		0.566	0.57	0.566	0.778	0.566	0.566	0.778	0.778
Range		0.0004	0.0017	2.1056	3.94	24.49	264.4	0.2349	27
Minimum		0	0	0.1444	0.26	2.16	9	0.0051	4
Maximum		0.0004	0.0017	2.25	4.2	26.65	273.4	0.24	31

		Mean Co, Ni, Cu	Mean Al, Fe, Ti	Ce/Lu	La/Yb	La/Lu	Sm/Yb	Ce/Yb	Sc/Ti
	Valid	35	70	70	68	70	68	68	69
N	Missing	35	0	0	2	0	2	2	1
Mean		6.719048	66866670	102.379442	8.790934	56.67774	1.65088	16.329942	0.00059
Median		5.5	52666671	53.197279	6.919077	33.32512	1.222001	12.762598	0.00053
Mode		2.6667[a]	11.6650[a]	7.6923[a]	2.0805[a]	20	.3509[a]	.6711[a]	.0001[a]
Std. Deviation		4.081036	55342366	151.2403407	8.408799	70.21532	1.580054	18.551238	0.00037
Variance		16.655	3.06E+15	22873.641	70.708	4930.191	2.497	344.148	0
Skewness		1.105	2.708	3.575	4.011	3.135	3.449	4.074	0.867
Std. Error of		0.398	0.287	0.287	0.291	0.287	0.291	0.291	0.289
Kurtosis		1.16	10.031	14.954	20.378	11.485	16.007	23.488	0.43
Std. Error of		0.778	0.566	0.566	0.574	0.566	0.574	0.574	0.57
Range		17	3.48E+08	867.561	57.2528	380.8537	10.3158	132.6622	0.0016
Minimum		2.3333	11.665	2.439	2.0805	4.1463	0.3509	0.6711	0.0001
Maximum		19.3333	3.48E+08	870	59.3333	385	10.6667	133.3333	0.0018

		Y/Ti	La/Ti	Ce/Ti	Sm/Ti	Eu/Ti	Dy/Ti	Yb/Ti	Lu/Ti
	Valid	34	69	69	69	63	69	67	69
N	Missing	36	1	1	1	7	1	3	1
Mean		0.001495	0.005995	0.010897	0.001098	0.000186	0.001057	0.00062	0.000149
Median		0.001319	0.003538	0.007019	0.000673	0.000069	0.000863	0.000501	0.000106
Mode		.0001[a]	.0002[a]	.0001[a]	.0000[a]	0	.0001[a]	.0001[a]	0.0001
Std. Deviation		0.001054	0.006205	0.0109018	0.001087	0.000283	0.000787	0.0003688	0.000123
Variance		0	0	0	0	0	0	0	0
Skewness		0.876	2.097	1.411	1.905	3.048	0.761	1.284	1.895
Std. Error of		0.403	0.289	0.289	0.289	0.302	0.289	0.293	0.289
Kurtosis		0.54	4.814	1.797	4.313	11.478	-0.276	1.465	4.499
Std. Error of		0.788	0.57	0.57	0.57	0.595	0.57	0.578	0.57
Range		0.0044	0.0305	0.0466	0.0057	0.0016	0.0032	0.0017	0.0006
Minimum		0.0001	0.0002	0.0001	0	0	0.0001	0.0001	0
Maximum		0.0045	0.0307	0.0467	0.0057	0.0016	0.0032	0.0018	0.0007

a. Multiple modes exist. The smallest value is shown

Appendix A.4 – Statistics: Soque Basin Sediment Samples

Soque Statistics

		U_ppm	Ag_ppm	Al_pct	Au_ppm	Be_ppm	Ca_pct	Ce_ppm
	Valid	65	32	65	32	31	0	65
N	Missing	0	33	0	33	34	65	0
Mean		18.837	0.2797	5.1111	0.032344	0.7758		468.138
Median		13.6	0.25	4.66	0.005	0.5		310
Mode		8.4	0.25	4.63	0.005	0.5		15.0[a]
Std. Deviation		17.2159	0.09826	1.94492	0.0955833	0.38381		615.5815
Variance		296.386	0.01	3.783	0.009	0.147		378940.53
Skewness		3.12	3.441	0.798	3.914	0.582		3.856
Std. Error of		0.297	0.414	0.297	0.414	0.421		0.297
Kurtosis		12.294	11.785	0.369	16.061	-0.642		17.412
Std. Error of		0.586	0.809	0.586	0.809	0.821		0.586
Range		95.6	0.45	8.8	0.471	1.25		3672
Minimum		4.5	0.25	1.48	0.005	0.25		15
Maximum		100.1	0.7	10.28	0.476	1.5		3687

		Co_ppm	Cr_ppm	Cu_ppm	Dy_ppm	Eu_ppm	F_ppm	Fe_pct
	Valid	32	31	32	65	63	33	65
N	Missing	33	34	33	0	2	32	0
Mean		3.719	7.581	6.938	36.0015	3.9444	193.848	2.8608
Median		2.5	7	5	25.2	2	150	2.51
Mode		2.5	7	3	14.90[a]	0.2	150	1.49[a]
Std. Deviation		2.102	4.96	5.8966	34.45583	5.09271	307.5299	1.5421
Variance		4.418	24.602	34.77	1187.204	25.936	94574.633	2.378
Skewness		1.69	3.115	1.741	2.464	2.157	3.54	1.435
Std. Error of		0.414	0.421	0.414	0.297	0.302	0.409	0.297
Kurtosis		1.96	14.02	2.672	7.488	6.597	13.662	2.758
Std. Error of		0.809	0.821	0.809	0.586	0.595	0.798	0.586
Range		7.5	27.5	23	184	27.4	1563	8.19
Minimum		2.5	2.5	2	3.9	0.2	20	0.57
Maximum		10	30	25	187.9	27.6	1583	8.76

		Hf_ppm	K_pct	La_ppm	Li_ppm	Lu_ppm	Mg_pct	Mn_ppm
	Valid	65	31	65	31	65	31	65
N	Missing	0	34	0	34	0	34	0
Mean		146.969	1.2452	257.492	6.339	4.695	0.195429	1192.923
Median		82	1	147	6	3.2	0.16	990
Mode		32.0[a]	0.6	118	6	1.0[a]	0.16	820
Std. Deviation		159.152	0.65668	362.8967	2.4474	4.4426	0.1121102	845.9642
Variance		25329.374	0.431	131694	5.99	19.736	0.013	715655.39
Skewness		2.268	0.537	4.128	0.398	1.97	2.144	2.451
Std. Error of		0.297	0.421	0.297	0.421	0.297	0.421	0.297
Kurtosis		5.419	-1.142	19.204	0.854	4.09	5.459	8.108
Std. Error of		0.586	0.821	0.586	0.821	0.586	0.821	0.586
Range		744	2.1	2094	10.5	21.1	0.5333	4820
Minimum		21	0.4	36	2.5	0.5	0.075	360
Maximum		765	2.5	2130	13	21.6	0.6083	5180

a. Multiple modes exist. The smallest value is shown

Soque Statistics

		Mo_ppm	Na_pct	Nb_ppm	Ni_ppm	P_ppm	Pb_ppm	Sc_ppm
	Valid	32	32	32	32	31	32	65
N	Missing	33	33	33	33	34	33	0
Mean		2.688	0.5162	17.453	5.172	1303.226	6.25	8.023
Median		2.5	0.475	17.5	2.5	1100	5	6.7
Mode		2.5	.31[a]	2.5	2.5	1000	5	4.9[a]
Std. Deviation		0.7487	0.24608	15.3015	3.9648	536.9568	2.8398	4.231
Variance		0.56	0.061	234.135	15.72	288322.6	8.065	17.901
Skewness		3.978	1.552	1.114	1.861	1.945	2.254	1.274
Std. Error of		0.414	0.414	0.414	0.414	0.421	0.414	0.297
Kurtosis		15.262	2.514	1.529	3.29	3.174	4.259	0.955
Std. Error of		0.809	0.809	0.809	0.809	0.821	0.809	0.586
Range		3.5	1.05	62.5	15.5	2000	10	17.3
Minimum		2.5	0.24	2.5	2.5	800	5	2.5
Maximum		6	1.29	65	18	2800	15	19.8

		Sm_ppm	Sn_ppm	Sr_ppm	Th_ppm	Ti_ppm	V_ppm	W_ppm
	Valid	65	32	31	64	65	65	32
N	Missing	0	33	34	1	0	0	33
Mean		78.308	8.141	25.839	74.922	21621.54	93.077	1.063
Median		34	5	25	45.5	16700	70	1
Mode		9.0a	5	25	21	22800	40	1
Std. Deviation		205.2846	5.0068	4.6697	103.1116	16750.14	65.8579	0.3536
Variance		42141.75	25.068	21.806	10632.01	2.81E+08	4337.26	0.125
Skewness		5.466	1.363	5.568	4.064	2.436	1.065	5.657
Std. Error of		0.297	0.414	0.421	0.299	0.297	0.297	0.414
Kurtosis		31.33	1.657	31	18.956	7.254	0.373	32
Std. Error of		0.586	0.809	0.821	0.59	0.586	0.586	0.809
Range		1391	20.5	26	631	92600	280	2
Minimum		4	2.5	25	7	4700	20	1
Maximum		1395	23	51	638	97300	300	3

		Y_ppm	Yb_ppm	Zn_ppm	Mean 9REE	Ti/9REE	U/9REE	Co/Fe (ppm)
	Valid	32	65	32	65	65	65	65
N	Missing	33	0	33	0	0	0	0
Mean		63.594	18.889	22.781	107.226902	361.4091	0.237243	0.000063
Median		40	13.9	21.5	65.655556	235.2156	0.227084	0
Mode		35	9.2	17.0a	13.5500a	39.5685a	.0861a	0
Std. Deviation		62.5659	14.9449	11.4377	145.059011	336.0018	0.117868	0.0000818
Variance		3914.491	223.349	130.822	21042.117	112897.2	0.014	0
Skewness		2.021	2.282	1.188	4.142	1.947	1.489	1.228
Std. Error of		0.414	0.297	0.414	0.297	0.297	0.297	0.297
Kurtosis		3.956	6.377	0.907	19.314	3.783	3.523	0.662
Std. Error of		0.809	0.586	0.809	0.586	0.586	0.586	0.586
Range		257.5	83.4	45	833.0833	1616.249	0.615	0.0003
Minimum		2.5	2.8	7	13.55	39.5685	0.0861	0
Maximum		260	86.2	52	846.6333	1655.818	0.7011	0.0003

a. Multiple modes exist. The smallest value is shown

Soque Statistics

		Cu/Fe (ppm)	U/Ti	U/Th	U/Pb	Heavy REE	Light REE	Lu/Zn	Mean Cu, Pb, Zn
	Valid	65	65	64	32	65	65	32	32
N	Missing	0	0	1	33	0	0	33	33
Mean		0.000103	0.000956	0.359646	3.048542	28.57492	221.1578	0.141057	11.98958
Median		0	0.000825	0.342045	2.33	17.44	137	0.073214	10.66667
Mode		0	.0002a	.1111a	.9000a	7.4600a	21.4000a	.0364a	7.6667a
Std. Deviation		0.000137	0.000534	0.1919206	2.063107	49.01763	290.2172	0.1676071	6.123276
Variance		0	0	0.037	4.256	2402.728	84226.04	0.028	37.495
Skewness		1.362	1.201	1.081	0.875	5.058	4.006	2.295	1.488
Std. Error of		0.297	0.297	0.299	0.414	0.297	0.297	0.414	0.414
Kurtosis		1.339	1.552	1.466	0.146	27.24	18.785	5.045	1.576
Std. Error of		0.586	0.586	0.59	0.809	0.586	0.586	0.809	0.809
Range		0.0006	0.0026	0.9197	8.17	321.54	1788.367	0.6708	22.6667
Minimum		0	0.0002	0.1111	0.59	5.14	21.4	0.0192	4.6667
Maximum		0.0006	0.0028	1.0308	8.76	326.68	1809.767	0.69	27.3333

		Mean Co, Ni, Cu	Mean Al, Fe, Ti	Ce/Lu	La/Yb	La/Lu	Sm/Yb	Ce/Yb	Sc/Ti
	Valid	32	65	65	65	65	65	65	65
N	Missing	33	0	0	0	0	0	0	0
Mean		5.276042	72071798	157.097839	13.98454	83.63863	3.4544	25.893312	0.000508
Median		4.083333	55666669	92.898551	9.782609	49.13044	1.904762	19.047619	0.000403
Mode		2.3333a	15666668.6933a	3.6585a	5.7609a	19.0000a	0.9783	1.1278a	.0001a
Std. Deviation		3.695539	55833784	186.1979045	11.63344	96.77218	4.189972	21.289234	0.000344
Variance		13.657	3.12E+15	34669.66	135.337	9364.855	17.556	453.231	0
Skewness		1.786	2.436	1.955	1.737	2.114	3.214	1.462	1.432
Std. Error of		0.414	0.297	0.297	0.297	0.297	0.297	0.297	0.297
Kurtosis		2.57	7.254	3.274	3.11	4.243	12.476	2.394	2.723
Std. Error of		0.809	0.586	0.586	0.586	0.586	0.586	0.586	0.586
Range		13	3.09E+08	748.7904	57.0135	411.9583	24.1941	101.7888	0.0018
Minimum		2.3333	15666669	3.6585	2.1532	5.3886	0.3226	1.1278	0.0001
Maximum		15.3333	3.24E+08	752.449	59.1667	417.3469	24.5167	102.9167	0.0019

		Y/Ti	La/Ti	Ce/Ti	Sm/Ti	Eu/Ti	Dy/Ti	Yb/Ti	Lu/Ti
	Valid	32	65	65	65	63	65	65	65
N	Missing	33	0	0	0	2	0	0	0
Mean		0.003972	0.012653	0.022912	0.003612	0.000251	0.00181	0.001004	0.00023
Median		0.003209	0.010568	0.019214	0.001891	0.000102	0.001481	0.000792	0.000198
Mode		.0002a	0.0043	.0008a	.0024a	.0000a	.0003a	.0002a	0.0003
Std. Deviation		0.004001	0.010918	0.0194478	0.006214	0.000443	0.001441	0.0006027	0.000173
Variance		0	0	0	0	0	0	0	0
Skewness		3.639	2.075	1.908	4.406	3.323	2.945	1.636	2.147
Std. Error of		0.414	0.297	0.297	0.297	0.302	0.297	0.297	0.297
Kurtosis		16.936	5.976	5.602	22.983	12.361	11.197	2.75	5.804
Std. Error of		0.809	0.586	0.586	0.586	0.595	0.586	0.586	0.586
Range		0.0228	0.06	0.1092	0.0414	0.0024	0.0085	0.0028	0.0009
Minimum		0.0002	0.0011	0.0008	0.0002	0	0.0003	0.0002	0
Maximum		0.023	0.061	0.1101	0.0416	0.0024	0.0088	0.003	0.0009

a. Multiple modes exist. The smallest value is shown

Appendix A.5 – Statistics: Upper Tugaloo Basin Sediment Samples

Tugaloo Statistics

		U_ppm	Ag_ppm	Al_pct	Au_ppm	Be_ppm	Ca_pct	Ce_ppm
	Valid	50	24	50	25	24	0	48
N	Missing	0	26	0	25	26	50	2
Mean		7.988	0.25	5.319	0.00784	0.8021		166.271
Median		6	0.25	5	0.005	0.75		49
Mode		2.1a	0.25	6.69	0.005	0.5		10
Std. Deviation		6.3492	0	1.8125	0.0142	0.39686		336.4932
Variance		40.312	0	3.285	0	0.157		113227.69
Skewness		1.789		0.685	5	1.263		3.879
Std. Error of		0.337	0.472	0.337	0.464	0.472		0.343
Kurtosis		3.705		-0.02	25	2.248		15.77
Std. Error of		0.662	0.918	0.662	0.902	0.918		0.674
Range		27.9	0	7.66	0.071	1.75		1738
Minimum		2	0.25	2.54	0.005	0.25		10
Maximum		29.9	0.25	10.2	0.076	2		1748

		Co_ppm	Cr_ppm	Cu_ppm	Dy_ppm	Eu_ppm	F_ppm	Fe_pct
	Valid	24	24	24	49	47	25	48
N	Missing	26	26	26	1	3	25	2
Mean		5.208	3.333	6.667	16.4663	1.6713	148.4	2.3365
Median		3.75	2.5	6	9.1	0.25	150	1.9
Mode		2.5	2.5	6	2.50a	0.25	150	1.09a
Std. Deviation		4.3487	2.0466	5.1302	19.44733	3.12357	112.5622	1.3912
Variance		18.911	4.188	26.319	378.198	9.757	12670.25	1.935
Skewness		2.748	2.436	2.24	2.313	3.735	3.382	1.81
Std. Error of		0.472	0.472	0.472	0.34	0.347	0.464	0.343
Kurtosis		9.406	5.087	6.486	5.333	16.666	15.655	3.613
Std. Error of		0.918	0.918	0.918	0.668	0.681	0.902	0.674
Range		19.5	7.5	24	89.45	17.75	620	6.46
Minimum		2.5	2.5	1	0.05	0.25	15	0.77
Maximum		22	10	25	89.5	18	635	7.23

		Hf_ppm	K_pct	La_ppm	Li_ppm	Lu_ppm	Mg_pct	Mn_ppm
	Valid	50	24	43	24	48	24	50
N	Missing	0	26	7	26	2	26	0
Mean		75.3	1.0083	86.814	6.396	2.317	0.214583	969
Median		27	1	43	6	1.65	0.2025	830
Mode		6.0a	1.1	3	2.5	0.1	.1300a	930
Std. Deviation		117.2058	0.42622	149.8538	3.9754	2.282	0.0818126	480.1796
Variance		13737.194	0.182	22456.16	15.804	5.207	0.007	230572.45
Skewness		3.045	0.974	3.53	0.808	1.879	0.6	1.008
Std. Error of		0.337	0.472	0.361	0.472	0.343	0.472	0.337
Kurtosis		10.932	1.425	12.974	-0.022	4.751	0.425	0.606
Std. Error of		0.662	0.918	0.709	0.918	0.674	0.918	0.662
Range		619	1.8	718	13.5	11.5	0.345	2140
Minimum		3	0.4	3	2.5	0.1	0.08	320
Maximum		622	2.2	721	16	11.6	0.425	2460

a. Multiple modes exist. The smallest value is shown

Tugaloo Statistics

		Mo_ppm	Na_pct	Nb_ppm	Ni_ppm	P_ppm	Pb_ppm	Sc_ppm
	Valid	24	25	24	24	24	24	50
N	Missing	26	25	26	26	26	26	0
Mean		2.5	1.0212	10	4.771	516.667	6.958	12.9
Median		2.5	0.95	5	2.5	400	5	10.3
Mode		2.5	1.71	2.5	2.5	300	5	14.7
Std. Deviation		0	0.64683	9.7524	2.9561	300.2414	3.9395	7.8098
Variance		0	0.418	95.109	8.739	90144.93	15.52	60.993
Skewness			0.388	1.261	1.176	0.929	2.184	0.929
Std. Error of		0.472	0.464	0.472	0.472	0.472	0.472	0.337
Kurtosis			-0.886	0.668	0.869	-0.15	4.601	0.007
Std. Error of		0.918	0.902	0.918	0.918	0.918	0.918	0.662
Range		0	2.27	32.5	10.5	1000	15	29.8
Minimum		2.5	0.12	2.5	2.5	200	5	2.6
Maximum		2.5	2.39	35	13	1200	20	32.4

		Sm_ppm	Sn_ppm	Sr_ppm	Th_ppm	Ti_ppm	V_ppm	W_ppm
	Valid	44	24	24	48	48	50	24
N	Missing	6	26	26	2	2	0	26
Mean		33.841	19.792	26.292	24.271	9572.917	83.2	1.167
Median		4	20	25	8	5950	70	1
Mode		.5a	20	25	4	3200.0a	60.0a	1
Std. Deviation		86.8916	11.5372	6.3278	44.8191	9655.287	52.6614	0.8165
Variance		7550.149	133.107	40.042	2008.755	93224570	2773.224	0.667
Skewness		3.774	0.353	4.899	3.788	1.795	1.441	4.899
Std. Error of		0.357	0.472	0.472	0.343	0.343	0.337	0.472
Kurtosis		14.95	-0.367	24	15.43	2.791	2.546	24
Std. Error of		0.702	0.918	0.918	0.674	0.674	0.662	0.918
Range		456.5	42.5	31	238	39900	250	4
Minimum		0.5	2.5	25	2	800	20	1
Maximum		457	45	56	240	40700	270	5

		Y_ppm	Yb_ppm	Zn_ppm	Mean 9REE	Ti/9REE	U/9REE	Co/Fe (ppm)
	Valid	24	42	24	50	50	50	48
N	Missing	26	8	26	0	0	0	2
Mean		25.083	11.052	23.875	38.379606	466.8952	0.399008	0.000105
Median		17.5	7.8	21	13.736111	296.1137	0.274087	0.000017
Mode		15	0.9	21	4.1250a	0	.0808a	0
Std. Deviation		26.0362	10.9366	13.0694	68.7313674	622.1909	0.363664	0.0001471
Variance		677.884	119.609	170.81	4724.001	387121.5	0.132	0
Skewness		2.537	1.978	3.07	3.916	3.894	2.385	1.955
Std. Error of		0.472	0.365	0.472	0.337	0.337	0.337	0.343
Kurtosis		7.486	4.432	12.283	16.003	18.454	6.291	4.613
Std. Error of		0.918	0.717	0.918	0.662	0.662	0.662	0.674
Range		117.5	50	70	347.2972	3832.924	1.8459	0.0006
Minimum		2.5	0.9	7	4.125	0	0.0808	0
Maximum		120	50.9	77	351.4222	3832.924	1.9267	0.0006

a. Multiple modes exist. The smallest value is shown

Tugaloo Statistics

		Cu/Fe (ppm)	U/Ti	U/Th	U/Pb	Heavy REE	Light REE	Lu/Zn	Mean Cu, Pb, Zn
	Valid	48	48	48	24	50	50	24	24
N	Missing	2	2	2	26	0	0	26	26
Mean		0.000131	0.001318	0.710151	1.133681	12.21122	76.03517	0.056435	12.5
Median		0.000028	0.000803	0.546429	0.955833	5.24125	27.25	0.04581	11
Mode		0	.0003a	0.9	.1300a	1.85	20.8000a	.0013a	10.3333
Std. Deviation		0.000175	0.001191	0.5192747	0.733137	22.01245	139.1292	0.042	6.924018
Variance		0	0	0.27	0.537	484.548	19356.93	0.002	47.942
Skewness		1.441	1.976	1.222	0.726	3.627	4.022	1.101	3.096
Std. Error of		0.343	0.343	0.343	0.472	0.337	0.337	0.472	0.472
Kurtosis		1.63	3.523	0.776	-0.462	13.98	17.071	1.564	12.282
Std. Error of		0.674	0.674	0.674	0.918	0.662	0.662	0.918	0.918
Range		0.0007	0.0051	1.9817	2.71	117.1775	755.2667	0.1737	36
Minimum		0	0.0003	0.1183	0.13	0.8625	9.2667	0.0013	4.6667
Maximum		0.0007	0.0053	2.1	2.84	118.04	764.5333	0.175	40.6667

		Mean Co, Ni, Cu	Mean Al, Fe, Ti	Ce/Lu	La/Yb	La/Lu	Sm/Yb	Ce/Yb	Sc/Ti
	Valid	24	50	48	40	43	40	42	48
N	Missing	26	0	2	10	7	10	8	2
Mean		5.548611	30943336	117.260512	8.798729	62.41488	1.893191	17.189298	0.004177
Median		4.25	19833335	43.178571	6.22991	35	1.065887	10.628019	0.001734
Mode		3	4.2650a	400	3.3333	20	.5556a	44.4444	.0001a
Std. Deviation		3.903572	32039757	160.9122347	9.852831	68.93955	2.507864	18.437994	0.007464
Variance		15.238	1.03E+15	25892.747	97.078	4752.661	6.289	339.96	0
Skewness		2.403	1.8	1.601	3.608	1.262	3.133	1.969	3.768
Std. Error of		0.472	0.337	0.343	0.374	0.361	0.374	0.365	0.343
Kurtosis		7.544	2.901	1.187	17.029	0.281	12.049	4.627	15.404
Std. Error of		0.918	0.662	0.674	0.733	0.709	0.733	0.717	0.674
Range		18	1.36E+08	566.9697	58.7381	225.5082	13.5761	88.0486	0.0404
Minimum		2	4.265	3.0303	0.1508	0.4918	0.0251	0.8403	0.0001
Maximum		20	1.36E+08	570	58.8889	226	13.6012	88.8889	0.0405

		Y/Ti	La/Ti	Ce/Ti	Sm/Ti	Eu/Ti	Dy/Ti	Yb/Ti	Lu/Ti
	Valid	23	42	46	43	46	47	41	46
N	Missing	27	8	4	7	4	3	9	4
Mean		0.005531	0.010793	0.019812	0.00358	0.000218	0.002273	0.001566	0.000318
Median		0.002941	0.006116	0.00908	0.000952	0.00008	0.001667	0.000938	0.000217
Mode		.0004a	0.005	.0003a	0.001	0.0001	.0000a	.0001a	.0001a
Std. Deviation		0.007416	0.010785	0.0232447	0.007946	0.000309	0.001943	0.001548	0.000307
Variance		0	0	0.001	0	0	0	0	0
Skewness		2.878	1.326	1.58	4.191	2.513	1.145	2.026	2.066
Std. Error of		0.481	0.365	0.35	0.361	0.35	0.347	0.369	0.35
Kurtosis		9.51	0.868	1.541	20.009	6.644	0.354	4.377	4.748
Std. Error of		0.935	0.717	0.688	0.709	0.688	0.681	0.724	0.688
Range		0.0334	0.0405	0.0927	0.0459	0.0014	0.0072	0.0069	0.0014
Minimum		0.0004	0.0003	0.0003	0.0001	0	0	0.0001	0
Maximum		0.0338	0.0409	0.093	0.0459	0.0014	0.0072	0.007	0.0014

a. Multiple modes exist. The smallest value is shown

Appendix B – Correlation Matrices

Appendix B.1 – Correlation Matrix: Tallulah Basin

Tallulah River - NURE sediment database
VassarStats: Correlation Matrix
Number of Variables = 37
Observations per variable = 70

r	U	Ag	Al	Au	Be	Ce	Co	Cr
U	1							
Ag	-0.032	1						
Al	-0.317	-0.181	1					
Au	-0.105	0.301	-0.031	1				
Be	-0.101	0.821	-0.083	0.324	1			
Ce	0.708	0.168	-0.064	-0.138	0.089	1		
Co	-0.164	0.808	-0.106	0.333	0.67	0.051	1	
Cr	-0.099	0.661	-0.242	0.159	0.665	0.111	0.74	1
Cu	-0.12	0.824	-0.127	0.224	0.622	0.122	0.947	0.719
Dy	0.635	-0.045	0.006	-0.195	-0.065	0.741	-0.049	-0.106
Eu	0.091	0.207	0.076	-0.058	0.324	0.303	0.265	0.279
fe	-0.057	-0.388	0.063	-0.112	-0.338	0.012	-0.331	-0.335
Fe	-0.229	0.19	-0.074	0.215	0.162	-0.133	0.469	0.388
Hf	0.742	-0.226	-0.489	-0.108	-0.259	0.217	-0.293	-0.159
K	0	0.579	-0.292	0.11	0.499	0.024	0.358	0.472
La	0.815	0.059	-0.086	-0.095	0.001	0.879	-0.078	-0.037
Li	-0.008	0.666	-0.259	0.128	0.652	0.069	0.484	0.525
Lu	0.456	-0.575	-0.095	-0.217	-0.51	0.279	-0.501	-0.454
Mg	-0.07	0.608	-0.281	0.071	0.581	0.058	0.604	0.754
Mn	0.17	-0.236	-0.133	-0.03	-0.234	-0.022	-0.042	-0.068
Mo	-0.046	0.889	-0.326	0.256	0.774	0.073	0.759	0.769
Na	-0.131	0.839	-0.008	0.2	0.74	0.057	0.799	0.567
Nb	0.026	0.669	-0.26	0.272	0.511	0.082	0.661	0.7
Ni	-0.141	0.801	-0.117	0.343	0.626	0.064	0.941	0.701
pb	0.013	0.863	-0.254	0.283	0.729	0.176	0.696	0.679
Pb	-0.067	0.943	-0.129	0.243	0.836	0.157	0.823	0.721
Sc	-0.128	0.08	0.144	0.159	0.087	0.099	0.288	0.268
Sm	0.69	0.347	-0.188	0.01	0.256	0.902	0.191	0.219
Sn	0.015	0.746	-0.23	0.06	0.552	0.144	0.517	0.464
Sr	-0.108	0.631	0.01	0.133	0.672	0.064	0.401	0.456
Th	0.77	0.216	-0.06	-0.134	0.152	0.868	0.012	0.056
Ti	0.14	-0.282	-0.187	-0.021	-0.222	-0.087	-0.17	-0.034
V	-0.239	-0.096	-0.017	0.036	-0.049	-0.206	0.141	0.124
W	-0.08	0.818	-0.263	0.214	0.733	0.057	0.721	0.751
Y	0.024	0.67	-0.334	0.043	0.487	0.146	0.524	0.597
Yb	0.598	-0.348	-0.034	-0.054	-0.351	0.369	-0.263	-0.257
Zn	-0.041	0.947	-0.205	0.282	0.747	0.152	0.894	0.667

r > 0.900	r < -0.600
r > 0.800	r < -0.500

Corrected ND values

Tallulah River - NURE sediment database
VassarStats: Correlation Matrix
Number of Variables = 37
Observations per variable = 70

r	Cu	Dy	Eu	fe	Fe	Hf	K	La
U								
Ag								
Al								
Au								
Be								
Ce								
Co								
Cr								
Cu	1							
Dy	0.008	1						
Eu	0.284	0.446	1					
fe	-0.324	0.046	-0.128	1				
Fe	0.476	-0.082	0.1	-0.114	1			
Hf	-0.258	0.248	-0.025	0.023	-0.154	1		
K	0.298	-0.128	0.137	-0.345	-0.112	-0.032	1	
La	-0.008	0.75	0.147	-0.044	-0.179	0.307	-0.063	1
Li	0.412	-0.079	0.175	-0.365	-0.078	-0.105	0.888	-0.037
Lu	-0.467	0.478	0.143	0.313	-0.131	0.582	-0.473	0.312
Mg	0.574	-0.08	0.086	-0.345	0.3	-0.125	0.601	-0.063
Mn	-0.02	0.189	0.028	0.111	0.652	0.366	-0.367	-0.015
Mo	0.743	-0.126	0.193	-0.436	0.204	-0.16	0.79	-0.026
Na	0.775	-0.074	0.195	-0.346	0.189	-0.306	0.497	-0.03
Nb	0.697	-0.134	0.167	-0.319	0.33	0.01	0.487	-0.025
Ni	0.965	-0.031	0.257	-0.329	0.514	-0.267	0.3	-0.039
pb	0.771	-0.025	0.219	-0.336	0.275	-0.145	0.37	0.123
Pb	0.8	-0.069	0.237	-0.39	0.178	-0.265	0.598	0.016
Sc	0.338	0.139	0.209	0.158	0.652	-0.187	-0.322	0.015
Sm	0.28	0.678	0.346	-0.111	-0.027	0.202	0.131	0.854
Sn	0.588	-0.095	-0.054	-0.3	0.204	-0.085	0.469	0.045
Sr	0.372	-0.098	0.14	-0.285	0.009	-0.194	0.61	-0.013
Th	0.067	0.679	0.177	-0.061	-0.252	0.235	0.065	0.88
Ti	-0.183	-0.014	-0.017	0.153	0.437	0.406	-0.238	-0.082
V	0.136	-0.045	0.009	0.049	0.882	-0.133	-0.251	-0.187
W	0.709	-0.053	0.305	-0.393	0.209	-0.173	0.718	-0.019
Y	0.551	-0.066	0.205	-0.343	0.125	-0.04	0.71	0.032
Yb	-0.241	0.549	0.086	0.167	0.093	0.594	-0.328	0.464
Zn	0.896	-0.021	0.242	-0.382	0.287	-0.219	0.533	0.028

r > 0.900	r < -0.600
r > 0.800	r < -0.500

Corrected ND values

Tallulah River - NURE sediment database
VassarStats: Correlation Matrix
Number of Variables = 37
Observations per variable = 70

r	Li	Lu	Mg	Mn	Mo	Na	Nb	Ni	pb
U									
Ag									
Al									
Au									
Be									
Ce									
Co									
Cr									
Cu									
Dy									
Eu									
fe									
Fe									
Hf									
K									
La									
Li	1								
Lu	-0.523	1							
Mg	0.69	-0.493	1						
Mn	-0.375	0.384	-0.064	1					
Mo	0.838	-0.623	0.792	-0.259	1				
Na	0.609	-0.564	0.622	-0.223	0.794	1			
Nb	0.478	-0.399	0.479	-0.028	0.732	0.539	1		
Ni	0.413	-0.487	0.584	-0.013	0.754	0.757	0.699	1	
pb	0.441	-0.48	0.431	-0.14	0.77	0.666	0.72	0.748	1
Pb	0.738	-0.59	0.677	-0.268	0.894	0.854	0.615	0.792	0.779
Sc	-0.258	0.022	0.133	0.61	0	0.117	0.178	0.354	0.185
Sm	0.177	0.153	0.14	-0.003	0.26	0.177	0.245	0.241	0.385
Sn	0.474	-0.437	0.526	-0.083	0.688	0.581	0.618	0.537	0.696
Sr	0.621	-0.465	0.629	-0.29	0.655	0.709	0.328	0.377	0.45
Th	0.137	0.151	0.1	-0.095	0.129	0.149	0.06	0.034	0.209
Ti	-0.278	0.367	-0.187	0.761	-0.266	-0.285	0.018	-0.195	-0.155
V	-0.224	0.013	0.096	0.736	-0.077	-0.063	0.016	0.172	-0.006
W	0.704	-0.555	0.71	-0.197	0.902	0.762	0.685	0.707	0.752
Y	0.708	-0.438	0.543	-0.222	0.788	0.527	0.707	0.505	0.634
Yb	-0.341	0.655	-0.301	0.552	-0.401	-0.358	-0.121	-0.259	-0.256
Zn	0.645	-0.559	0.619	-0.165	0.876	0.848	0.698	0.883	0.825

r > 0.900	r < -0.600
r > 0.800	r < -0.500

Corrected ND values

Tallulah River - NURE sediment database
VassarStats: Correlation Matrix
Number of Variables = 37
Observations per variable = 70

r	Pb	Sc	Sm	Sn	Sr	Th	Ti	V	W	Y	Yb	Zn
U												
Ag												
Al												
Au												
Be												
Ce												
Co												
Cr												
Cu												
Dy												
Eu												
fe												
Fe												
Hf												
K												
La												
Li												
Lu												
Mg												
Mn												
Mo												
Na												
Nb												
Ni												
pb												
Pb	1											
Sc	0.063	1										
Sm	0.312	0.134	1									
Sn	0.691	-0.001	0.26	1								
Sr	0.628	-0.065	0.073	0.505	1							
Th	0.206	-0.003	0.835	0.177	0.128	1						
Ti	-0.279	0.335	-0.099	-0.19	-0.253	-0.15	1					
V	-0.092	0.576	-0.168	-0.021	-0.117	-0.277	0.638	1				
W	0.792	0.064	0.26	0.595	0.6	0.086	-0.233	-0.06	1			
Y	0.646	-0.118	0.286	0.648	0.418	0.132	-0.191	-0.113	0.758	1		
Yb	-0.38	0.242	0.317	-0.245	-0.358	0.33	0.46	0.145	-0.324	-0.236	1	
Zn	0.922	0.122	0.32	0.71	0.556	0.16	-0.266	-0.027	0.803	0.666	-0.322	1

r > 0.900	r < -0.600
r > 0.800	r < -0.500

Corrected ND values

Appendix B.2 – Correlation Matrix: Soque Basin

Soque River: NURE Sediment Database
VassarStats: Correlation Matrix
Number of Variables = 37
Observations per variable = 65

r	U	Ag	Al	Au	Be	Ce	Co	Cr
U	1							
Ag	0.044	1						
Al	-0.041	-0.103	1					
Au	0.489	0.348	-0.108	1				
Be	-0.045	0.641	-0.069	0.085	1			
Ce	0.901	0.153	0.031	0.605	-0.035	1		
Co	0.119	0.901	0.018	0.372	0.602	0.191	1	
Cr	0.046	0.579	-0.301	0.344	0.579	0.02	0.618	1
Cu	0.135	0.841	0.15	0.412	0.432	0.291	0.887	0.379
Dy	0.908	-0.011	-0.115	0.45	-0.132	0.852	0.045	0.007
Eu	0.388	0.18	-0.085	0.188	0.259	0.35	0.163	0.151
fe	-0.024	-0.369	-0.021	-0.097	-0.33	-0.064	-0.323	-0.297
Fe	0.528	0.429	-0.019	0.51	0.122	0.594	0.423	0.268
Hf	0.361	-0.174	-0.288	-0.031	-0.093	-0.013	-0.156	0.042
K	-0.023	0.616	-0.101	0.028	0.907	-0.066	0.549	0.53
La	0.917	0.093	0.059	0.547	-0.062	0.988	0.15	-0.011
Li	0.032	0.715	-0.196	0.26	0.834	0.09	0.684	0.573
Lu	0.461	-0.496	-0.156	-0.037	-0.457	0.219	-0.446	-0.347
Mg	0.015	0.719	-0.179	0.218	0.561	0.099	0.692	0.567
Mn	0.393	-0.154	-0.088	0.086	-0.245	0.223	-0.134	-0.082
Mo	-0.006	0.827	-0.218	0.196	0.756	0.091	0.731	0.657
Na	-0.047	0.79	0.005	0.164	0.789	0.013	0.793	0.579
Nb	0.106	0.579	-0.175	0.131	0.499	0.037	0.605	0.585
Ni	0.14	0.866	0.097	0.428	0.468	0.292	0.802	0.411
pb	0.158	0.748	-0.203	0.375	0.743	0.224	0.7	0.66
Pb	0.146	0.858	-0.138	0.423	0.703	0.227	0.825	0.571
Sc	-0.085	0.151	0.359	0.043	-0.126	0.074	0.204	-0.02
Sm	0.84	0.21	0.019	0.701	-0.01	0.933	0.258	0.049
Sn	0.023	0.804	-0.041	0.165	0.656	0.072	0.764	0.447
Sr	-0.034	0.812	-0.221	0.224	0.807	0.024	0.77	0.716
Th	0.889	0.178	-0.001	0.626	-0.027	0.99	0.213	0.034
Ti	0.493	-0.201	-0.172	0.101	-0.208	0.277	-0.177	-0.049
V	0.353	0.011	0.296	0.287	-0.268	0.546	0.087	-0.08
W	-0.056	0.807	-0.259	0.195	0.703	0.018	0.689	0.608
Y	0.394	0.553	-0.288	0.572	0.388	0.42	0.533	0.524
Yb	0.806	-0.192	-0.231	0.293	-0.287	0.648	-0.162	-0.123
Zn	0.063	0.915	0.085	0.302	0.712	0.175	0.92	0.489

r > 0.900	r < -0.400
r > 0.800	r < -0.300

Corrected ND values

Soque River: NURE Sediment Database
VassarStats: Correlation Matrix
Number of Variables = 37
Observations per variable = 65

r	Li	Lu	Mg	Mn	Mo	Na	Nb	Ni	pb
U									
Ag									
Al									
Au									
Be									
Ce									
Co									
Cr									
Cu									
Dy									
Eu									
fe									
Fe									
Hf									
K									
La									
Li	1								
Lu	-0.482	1							
Mg	0.634	-0.414	1						
Mn	-0.277	0.673	-0.109	1					
Mo	0.806	-0.522	0.756	-0.201	1				
Na	0.744	-0.487	0.783	-0.216	0.734	1			
Nb	0.409	-0.279	0.616	0.074	0.524	0.686	1		
Ni	0.536	-0.394	0.55	-0.131	0.655	0.663	0.337	1	
pb	0.761	-0.422	0.832	-0.035	0.857	0.748	0.635	0.591	1
Pb	0.837	-0.468	0.584	-0.192	0.769	0.747	0.498	0.737	0.761
Sc	-0.169	-0.141	0.264	0.173	0.021	0.198	0.174	0.188	0.063
Sm	0.161	0.149	0.126	0.156	0.073	0.077	0.06	0.339	0.256
Sn	0.6	-0.431	0.451	-0.209	0.674	0.645	0.455	0.631	0.546
Sr	0.857	-0.515	0.866	-0.206	0.879	0.879	0.692	0.587	0.867
Th	0.121	0.184	0.125	0.191	0.113	0.038	0.063	0.309	0.246
Ti	-0.267	0.725	-0.139	0.945	-0.195	-0.233	0.085	-0.166	-0.027
V	-0.223	0.051	0.104	0.235	-0.1	-0.001	-0.02	0.138	-0.011
W	0.822	-0.509	0.703	-0.232	0.841	0.739	0.55	0.586	0.757
Y	0.552	-0.19	0.548	0.001	0.539	0.432	0.52	0.437	0.618
Yb	-0.209	0.809	-0.174	0.632	-0.251	-0.288	-0.075	-0.128	-0.114
Zn	0.734	-0.486	0.695	-0.175	0.769	0.884	0.543	0.868	0.735

r > 0.900	r < -0.400
r > 0.800	r < -0.300

Corrected ND values

Soque River: NURE Sediment Database
VassarStats: Correlation Matrix
Number of Variables = 37
Observations per variable = 65

r	Cu	Dy	Eu	fe	Fe	Hf	K	La
U								
Ag								
Al								
Au								
Be								
Ce								
Co								
Cr								
Cu	1							
Dy	0.069	1						
Eu	0.15	0.495	1					
fe	-0.266	0.031	-0.167	1				
Fe	0.524	0.466	0.34	-0.144	1			
Hf	-0.252	0.244	0.088	0.116	0.117	1		
K	0.363	-0.13	0.2	-0.323	0.095	0.003	1	
La	0.238	0.864	0.351	-0.05	0.541	-0.008	-0.087	1
Li	0.534	-0.022	0.25	-0.352	0.209	-0.175	0.811	0.054
Lu	-0.391	0.514	0.129	0.225	0.125	0.693	-0.413	0.245
Mg	0.684	0.014	0.292	-0.313	0.43	-0.155	0.511	0.053
Mn	-0.092	0.342	0.101	0.194	0.524	0.714	-0.199	0.199
Mo	0.64	-0.044	0.224	-0.382	0.29	-0.163	0.708	0.025
Na	0.748	-0.109	0.245	-0.342	0.351	-0.189	0.75	-0.015
Nb	0.437	0.014	0.205	-0.261	0.358	0.164	0.567	0.012
Ni	0.9	0.069	0.158	-0.281	0.436	-0.215	0.445	0.23
pb	0.624	0.09	0.36	-0.347	0.482	-0.049	0.681	0.165
Pb	0.699	0.072	0.219	-0.347	0.374	-0.156	0.65	0.181
Sc	0.34	-0.048	-0.061	-0.017	0.508	-0.275	-0.194	0.042
Sm	0.356	0.74	0.294	-0.056	0.614	-0.043	-0.024	0.934
Sn	0.579	-0.044	0.252	-0.312	0.242	-0.132	0.628	0.032
Sr	0.642	-0.075	0.217	-0.386	0.319	-0.136	0.779	-0.022
Th	0.317	0.833	0.347	-0.078	0.577	-0.028	-0.048	0.983
Ti	-0.164	0.422	0.131	0.23	0.424	0.812	-0.159	0.259
V	0.258	0.406	0.057	0.062	0.619	-0.304	-0.331	0.535
W	0.55	-0.109	0.196	-0.372	0.242	-0.148	0.709	-0.034
Y	0.407	0.433	0.563	-0.243	0.429	0.05	0.394	0.36
Yb	-0.128	0.838	0.32	0.085	0.45	0.543	-0.245	0.666
Zn	0.916	-0.019	0.204	-0.337	0.439	-0.222	0.641	0.128

r > 0.900	r < -0.400
r > 0.800	r < -0.300

Corrected ND values

Soquee River: NURE Sediment Database
VassarStats: Correlation Matrix
Number of Variables = 37
Observations per variable = 65

r	Pb	Sc	Sm	Sn	Sr	Th	Ti	V	W	Y	Yb	Zn
U												
Ag												
Al												
Au												
Be												
Ce												
Co												
Cr												
Cu												
Dy												
Eu												
fe												
Fe												
Hf												
K												
La												
Li												
Lu												
Mg												
Mn												
Mo												
Na												
Nb												
Ni												
pb												
Pb	1											
Sc	-0.005	1										
Sm	0.307	0.05	1									
Sn	0.706	0.042	0.089	1								
Sr	0.758	0.06	0.067	0.619	1							
Th	0.255	0.047	0.949	0.07	0.051	1						
Ti	-0.19	0.032	0.182	-0.228	-0.209	0.244	1					
V	-0.058	0.799	0.493	-0.097	-0.108	0.52	0.135	1				
W	0.752	-0.018	0.052	0.711	0.855	0.037	-0.234	-0.167	1			
Y	0.606	-0.039	0.418	0.418	0.575	0.44	0.037	0.042	0.481	1		
Yb	-0.147	-0.11	0.59	-0.224	-0.253	0.629	0.672	0.265	-0.265	0.19	1	
Zn	0.846	0.207	0.242	0.759	0.782	0.194	-0.221	0.066	0.721	0.45	-0.224	1

r > 0.900	r < -0.400
r > 0.800	r < -0.300

Corrected ND values

Appendix B.3 – Correlation Matrix: Upper Tugaloo Basin

Tugaloo River: NURE Sediment Database
VassarStats: Correlation Matrix
Number of Variables = 37
Observations per variable = 50

r	U	Ag	Al	Au	Be	Ce	Co	Cr
U	1							
Ag	-0.114	1						
Al	0.034	-0.277	1					
Au	-0.118	0.366	-0.234	1				
Be	-0.226	0.83	-0.277	0.359	1			
Ce	0.751	0.045	0.099	-0.051	-0.114	1		
Co	-0.12	0.662	-0.034	0.235	0.778	0.087	1	0.381
Cr	-0.048	0.768	-0.295	0.23	0.694	-0.011	0.381	1
Cu	-0.027	0.691	0.052	0.123	0.677	0.167	0.892	0.384
Dy	0.77	-0.048	0.221	-0.093	-0.205	0.879	-0.016	-0.044
Eu	0.686	0.16	0.006	-0.026	-0.059	0.91	0.143	0.065
fe	-0.023	-0.662	0.241	-0.255	-0.55	-0.021	-0.438	-0.509
Fe	0.188	0.337	0.319	0.029	0.196	0.446	0.346	0.111
Hf	0.532	-0.227	-0.21	-0.104	-0.161	-0.103	-0.238	-0.063
K	-0.07	0.867	-0.256	0.177	0.798	0.056	0.58	0.854
La	0.732	0.008	0.032	-0.052	-0.134	0.981	0.042	-0.022
Li	-0.155	0.764	-0.308	0.155	0.856	-0.027	0.773	0.629
Lu	0.511	-0.464	0.158	-0.215	-0.429	0.529	-0.349	-0.313
Mg	-0.18	0.888	-0.203	0.354	0.85	0.027	0.842	0.551
Mn	0.349	-0.262	0.676	-0.187	-0.349	0.335	-0.22	-0.229
Mo	-0.114	1	-0.277	0.366	0.83	0.045	0.662	0.768
Na	-0.038	0.73	0.02	0.203	0.428	0.103	0.447	0.395
Nb	-0.018	0.603	-0.265	0.099	0.731	-0.024	0.501	0.619
Ni	-0.027	0.765	-0.096	0.183	0.724	0.199	0.915	0.453
pb	0.134	0.785	-0.199	0.158	0.608	0.29	0.459	0.803
Pb	-0.025	0.793	0.018	0.231	0.748	0.145	0.836	0.527
Sc	-0.125	-0.041	0.387	0.168	-0.091	-0.123	0.001	-0.213
Sm	0.698	0.085	0.012	-0.029	-0.099	0.952	0.121	0.009
Sn	-0.104	0.784	-0.135	0.396	0.566	0.079	0.575	0.494
Sr	-0.132	0.951	-0.244	0.336	0.807	0.027	0.649	0.713
Th	0.753	0.069	0.064	-0.045	-0.113	0.994	0.083	0.007
Ti	0.627	-0.128	0.107	-0.135	-0.169	0.553	-0.132	0.014
V	0.386	-0.136	0.594	-0.068	-0.224	0.606	0.059	-0.278
W	-0.106	0.725	-0.003	0.238	0.54	0.006	0.474	0.519
Y	0.328	0.579	-0.1	0.15	0.484	0.499	0.507	0.521
Yb	0.664	-0.151	-0.077	-0.104	-0.207	0.763	-0.115	-0.114
Zn	-0.117	0.803	-0.073	0.142	0.845	0.045	0.925	0.538

r > 0.900	r < -0.400
r > 0.800	r < -0.300

Corrected ND values

Tugaloo River: NURE Sediment Database
VassarStats: Correlation Matrix
Number of Variables = 37
Observations per variable = 50

r	Cu	Dy	Eu	fe	Fe	Hf	K	La
U								
Ag								
Al								
Au								
Be								
Ce								
Co								
Cr								
Cu	1							
Dy	0.109	1						
Eu	0.225	0.743	1					
fe	-0.458	0.023	-0.095	1				
Fe	0.395	0.304	0.567	-0.213	1			
Hf	-0.24	-0.035	-0.072	0.016	-0.294	1		
K	0.572	-0.025	0.128	-0.574	0.171	-0.161	1	
La	0.117	0.852	0.886	0.002	0.399	-0.106	0.031	1
Li	0.681	-0.103	0.025	-0.506	0.136	-0.138	0.762	-0.063
Lu	-0.338	0.6	0.351	0.21	0.08	0.044	-0.372	0.551
Mg	0.793	-0.107	0.149	-0.588	0.455	-0.252	0.714	-0.007
Mn	-0.1	0.407	0.305	0.102	0.588	-0.037	-0.28	0.313
Mo	0.691	-0.048	0.16	-0.662	0.337	-0.227	0.867	0.008
Na	0.622	0.042	0.169	-0.518	0.317	-0.214	0.583	0.069
Nb	0.468	-0.098	0.028	-0.399	0.198	0.037	0.685	-0.061
Ni	0.921	0.092	0.283	-0.507	0.367	-0.252	0.655	0.151
pb	0.561	0.213	0.394	-0.52	0.347	-0.132	0.747	0.239
Pb	0.9	0.083	0.224	-0.525	0.386	-0.228	0.685	0.087
Sc	-0.004	-0.218	-0.064	-0.012	0.397	-0.056	-0.177	-0.132
Sm	0.185	0.778	0.922	-0.05	0.438	-0.093	0.075	0.926
Sn	0.53	-0.001	0.147	-0.519	0.288	-0.268	0.687	0.052
Sr	0.651	-0.069	0.137	-0.63	0.355	-0.233	0.808	-0.011
Th	0.173	0.877	0.918	-0.038	0.433	-0.099	0.079	0.98
Ti	-0.077	0.593	0.549	0.046	0.512	0.217	-0.081	0.56
V	0.132	0.555	0.513	0.078	0.685	-0.216	-0.223	0.57
W	0.488	-0.046	0.056	-0.48	0.266	-0.198	0.61	-0.048
Y	0.545	0.315	0.617	-0.383	0.521	-0.07	0.598	0.424
Yb	-0.049	0.783	0.653	0.069	0.232	-0.003	-0.119	0.771
Zn	0.918	-0.048	0.128	-0.532	0.392	-0.209	0.731	0.002

r > 0.900	r < -0.400
r > 0.800	r < -0.300

Corrected ND values

Tugaloo River: NURE Sediment Database
VassarStats: Correlation Matrix
Number of Variables = 37
Observations per variable = 50

r	Li	Lu	Mg	Mn	Mo	Na	Nb	Ni	pb
U									
Ag									
Al									
Au									
Be									
Ce									
Co									
Cr									
Cu									
Dy									
Eu									
fe									
Fe									
Hf									
K									
La									
Li	1								
Lu	-0.384	1							
Mg	0.797	-0.461	1						
Mn	-0.388	0.468	-0.231	1					
Mo	0.764	-0.464	0.888	-0.262	1				
Na	0.294	-0.377	0.643	-0.07	0.73	1			
Nb	0.806	-0.248	0.59	-0.186	0.603	0.107	1		
Ni	0.778	-0.367	0.866	-0.192	0.765	0.584	0.501	1	
pb	0.592	-0.267	0.62	-0.096	0.785	0.556	0.481	0.616	1
Pb	0.669	-0.347	0.783	-0.122	0.793	0.679	0.485	0.836	0.648
Sc	-0.272	-0.297	0.081	0.371	-0.041	0.222	-0.22	-0.072	-0.179
Sm	0.01	0.431	0.069	0.23	0.085	0.124	-0.011	0.232	0.327
Sn	0.542	-0.359	0.685	-0.179	0.784	0.638	0.302	0.639	0.533
Sr	0.685	-0.462	0.867	-0.248	0.951	0.712	0.532	0.731	0.703
Th	-0.023	0.513	0.032	0.313	0.069	0.124	-0.019	0.205	0.308
Ti	-0.126	0.636	-0.135	0.655	-0.128	-0.204	0.073	-0.094	0.119
V	-0.225	0.272	0.005	0.691	-0.136	0.097	-0.192	0.065	-0.028
W	0.461	-0.298	0.566	-0.108	0.725	0.654	0.347	0.482	0.504
Y	0.456	-0.119	0.546	0.037	0.579	0.372	0.553	0.59	0.717
Yb	-0.122	0.721	-0.184	0.232	-0.151	-0.167	-0.044	-0.054	0.05
Zn	0.85	-0.399	0.893	-0.192	0.803	0.557	0.681	0.903	0.596

r > 0.900	r < -0.400
r > 0.800	r < -0.300

Corrected ND values

Tugaloo River: NURE Sediment Database
VassarStats: Correlation Matrix
Number of Variables = 37
Observations per variable = 50

r	Pb	Sc	Sm	Sn	Sr	Th	Ti	V	W	Y	Yb	Zn
U												
Ag												
Al												
Au												
Be												
Ce												
Co												
Cr												
Cu												
Dy												
Eu												
fe												
Fe												
Hf												
K												
La												
Li												
Lu												
Mg												
Mn												
Mo												
Na												
Nb												
Ni												
pb												
Pb	1											
Sc	-0.046	1										
Sm	0.14	-0.088	1									
Sn	0.689	-0.03	0.099	1								
Sr	0.734	0.076	0.062	0.693	1							
Th	0.162	-0.148	0.947	0.111	0.04	1						
Ti	-0.079	-0.138	0.471	-0.127	-0.155	0.545	1					
V	0.045	0.521	0.522	-0.07	-0.091	0.571	0.397	1				
W	0.757	0	0.016	0.767	0.68	0.021	-0.142	-0.071	1			
Y	0.555	-0.048	0.588	0.402	0.554	0.509	0.256	0.178	0.35	1		
Yb	-0.097	-0.33	0.761	-0.145	-0.175	0.758	0.595	0.327	-0.18	0.251	1	
Zn	0.896	-0.047	0.071	0.629	0.742	0.052	-0.091	-0.009	0.583	0.558	-0.138	1

r > 0.900	r < -0.400
r > 0.800	r < -0.300

Corrected ND values

Appendix C – Histograms of Rare Earth Element Concentrations

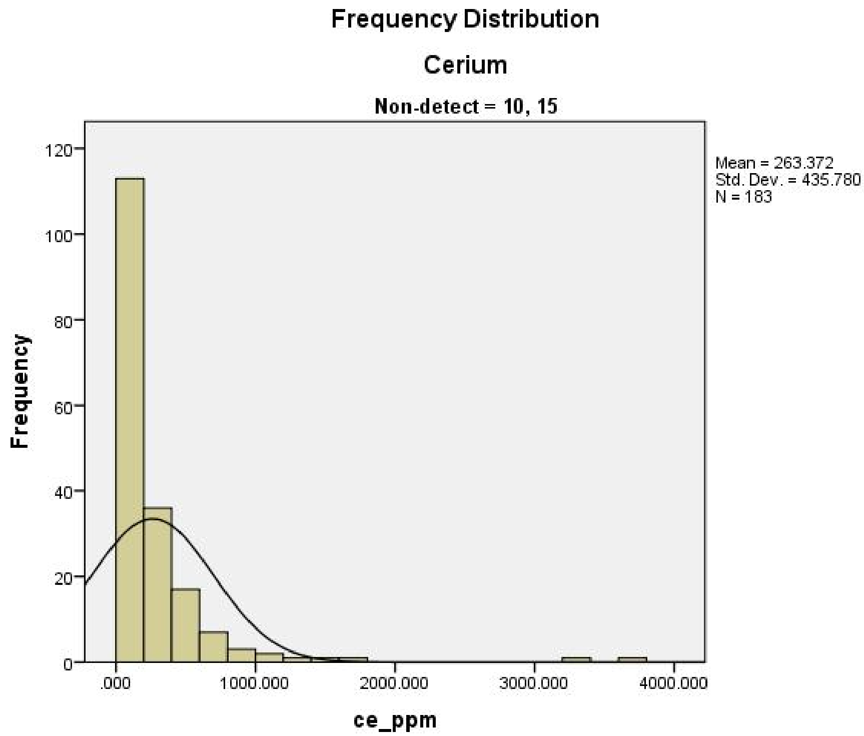

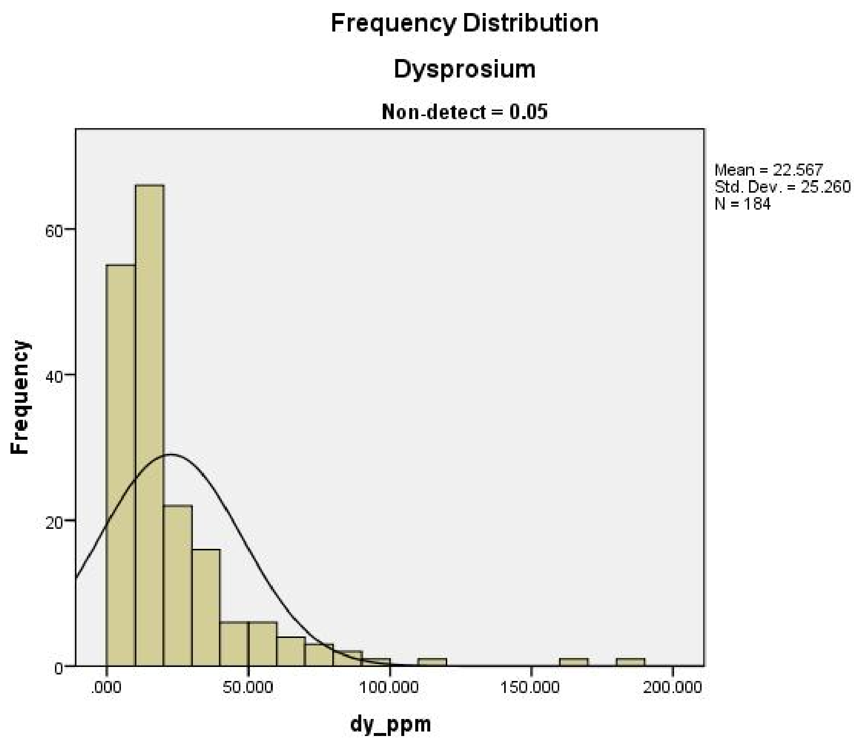

Frequency Distribution

Europium

Non-detect = 0.2, 0.25, 0.35

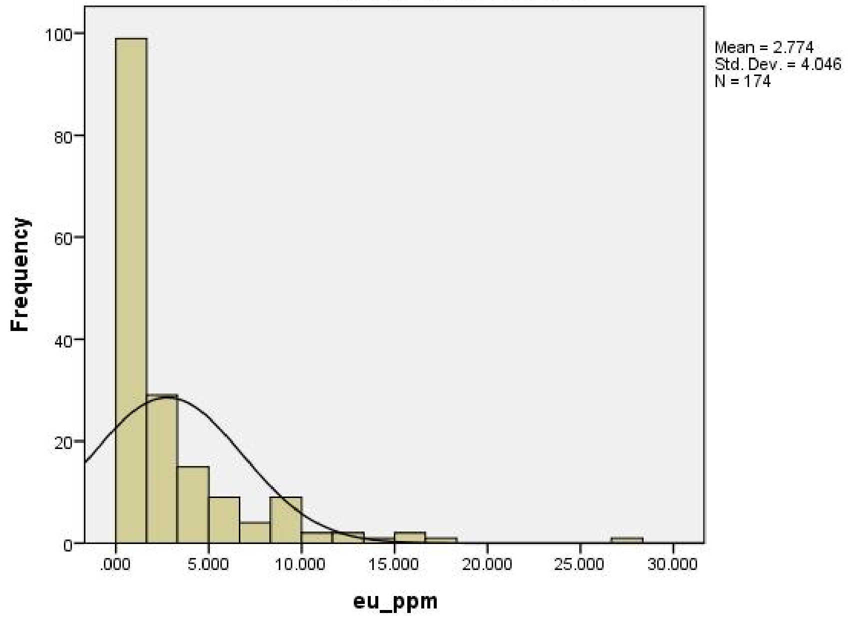

Frequency Distribution

Lanthanum

Non-detect = 3

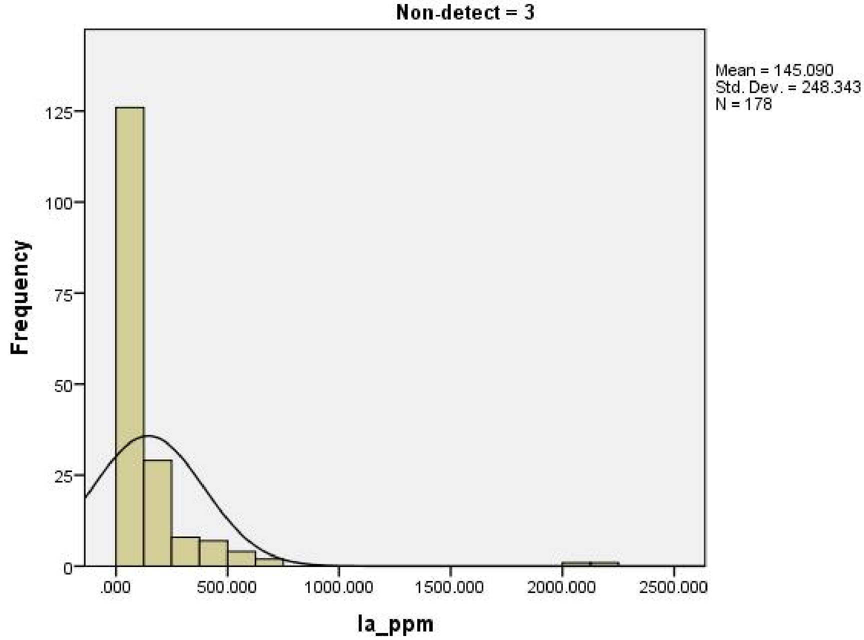

Frequency Distribution

Lutetium

Non-detect = 0.1, 0.2

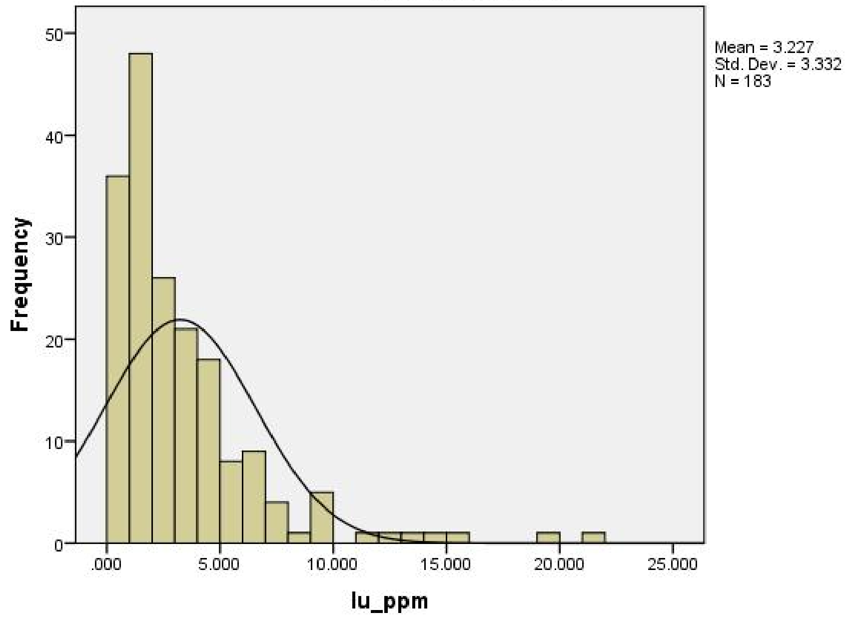

Frequency Distribution

Samarium

Non-detect = 0.5

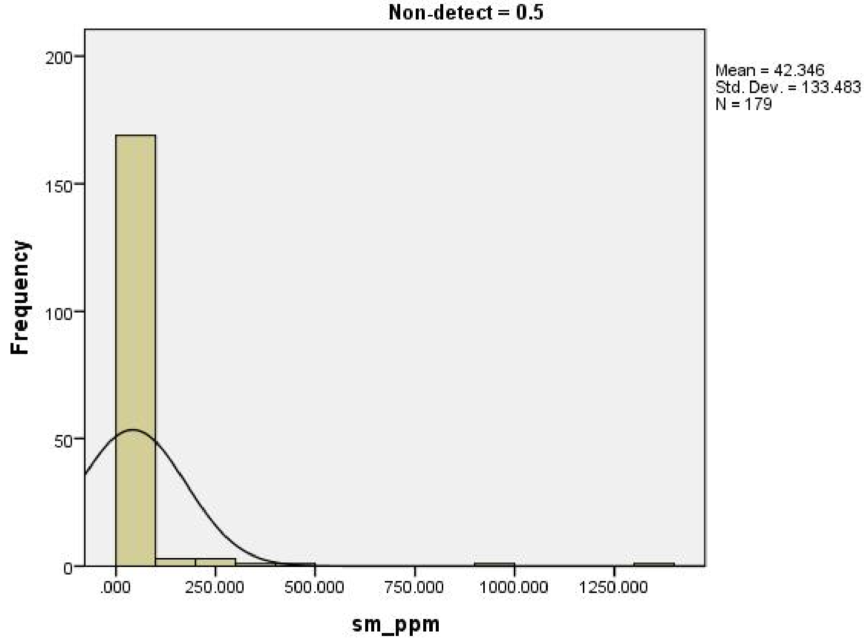

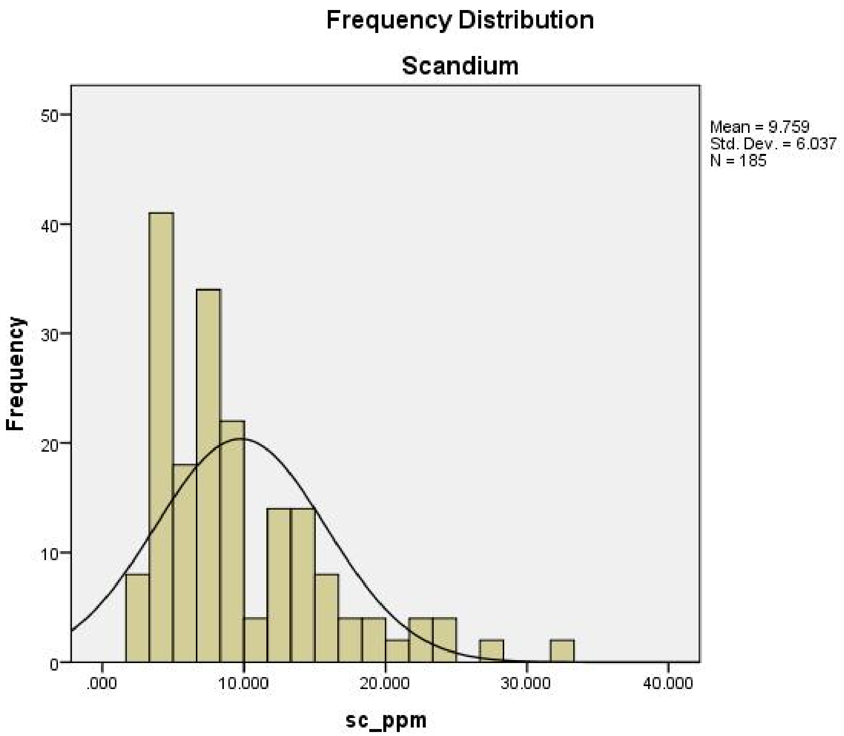
Frequency Distribution
Scandium
Mean = 9.759
Std. Dev. = 6.037
N = 185
Frequency
0
10
20
30
40
50
.000
10.000
20.000
30.000
40.000
sc_ppm

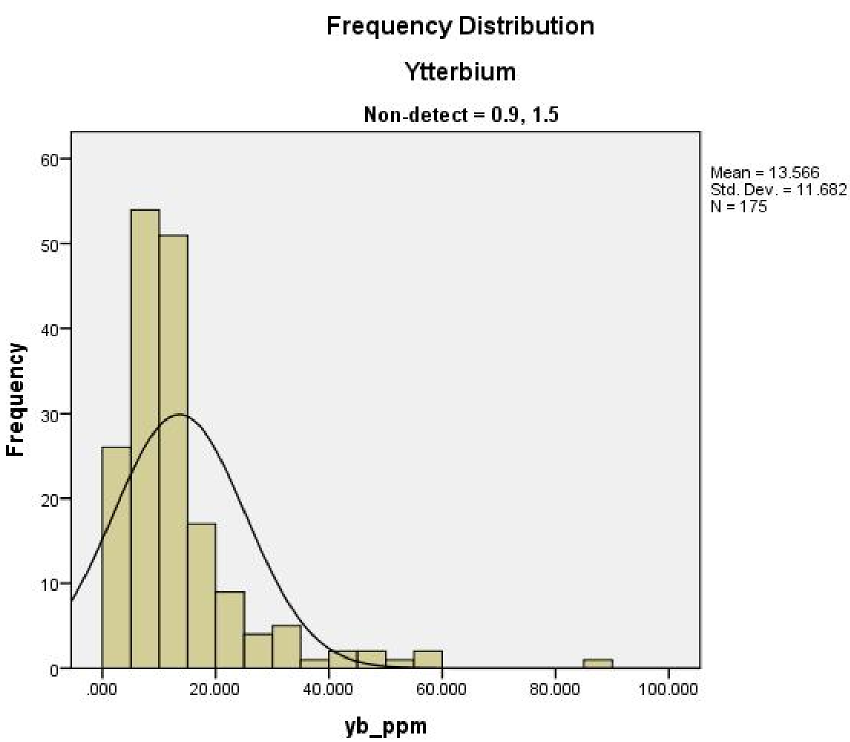
Frequency Distribution
Ytterbium
Non-detect = 0.9, 1.5
Mean = 13.566
Std. Dev. = 11.682
N = 175
Frequency
0
10
20
30
40
50
60
.000
20.000
40.000
60.000
80.000
100.000
yb_ppm

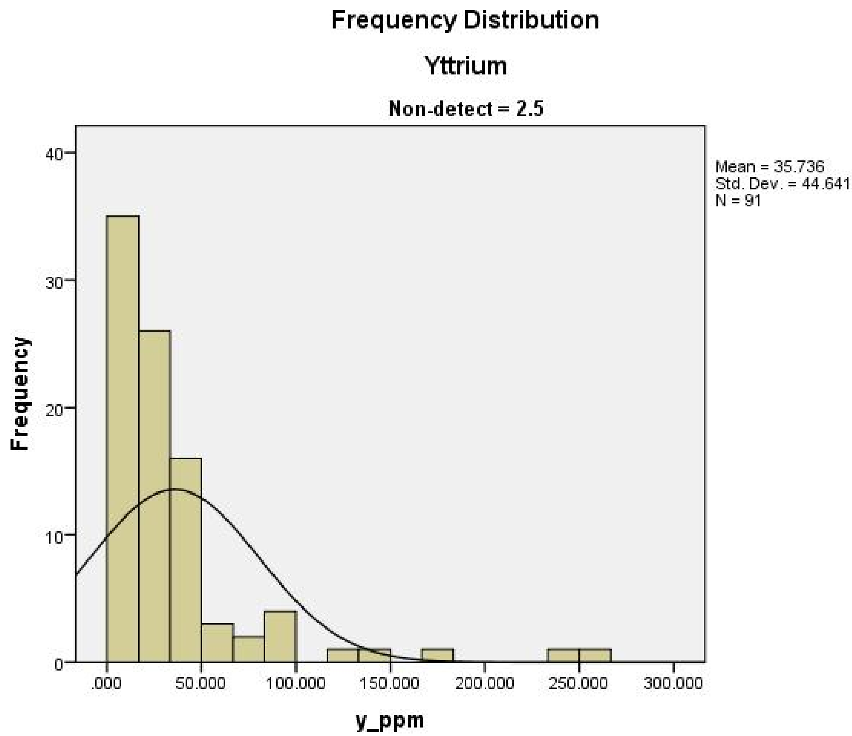
Frequency Distribution
Yttrium
Non-detect = 2.5
Mean = 35.736
Std. Dev. = 44.641
N = 91
Frequency
0
10
20
30
40
.000
50.000
100.000
150.000
200.000
250.000
300.000
y_ppm